Constitutive modelling of polymer glasses : finite, nonlinear viscoelastic behaviour of polycarbonate

Constitutive Modelling of Polymer Glasses

Finite, Nonlinear Viscoelastic Behaviour of Polycarbonate

PROEFSCHRIFT

ter verkrijging van de graad van doctor aan de Technische Universiteit Eindhoven, op gezag van de Rector Magnificus, prof.dr. J.H. van Lint, voor een commissie aangewezen door het College van Dekanen in het openbaar te verdedigen op woensdag 28 februari 1996 om 16.00 uur

door

THEODORUS ANTHONIUS TERVOORT

geboren te Haarlem

Dit proefschrift is goedgekeurd door de promotoren:

prof.dr.ir. H.E.H. Meijer
prof.dr. P.J. Lemstra

en de co-promotor:

dr.ir. L.E. Govaert

Constitutive Modelling of Polymer Glasses

Finite, Nonlinear Viscoelastic Behaviour of Polycarbonate

CIP-GEGEVENS KONINKLIJKE BIBLIOTHEEK, DEN HAAG

Tervoort, Theodorus Anthonius

Constitutive Modelling of Polymer Glasses : finite
non-linear viscoelastic behaviour of polycarbonate /
Theodorus Anthonius Tervoort. - Eindhoven : Eindhoven
University of Technology
Thesis Technische Universiteit Eindhoven. - With ref. -
With summary in Dutch.
ISBN 90-386-0357-6
Subject headings: polymer glasses / viscoelasticity.

This thesis was prepared with LaTeX 2_ε, and reproduced by de Witte
offsetdrukkerij bv, Eindhoven, from camera-ready copy supplied by the author.

Voor mijn ouders

Table of Contents

Summary

When studying the deformation behaviour of glassy polymers, a distinction can be made between the linear viscoelastic region, the nonlinear viscoelastic response and the yield behaviour at high stress levels. The linear viscoelastic deformation is adequately described using linear response theory, resulting in the well known Boltzmann single integral representation. The non-linear regime has been, and still is, an active field of research and a large number of theories have been put forward. Most of these theories aim at a one-dimensional description of the non-linear behaviour at moderate strain, often for a special deformation mode like for instance creep. Yield of polymer materials is classically described by using yield criteria, of which the pressure and rate-dependent Von Mises criterion seems to be most successful. After yielding, strain hardening sets in, sometimes preceded by intrinsic strain softening.

In this thesis, an attempt is made to combine all these aspects of the deformation behaviour of polymer glasses into a single constitutive equation. To this extent, the "time-stress superposition principle" is invoked, sometimes referred to as a "stress clock", which states that the main influence of stress is to change all relaxation times in a similar way, i.e. to alter the intrinsic time scale of the material. This is analogous to the well known "time-temperature superposition", according to which all relaxation times depend equally on temperature. This nonlinear influence of stress on the deformation behaviour, originating from stress-biased segmental diffusion, is quantitatively described by the Eyring theory, which defines to what extent the relaxation times change as a function of stress. The applicability of time-stress superposition is demonstrated for polycarbonate, that can be considered as a relatively simple model system since it has only a single molecular mechanism active from room temperature to the glass-transition temperature. It is shown that the complete nonlinear viscoelastic behaviour of polycarbonate, including rate-dependent "yield" behaviour, is determined by the linear relaxation time spectrum combined with a single nonlinearity parameter, which emerges from the Eyring theory, the so-called "activation volume". In essence, the applicability of time-stress superposition states that "yielding" can be envisaged as a stress-induced glass transition.

The strain-hardening response of polycarbonate was investigated by means of large homogeneous deformations above and below the glass-transition temperature. To ensure homogeneous behaviour below the glass-transition temperature during mechanical testing at large strains, the samples were conditioned mechanically, prior to testing. During this conditioning technique, consisting of large to and fro torsion of the cylindrical specimen, intrinsic strain softening, which is the main cause for strain localisation, proceeds up to a saturation level. Upon reloading, the material does not soften anymore, resulting in a homogeneous deformation, even under tensile loading.

Using the preconditioned polycarbonate samples, it was shown experimentally that the strain hardening response of polycarbonate at room temperature, in uniaxial tensile and compression, and in shear deformation, is accurately described by neo-Hookean behaviour, with a (shear) modulus $G = 26$ MPa. Neo-Hookean behaviour was observed up to fracture, which occurred at draw ratios $\lambda = 3$ in uniaxial tensile deformation. In particular, no upswing in stress, indicative for a finite extensibility (maximum draw ratio) of the entanglement network, was observed. The temperature dependence of the strain-hardening modulus below the glass-transition temperature corresponds to the temperature dependence of the "plateau modulus", as observed with mechanical spectroscopy above the glass-transition temperature. This indicates that strain hardening in glassy polymers results from a rubber-elastic response of the entanglement network.

To combine all these aspects of the deformation behaviour of glassy polymers into a single constitutive equation, a basic model, a so-called "Leonov mode", is presented. A single Leonov mode is a Maxwell model employing a relaxation time that is dependent on an equivalent stress proportional to the Von Mises stress. Furthermore, a Leonov mode correctly separates the (elastic) hydrostatic and (viscoelastic) deviatoric stress response and accounts for the geometrical complexities associated with simultaneous finite elastic and plastic deformations. Subsequently, this Leonov mode is combined into a "multi-mode" expression that is able to describe the bimodal spectrum of relaxation times which rules the complete deformation behaviour of polymer glasses. It is demonstrated that the model is able to describe the three-dimensional, finite non-linear viscoelastic behaviour of polycarbonate in creep, stress relaxation and tensile experiments, including strain-rate dependent yield behaviour. It is also capable of describing three-dimensional aspects of the strain-hardening behaviour, such as the development of anisotropy during plastic flow.

The present research establishes the linear shear relaxation time spectrum as the key quantity, determining the nonlinear viscoelastic behaviour of glassy polymers. Deviatoric stress (and temperature) merely distort the time scale. It should be noted, however, that mechanical properties in general, and viscoelastic behaviour especially, are profoundly influenced by physical aging. It is now well established that, under influence of aging, the creep compliance curve shifts toward longer times. All samples used in this study, however, had the same age,

which by far exceeded the longest times in the experiments. Therefore, to a first approximation, aging was not taken into account (which causes the model to be less accurate for differently aged samples). As opposed to aging, it is also observed that plastic deformation beyond the "yield point" results in a decrease of the viscosity, leading to intrinsic strain softening. This phenomenon is called "rejuvenation" and is thought to be the result of mechanically "de-aging" the sample by plastic deformation. The good agreement between experiments and predictions for the stress-relaxation experiments, as well as the applicability of time-stress superposition, indicate that, for polycarbonate, rejuvenation effects are not important for monotonic loading paths up to the "yield stress", and for loading times which are short relative to the age of the material. Although a quantitative description of rejuvenation (and aging) at moderate stresses has yet to be developed, several phenomenological models have been proposed in literature, that give an adequate description of strain softening in monotone loading paths after the yield point (Boyce *et al.*, 1988; Hasan *et al.*, 1993). In this thesis, rejuvenation was not taken into account. Some consequences with respect to aging and rejuvenation of the modelling strategy applied, are addressed at the end of the thesis.

An important consequence of the nonlinear flow behaviour of polymers in general, and polymer glasses specifically, is their sensitivity to strain localisation. Strain localisation, loosely defined as amplification of non-homogeneous deformation due to small fluctuations in the stress- or strain field, manifests itself in the form of shear bands or crazes. Using a brittle polystyrene, it was shown experimentally that both, fracture and yield, possess the same strain-rate dependence. This given indicates that the occurrence of small deformation zones (micro-shear bands or "slip patches") is the rate-determining step in craze initiation. This offers a possibility to define a local (time-independent) craze initiation criterion. By comparing local finite-element calculations, given a specific micro-structure, with experimental craze studies, this local criterion could be identified and could serve as a powerful tool in the computer-aided design of new heterogeneous polymer systems, where the morphology is optimized in such a way that shear yielding prevails crazing.

Notation

Tensorial Quantities

α, a, A	scalar
$\mathbf{a}$, $\mathbf{A}$	vector
$\boldsymbol{\alpha}$, $\mathbf{A}$	second order tensor
$\underline{\boldsymbol{\alpha}}$, $\underline{\mathbf{A}}$	fourth order tensor

Operations and functions

$\mathbf{ab}$, $\mathbf{AB}$	dyadic product
$\mathbf{a} \cdot \mathbf{b}$, $\mathbf{A} \cdot \mathbf{B}$	inner product
$\mathbf{A} : \mathbf{B}$	double inner product
$\mathbf{A}^T$	transposition
$\mathbf{A}^{-1}$	inversion
$\mathrm{tr}(\mathbf{A})$	trace
$\det(\mathbf{A})$	determinant
$I_A \equiv \mathrm{tr}(\mathbf{A})$	first invariant of $\mathbf{A}$
$II_A \equiv \frac{1}{2}(I_A^2 - \mathrm{tr}(\mathbf{A} \cdot \mathbf{A})$	second invariant of $\mathbf{A}$
$III_A \equiv \det(\mathbf{A})$	third invariant of $\mathbf{A}$
$\mathbf{A}^d = \mathbf{A} - \frac{1}{3}\mathrm{tr}(\mathbf{A})\mathbf{I}$	deviatoric part of $\mathbf{A}$
$\dot{\mathbf{A}}$	material time derivative of $\mathbf{A}$
$\mathring{\mathbf{A}}$	Jaumann (co-rotational) derivative of $\mathbf{A}$
$\overset{\nabla}{\mathbf{A}}$	Truesdell (upper-convected) derivative of $\mathbf{A}$
$\mathrm{div}(\mathbf{a})$	divergence of $\mathbf{a}$

Chapter 1

Introduction

1.1 General Introduction

Polymers, as a group of materials, often offer an attractive compromise between ease of processability and final mechanical and thermal properties. It is, therefore, not surprising, that, since their introduction in the beginning of this century, nowadays structural and other applications of polymers have become widespread. Nevertheless, a thorough understanding of their mechanical behaviour is still lacking.

There are a number of reasons to strive for a better comprehension of the deformation behaviour of polymer systems. In case of structural applications, the need for an adequate description of mechanical properties like creep and stress-relaxation, is obvious. Second, at high stress, polymers are prone to strain localisation, which manifests itself in the form of shear bands and crazes, and which is often a prelude to failure. In heterogeneous polymer systems, this process of strain localisation is strongly influenced by the specific micro-structure (*morphology*), which determines the local state-of stress and strain. A thorough understanding of this process is, however, still lacking and researchers in the area of polymer development have to rely on an empirical approach, characterized by the impossibility to transfer knowledge, obtained in one polymer system, to the other. Utilizing detailed finite element calculations might remove some of this empiricism, by resolving the complicated interaction between structure development and strain localisation, and, thereby, determine which aspects of the morphology govern the localisation process on a mesoscopic scale. However, for this, a proper constitutive equation, which allows for a quantitative description of the constituent polymers, is essential. Last but not least, an accurate continuum mechanical description would identify the essential material parameters which control the mechanical behaviour of polymer materials. Relating these parameters to the molecular structure of a polymer, would open an efficient way of developing new polymers with tailored mechanical properties.

With respect to micro-structure, it is possible to distinguish between semi-crystalline and amorphous polymers. Semi-crystalline polymers generally have a spherulitic structure, consisting of crystalline lamellae, separated by amorphous material. Consequently, semi-crystalline polymers exhibit a complex deformation behaviour, which, at this moment, is difficult to describe, especially since the mechanical behaviour of the constituent amorphous and crystalline phases is not understood completely, let it be their mutual interaction[1]. Therefore, this thesis is primarily concerned with amorphous polymers, also called *polymer glasses*.

The structure of a polymer glass is essentially the same as the melt from which it solidifies, and can be envisaged as a random assembly of covalent bonded chains, held together by secondary forces. Many aspects of the physical and mechanical properties of (glassy) polymers are governed by the comparatively weak secondary bonds, and polymers are, therefore, sometimes referred to as "soft-condensed matter". An important consequence of the weakness of the secondary bonds is the considerable thermally (and stress) activated segmental motion, resulting in complicated time and temperature dependent mechanical behaviour, which is the topic of this thesis.

1.2 Deformation Behaviour of Polymer Glasses

In the description of the deformation behaviour of solid polymers, usually a distinction is made between the linear viscoelastic regime at very low stress, the non-linear viscoelastic response at moderate stress, and the yield behaviour at high stress (Ward, 1990). The linear viscoelastic deformation is adequately described using linear response theory, which results in the well-known Boltzmann single integral representation. The non-linear regime has been, and still is, an active field of research, and a large number of theories have been put forward. Most of these theories aim at a one-dimensional description of the non-linear behaviour at moderate strain, often for a special deformation mode like, for instance, creep. An extensive survey of these theories can be found in the monograph by Ward (1990). Yield of polymer materials is classically described by using yield criteria, of which the pressure and rate- dependent Von Mises criterion seems to be most successful. After yielding, strain hardening sets in, sometimes preceded by intrinsic strain softening. A typical stress-strain curve of an amorphous polymer, displaying these features of mechanical behaviour, is depicted in Figure 1.1. It should be noted that most of the response, as depicted in Figure 1.1, is highly nonlinear, since the true linear range for polymers is very small[2].

[1] A nice example of the complicated effects which can occur in semi-crystalline polymers, is the dramatic embrittlement of poly[(R)-3-hydroxybutyrate] upon secondary crystallization, and the relatively simple solution, to this problem (De Koning and Lemstra, 1993).

[2] For polycarbonate in uniaxial tensile deformation, the critical stress is about 1.7 MPa, which corresponds to approximately 0.06% strain in a normal tensile test, see Chapter 3.

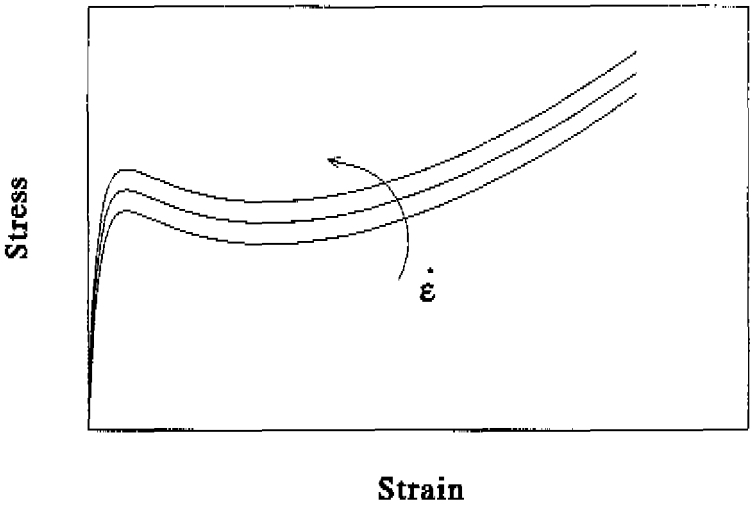

Figure 1.1 *Schematic stress-strain curves of an (amorphous) polymer below the glass-transition temperature, at different strain rates $\dot{\varepsilon}$.*

The main features of the linear viscoelastic behaviour of glassy polymers are determined by two characteristic relaxation mechanisms, the glass transition and the reptation process (Struik, 1990). This is depicted in Figure 1.2, showing a schematic dubbel-logarithmic plot of the shear-relaxation modulus versus time. At short times, only limited segmental motion is possible, resulting in a solid-like behaviour. At the glass transition, segmental diffusion becomes unbounded, but large scale motion of the polymer chain is still prohibited because of steric hindrance between the chains. On these time scales, the polymer effectively behaves like a rubber. From the (plateau) modulus G_r in this region, a molecular weight between entanglements can be defined, using the classical theory of rubber elasticity. Here, *entanglements* are envisaged as physical knots, as opposed to chemical (permanent) cross-links in a real rubber, and the molecular weight between entanglements provides a scalar measure of the steric hindrance between the polymer chains. At still longer time scales, the reptation process enables main-chain diffusion (centre-of mass diffusion), and the polymer behaves like a melt, not able to sustain any load.

The overall shape of the relaxation modulus of an amorphous polymer, as depicted in Figure 1.2, is rather insensitive to the exact chemical composition. Details of the molecular structure determine the glass-transition temperature and the value of the plateau modulus (disproportional to the molecular weight between entanglements), whereas the length of the plateau zone depends on the molecular

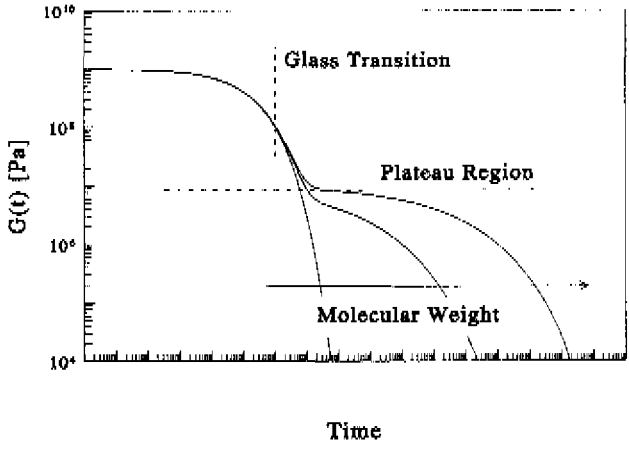

Figure 1.2 *Relaxation modulus of a glassy polymer (far) below the glass-transition temperature; schematic*

weight (which is proportional to degree-of polymerisation).

It was already observed by Leaderman (1943), that, to a good approximation, temperature does not influence the shape of the relaxation modulus, but only determines its position on a logarithmic time-scale. This is called *time-temperature superposition* or *thermo-rheological simple behaviour*. With respect to modelling, it implies that the main influence of temperature is to change all the relaxation times, which determine the decay of the relaxation modulus in time, in an identical way. If it is assumed that this is the *only* effect of temperature, then a so-called reduced time φ can be defined, on which isothermal linear behaviour is recovered:

$$\varphi = \int_0^t \frac{dt'}{a_T[T(t')]} \tag{1.1}$$

Here, $T(t')$ is the applied temperature history, and a_T is the temperature *shift factor*, defined as the ratio of the relaxation times at a given temperature with respect to a reference temperature. Thus, a higher temperature only accelerates relaxation, and, therefore, only distorts the time scales of the material.

An important feature of the mechanical behaviour of glassy polymers is the similarity between Figures 1.1 and 1.2. At low stress/short times, the response is solid-like, with a modulus of 1-5 GPa. At higher stress/longer times, there is a gradual change to rubber-like behaviour, with a good correspondence between the value of the strain-hardening modulus in Figure 1.1, and the plateau modulus

in Figure 1.2. Finally, at the highest stress/longest time, there is a transition to fluid-like behaviour, and the polymer will break/flow. Only the time-scales are not correct, for polycarbonate at room temperature, the linear relaxation times associated with the glass-transition are in the order of 10^{15}-10^{16} s, whereas the transition to rubber-like behaviour in a standard uniaxial tensile test, at high stress, only takes $\approx$ 100 s. This indicates that stress, like temperature, accelerates relaxation. If this concept of stress-induced relaxation is correct, it is important both from a modelling and from a physics point-of view. For example, with respect to molecular interpretation, it indicates that the yield point can be envisaged as a stress-induced glass transition. With respect to modelling, the concept of stress-induced relaxation suggests the use of a reduced time, or, equivalently, the use of stress-dependent relaxation times, to describe the nonlinear effect of high stresses.

The principle to describe yield-like behaviour of polymeric materials, by use of a stress-dependent relaxation time, dates back to Tobolsky and Eyring (1943). It was used later by Haward and Thackray (1968) who added a finite-extendable spring (a so-called "Langevin" spring) to account for a maximum draw ratio during strain hardening (see Figure 1.3).

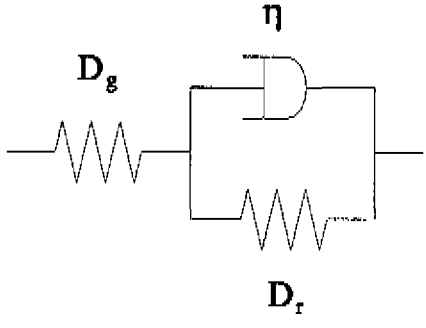

Figure 1.3 *Mechanical analogue of the Haward-Thackray model. The initial elastic response is described by the compliance D_g, the yield point is determined by a stress-dependent viscosity η, and the strain-hardening response follows from D_r.*

The stress dependence of the relaxation time in the Haward-Thackray model is incorporated using a stress shift factor a_σ, defined as the ratio of the relaxation time at a given stress level and the linear relaxation time at zero (very low) stress. The effect of a stress-dependent relaxation time is revealed most clearly in creep tests at different stress levels, see Figure 1.4. At very low stress levels, the relaxation time is constant, and the behaviour is linear (the creep compliance is independent of stress). At higher stress levels, the relaxation time is reduced by a factor $a_\sigma(\tau)$. On a logarithmic time axis, this results in a horizontal shift of the compliance curve.

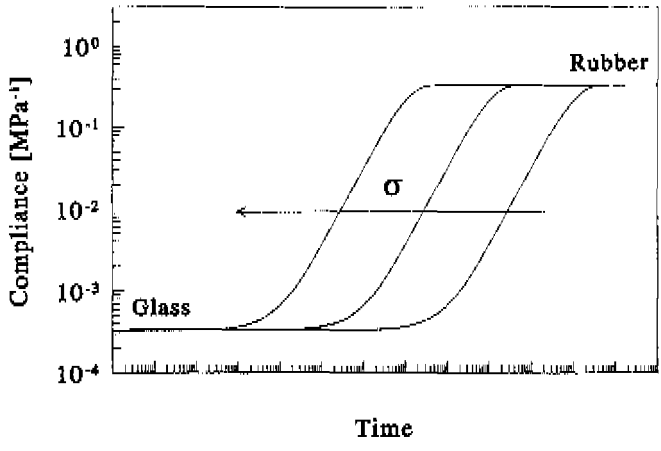

Figure 1.4 *Schematic representation of the creep compliance of the Haward-Thackray model at different stress levels.*

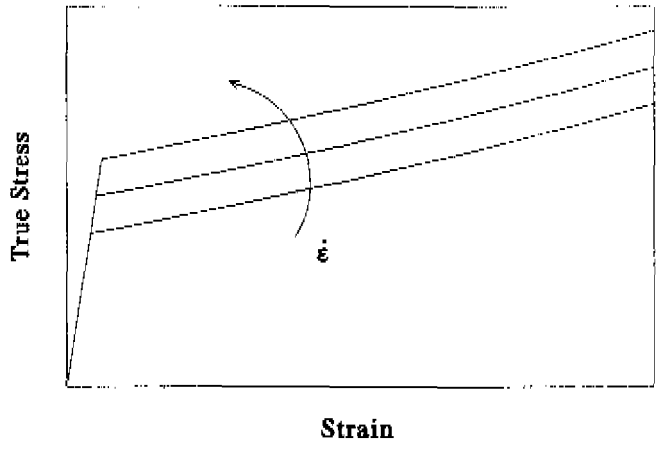

Figure 1.5 *Schematic representation of stress-strain curves, according to the Haward-Thackray model at different strain rates.*

Haward and Thackray assumed, that the stress dependence of the relaxation time originated solely from the plastic flow process (the dashpot in Figure 1.3). They used the Eyring expression for the viscosity, a semi-empirical relation, which describes stress-activated flow of structural units in a material, like segments in case of polymers. The Eyring equation is known to give a good description of the strain rate dependence of plastic flow in polymers and other materials (Krausz and Eyring, 1975; Ward, 1990, Chapter 11). Other expressions for the stress dependence of the viscosity have been derived, with more molecular detail, like the Argon theory, in which plastic flow is regarded as stress-activated nucleation of kink bands in a polymer chain. However, on a fitting level, these theories are almost indistinguishable (Hasan and Boyce, 1995; Ward, 1990).

A schematic drawing of a set of calculated true stress-strain curves, at different strain rates, using the Haward-Thackray model, is depicted in Figure 1.5. From this figure, it is clear that the model correctly accounts for the rate-dependence of the yield stress and the initial "glassy" modulus. However, the use of a single stress-dependent relaxation time results in an abrupt transition from elastic to plastic behaviour, similar to elasto-plastic behaviour, employing a rate-dependent yield criterion. Moreover, using only a single relaxation time, it is not possible to describe an experimental linear relaxation modulus (see Figure 1.2). Particularly, the Haward-Thackray model considers a polymer to be a thermo*set*, incapable of (irreversible) plastic deformation, whereas many polymers are thermo*plasts*, which ultimately can flow (see Figure 1.2).

More recently, Boyce *et al.* (1988) introduced the "BPA-model", which is essentially an extension of the Haward-Thackray model to three-dimensional finite deformations, using the Argon theory and the three-chain model (James and Guth, 1943) to describe, respectively, the plastic flow process and the strain-hardening response. The BPA-model was later refined by Arruda (1992) and Wu and van der Giessen (1993) with respect to the strain-hardening response and by Hasan *et al.* (1993) to include the effect of aging and rejuvenation. In all these models, no explicit use is made of a yield criterion. Instead, like in the Haward-Thackray model, the deformation behaviour is determined by a single relaxation time that is dependent on an equivalent stress (proportional to the Von Mises stress). Consequently, these models suffer from the same drawbacks as the Haward-Thackray model, as described above.

A way to improve the Haward-Thackray model, with respect to its poor description of the linear viscoelastic deformation behaviour, would be to use a *spectrum* of relaxation times rather than one (see Figure 1.6). In this case, additional assumptions have to be made concerning the stress dependence of these relaxation times. If it is assumed that all the relaxation times are dependent on the *total* stress in the same way, then the only nonlinear effect of stress is to alter the time scale of the material. This is called a "stress clock" (Bernstein and Shokooh, 1980), or *time-stress superposition*, analogous to time-temperature superposition. From time-stress superposition it follows that, like with temperature, a reduced

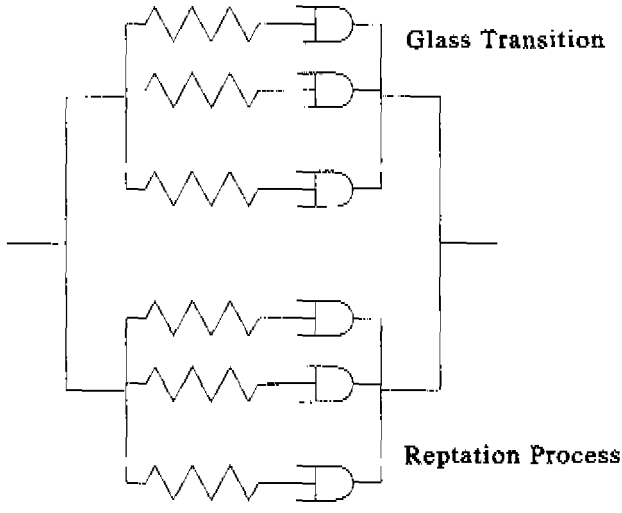

Figure 1.6 *Mechanical analogue of the bimodal spectrum of relaxation times of a polymer glass, composed of the glass transition and the reptation process. In principle, both sets of relaxation times can have their own temperature and stress dependence.*

time φ can be defined on which linear behaviour is recovered (Schapery, 1969):

$$\varphi(t) = \int_0^t \frac{dt'}{a_\sigma[\tau(t')]} \tag{1.2}$$

where $\tau(t')$ is the stress history of the material.

The principle to use a shift function to incorporate the effect of an experimental parameter is not limited to temperature and stress alone. Schapery (1969) and Valanis (1971) assumed that strain affects relaxation processes in a material. Shay, Jr. and Caruthers (1986) and O'Dowd and Knauss (1995) considered a free-volume clock to describe nonlinear viscoelastic behaviour and yielding, and Struik (1978) found that, during aging of a glassy polymer, the retardation times increase proportional to the aging time. All these theories imply, that the linear compliance curve or, more general, the linear response characteristic, is the key material function. The main influence of parameters like stress and temperature, is to distort the time scale. In Chapter 3, the time-stress superposition superposition principle will be used to formulate a constitutive equation for the finite nonlinear viscoelastic behaviour of glassy polymers up to the yield point.

As mentioned before, the Haward-Thackray model is only an approximation of the experimental relaxation modulus, assuming elastic behaviour before and after the glass transition. Moreover, in their original treatment of the subject,

Haward and Thackray (1968) assumed that the entanglement network, like a chemically cross-linked network, has a limited extensibility. They used a non-Gaussian rubber elastic model, a so-called "Langevin spring" (Kuhn and Grün, 1942), to describe the expected upswing in stress at limiting chain stretches. This concept of a *maximum draw ratio* was retained in all three-dimensional extensions of the Haward-Thackray model by Boyce *et al.* (1988); Arruda and Boyce (1993a) and Wu and van der Giessen (1993). Donald and Kramer (1982b, 1982a) showed that the maximum extensibility of a single strand in the entanglement network correlates well with the extension ratio inside craze fibrils and shear-deformation zones.

Although finite extensibility is relevant for a *chemically* cross-linked rubber, it is less obvious that it also applies to a (thermoplastic) glassy polymer, which ultimately flows. In fact, for a number of (semi-crystalline) polymers, the upswing in stress, associated with finite extensibility, was not observed experimentally (G'Sell *et al.*, 1992). In later expositions on the subject, Haward (1993) abandoned the Langevin spring, and adopted standard neo-Hookean behaviour to describe the strain-hardening response of polymeric materials. The deformation-state dependence of strain hardening and the issue of finite extensibility will be discussed in more detail in Chapter 5.

Important aspects of the deformation behaviour of glassy polymers, which have not been discussed so far, are "physical aging", and "rejuvenation". During cooling of a (polymer) melt around the glass-transition temperature, the relaxation times exceed the observational time scale, the material is unable to reach thermodynamic equilibrium, and turns into a glass. In the non-equilibrium glassy state, thermodynamic quantities like volume and enthalpy are not constant, but slowly evolve towards their equilibrium value. This process is called *physical aging* and is also known to have a profound influence on the viscoelastic behaviour. It was found in the sixties (Struik, 1978), that the main influence of physical aging far below the glass-transition temperature, on viscoelastic behaviour is to increase the retardation times proportional to the aging time. In other words, an aging-time shift factor a_t can be defined, analogous to the temperature shift factor a_T and the stress shift factor a_σ. On the other hand, it was shown (Bauwens, 1987), that aging far below the glass-transition temperature did not result in large changes of the yield stress. The effect of physical aging can be erased by bringing the sample above the glass-transition temperature, or by the application of plastic deformation. The latter observation is called *rejuvenation*, and is in accordance with the point of view that yielding can be envisaged as a stress-induced glass transition. Rejuvenation results in a significant decrease of the viscosity after the "yield point", and, consequently, strongly amplifies non-homogeneous behaviour. It is, therefore, also referred to as *intrinsic strain softening*, and plays an important role in the evolution of strain inhomogeneities such as shear bands and crazes.

Qualitatively, changes in mobility during aging and rejuvenation are often at-

tributed to changes in the so-called *free volume* (Struik, 1978; Hasan *et al.*, 1993), loosely defined as free space, available for segment diffusion. Unfortunately, attempts to quantify the free-volume concept have met serious difficulties, since there is no known definition of "free volume" that provides a satisfactory relation between "free volume" and mobility, especially below the glass transition temperature (Struik, 1978, Chapter 13). This is related to the fact that a thorough theoretical understanding of the glass transition is still lacking (Mansfield, 1995), which, in general, frustrates attempts to identify measurable parameters that are able to describe "mobility" (relaxation behaviour) around and below the glass transition temperature (Hodge, 1995).

1.3 Scope of the Thesis

The main objective of this thesis, is to derive a structured phenomenological constitutive equation for the three-dimensional, finite, nonlinear viscoelastic behaviour of glassy polymers. To this extent, the correspondence between the linear response characteristics of glassy polymers and the nonlinear deformation behaviour at high stress, as discussed in the preceding section, is taken as a starting point. It is assumed that each molecular relaxation process is described by a spectrum of relaxation times, all of which are equally dependent on stress and temperature. This implies, that the initial "yield point" is regarded as a stress-induced glass transition, whereas the temperature dependence of the strain-hardening response is assumed to originate from relaxation of the entanglement network.

In the present investigation, all experiments were performed on separate samples of identical thermal history, their age exceeding by far the longest time in the experiments. It is, therefore, assumed that all samples were equally affected by physical aging at the start of the experiment, and, moreover, that aging during the experiments could be neglected. Therefore, to a first approximation, aging was not taken into account. In this thesis, also the complicated effects of stress on the aging process, such as accelerated aging at higher stress levels and rejuvenation above the "yield stress", are not considered. It is, therefore, to be expected that especially in cyclic loading situations the model proposed will be less accurate.

1.4 Survey of the Thesis

To describe relaxation behaviour at large deformations, one needs to take into account complexities which can arise when combining simultaneously large elastic and plastic deformations. To this extent, a basic model, a so-called "Leonov mode", is presented in **Chapter 2**. A single Leonov mode is a Maxwell model employing a relaxation time that is dependent on an equivalent stress, proportional to the Von Mises stress. Furthermore, a Leonov mode correctly separates the

(elastic) hydrostatic stress and the (viscoelastic) deviatoric stress.

In **Chapter 3**, this Leonov mode is combined into a "multi-mode" expression to describe the spectrum of relaxation times which rules the deformation behaviour up to the yield point. Using polycarbonate as a model polymer, it is shown that the multi-mode Leonov model is able to describe the three-dimensional, finite, nonlinear viscoelastic behaviour in creep, stress relaxation, and tensile experiments.

Some consequences of the proposed constitutive behaviour with respect to strain localisation are discussed in **Chapter 4**. Using an extremely brittle polystyrene grade as a model system, it is shown that the kinetics of craze initiation are determined by the nonlinear flow process. Cavitation of a plastically deforming zone, which marks the onset of crazing, is either a very fast, or time-independent process.

Chapter 5 describes the state-of deformation dependence and the influence of temperature on the strain-hardening response of polymer glasses. Using polycarbonate as a model system, it is shown that the three-dimensional aspects of strain-hardening are adequately described by simple neo-Hookean behaviour. Deviations due to a finite extensibility, such as an asymptotic upswing in stress, were not observed. It is also shown, that the temperature dependence of the strain-hardening response is in accordance with the relaxation behaviour of the entanglement network, as observed in the melt (reptation process).

Chapter 6 discusses some of the implications of the applied model strategy with respect to aging and rejuvenation. It is shown that the free-volume approach, employing the Doolittle equation, is not able to describe three dimensional aging and rejuvenation. Moreover, it will be argued that it probably is not possible to define a aging-time shift factor for the *complete* relaxation-time spectrum. This would imply that during aging the relaxation-time spectrum not only shifts, but also changes shape.

Finally, some of the conclusions and recommendations are summarized in **Chapter 7**.

Chapter 2

Continuum Mechanical Modelling

2.1 Introduction

In the introductory Chapter, a one-dimensional outline of the deformation behaviour of glassy polymers was discussed. In order to develop a three-dimensional model, some continuum mechanical aspects have to be taken into account, which is the subject of this Chapter. In Section 2.2 the most frequently used kinematic quantities are introduced together with their notation. Section 2.3 gives an overview of the balance laws of continuum mechanics. In Section 2.4 a formalism to derive thermodynamic consistent constitutive equations is presented. This formalism is then used to derive a basic non-linear relaxation model which will serve as a "building block" for a detailed description of the finite non-linear viscoelastic behaviour of polymer glasses in Chapters 3 and 5. In Section 2.5, some of the features of this basic model, the so-called "compressible Leonov model", are shown and compared with some of the "standard" relaxation models used in plasticity and in polymer rheology. The Chapter ends with a short discussion in Section 2.6.

2.2 Kinematics

In this section we briefly introduce some of the kinematic quantities used in this thesis. A more complete discussion on this subject can be found in the literature (Astarita and Marrucci, 1974, Chapter 2).

A material body $\mathcal{B}$ consists of material points $\mathcal{P}$ which, at a certain time t, occupy a region in space. This region is called a configuration of $\mathcal{B}$ at time t. The motion of $\mathcal{B}$ in space generates a family of configurations which are related by the function φ with inverse φ^{-1}:

$$\mathbf{x} = \varphi(\mathbf{X}, t) \quad \text{and} \quad \mathbf{X} = \varphi^{-1}(\mathbf{x}, t) \tag{2.1}$$

Here $\mathbf{x}$ is the position vector in the current configuration (at time t) of a material point which was located at $\mathbf{X}$ in an arbitrary reference configuration. In this thesis

the initial (undeformed) configuration is chosen as reference, which is called the Lagrangian description of deformation. Since it is assumed that the inverse φ^{-1} exists, catastrophic motions like ripping and interpenetration of matter are not allowed.

The function φ fully specifies the deformation history of $\mathcal{B}$. The gradient of $\varphi(\mathbf{X}, t)$ with respect to $\mathbf{X}$ is a measure of the deformation and is called the deformation gradient tensor $\mathbf{F}$:

$$\mathbf{F} = \frac{\partial \varphi(\mathbf{X}, t)}{\partial \mathbf{X}} = \frac{\partial \mathbf{x}}{\partial \mathbf{X}} \tag{2.2}$$

The change in volume between the reference and current configuration of the infinitesimal neighbourhood of a material point $\mathcal{P}$ is related to the determinant of $\mathbf{F}$:

$$\frac{dV}{dV_0} = J = \det \mathbf{F} \tag{2.3}$$

The determinant of the deformation gradient tensor is, therefore, on physical grounds, always positive.

From the deformation gradient tensor, several strain measures can be derived, the most important of which are the left and right Cauchy-Green strain tensors:

$$\mathbf{B} = \mathbf{F} \cdot \mathbf{F}^T \quad \text{and} \quad \mathbf{C} = \mathbf{F}^T \cdot \mathbf{F} \tag{2.4}$$

Throughout this thesis, the rate of an arbitrary field quantity ϕ over the body $\mathcal{B}$ denotes the time derivative of that quantity at a constant value of $\mathbf{X}$:

$$\dot{\phi} = \frac{D\phi}{Dt} = \frac{\partial \phi(\mathbf{X}, t)}{\partial t} \tag{2.5}$$

The velocity is the rate of position of the material points:

$$\mathbf{v} = \dot{\mathbf{x}} = \frac{\partial \varphi(\mathbf{X}, t)}{\partial t} \tag{2.6}$$

The gradient of the velocity field gives the rate of deformation and is denoted by $\mathbf{L}$:

$$\mathbf{L} = \frac{\partial \mathbf{v}}{\partial \mathbf{x}} = \frac{\partial^2 \varphi(\mathbf{X}, t)}{\partial t \partial \mathbf{x}} = \frac{\partial^2 \varphi(\mathbf{X}, t)}{\partial \mathbf{X} \partial t} \cdot \frac{\partial \mathbf{X}}{\partial \mathbf{x}} = \dot{\mathbf{F}} \cdot \mathbf{F}^{-1} \tag{2.7}$$

The symmetric part of $\mathbf{L}$ is the rate-of-strain tensor

$$\mathbf{D} = \frac{1}{2}(\mathbf{L} + \mathbf{L}^T) \tag{2.8}$$

and the skew symmetric part is the vorticity tensor

$$\mathbf{W} = \frac{1}{2}(\mathbf{L} - \mathbf{L}^T) \tag{2.9}$$

The trace of $\mathbf{D}$ is related to the rate of volume $\dot{J}$:

$$\dot{J} = \frac{d(\det \mathbf{F})}{dt} = \det(\mathbf{F}) \mathbf{F}^{-T} : \dot{\mathbf{F}} = J \operatorname{tr}(\dot{\mathbf{F}} \cdot \mathbf{F}^{-1}) = J \operatorname{tr} \mathbf{L} = J \operatorname{tr} \mathbf{D} \tag{2.10}$$

2.3 Balance Laws

For a material body $\mathcal{B}$, mass, momentum, moment of momentum and energy are conserved quantities. This is expressed in the balance equations of continuum mechanics. The *law of conservation of mass* reads in its local form:

$$\dot{\rho} + \rho \operatorname{div} \mathbf{v} = 0 \tag{2.11}$$

where ρ is the mass density of the body.

According to Cauchy, the state of stress of a material body $\mathcal{B}$ is completely determined by the Cauchy-stress tensor field $\mathbf{T}$. This second order tensor maps the outward unit normal $\mathbf{n}$ of a surface element dS in $\mathcal{B}$ to the traction vector $\mathbf{t}$ on dS:

$$\mathbf{t} = \mathbf{T} \cdot \mathbf{n} \tag{2.12}$$

The Cauchy-stress tensor field is determined by the *law of conservation of momentum*, which reads in its local form:

$$\rho \dot{\mathbf{v}} = \operatorname{div} \mathbf{T} + \rho \mathbf{b} \tag{2.13}$$

Here, $\mathbf{b}$ is the external body force field per unit mass.

For some materials (fluids), large deformations can be obtained without a notable change in the volume. This kind of behaviour is often idealised by assuming that the material is "incompressible". In case of such an incompressibility constraint, the hydrostatic part of the Cauchy-stress tensor is undetermined, which gives rise to a so-called *extra stress tensor* $\mathbf{T}_E$, of which only the deviatoric part is of importance:

$$\mathbf{T} = -p\mathbf{I} + \mathbf{T}_E \tag{2.14}$$

Here, the unknown quantity p is determined by the boundary conditions. The hydrostatic (thermodynamic) pressure $-p_0$ equals $-p + \frac{1}{3} \operatorname{tr} \mathbf{T}_E$ and, therefore, Eq. (2.14) can also be written as:

$$\mathbf{T} = -p_0 + \mathbf{T}_E^d \tag{2.15}$$

For ordinary continua the *law of conservation of moment of momentum* states that the Cauchy-stress tensor is symmetric:

$$\mathbf{T} = \mathbf{T}^T \tag{2.16}$$

In addition to the balance laws of mass, momentum and moment of momentum, the material body $\mathcal{B}$ must also obey the *first and second law of thermodynamics*. The first law of thermodynamics is the *law of conservation of (internal)*

energy, which states that the rate of internal energy per unit volume, $\dot{U}$, equals the heat, $\dot{Q}$, plus the power, $\dot{W}$, supplied to the material body.

$$\dot{U} = \dot{Q} + \dot{W} = \dot{Q} + \mathbf{T} : \mathbf{L} \tag{2.17}$$

Note that $\dot{Q}$ and $\dot{W}$ are inexact differentials, only their sum $\dot{U}$ is path independent.

The second law of thermodynamics states that the entropy production is always positive. Since, in this thesis, thermal effects are not considered directly, the first and second law are not of immediate concern. However, from the second law a dissipation rate may be defined as will be discussed in the next section on constitutive principles.

2.4 Constitutive Principles

2.4.1 Restrictions on Constitutive Equations

Constitutive equations are material specific relations necessary to close the set of equations which describe the behaviour of the material body $\mathcal{B}$. This thesis is concerned with *rheological* constitutive equations, which typically relate kinematic quantities to the six independent components of the Cauchy-stress tensor. Although these equations cannot be derived from any balance law, there are some general aspects of material behaviour which lead to widely accepted restrictions on the form of constitutive equations. The two most important thereof are the starting point of the famous *simple fluid theory* of Noll (1958): the principles of local action and material frame indifference.

The *principle of local action* states that the stress in a material point $\mathcal{P}$ is completely determined by the deformation history of that point. In a mathematical sense it states that the stress tensor in $\mathcal{P}$ is a *functional* of the history of the deformation gradient tensor in $\mathcal{P}$.

According to the *principle of material frame indifference*, also called the *principle of objectivity*, a constitutive equation must be invariant under a Galilei transformation. This means that the material behaviour must appear the same for two observers moving with different speed and/or undergoing a relative rotation $\mathbf{Q}(t)$ with respect to each other ($\mathbf{Q}(t)$ is orthogonal).

An objective quantity is one which is subdue to certain transformation rules dependent on the tensorial order: a scalar is always objective, a vector is objective if it transforms like $\mathbf{a}^* = \mathbf{Q}\cdot\mathbf{a}$ and a second order tensor is objective if it transforms like $\mathbf{A}^* = \mathbf{Q}\cdot\mathbf{A}\cdot\mathbf{Q}^T$. An invariant quantity is not affected by a rigid body rotation $\mathbf{Q}$. A scalar is always invariant. As an example, the left Cauchy-Green strain tensor $\mathbf{B}$ and the Cauchy-stress tensor $\mathbf{T}$ are objective quantities and the right Cauchy-Green strain tensor is an invariant quantity. The velocity gradient $\mathbf{L}$ transforms like: $\mathbf{L}^* = \dot{\mathbf{Q}}\cdot\mathbf{Q}^T + \mathbf{Q}\cdot\mathbf{L}\cdot\mathbf{Q}^T$ and is, therefore, neither objective nor

invariant. An easy way to ensure objectivity of a constitutive equation is to relate only objective quantities or invariant quantities.

Of particular importance is that the material derivative of an objective quantity is neither objective nor invariant. Therefore, objective rates have been defined, of which the most important are the *Truesdell* (or *upper-convected*) and the *Jaumann* (or *corotational*) time derivative. The Truesdell time derivative $\overset{\nabla}{\mathbf{A}}$ of an objective tensor $\mathbf{A}$, is the derivative with respect to a co-deforming frame-of reference (Astarita and Marrucci, 1974):

$$\overset{\nabla}{\mathbf{A}} = \dot{\mathbf{A}} - \mathbf{L} \cdot \mathbf{A} - \mathbf{A} \cdot \mathbf{L}^T \tag{2.18}$$

The Jaumann time derivative $\mathring{\mathbf{A}}$ is the derivative with respect to a co-rotating frame-of reference:

$$\mathring{\mathbf{A}} = \dot{\mathbf{A}} - \mathbf{W} \cdot \mathbf{A} - \mathbf{A} \cdot \mathbf{W}^T \tag{2.19}$$

In principle, an infinite amount of objective rates can be defined.

2.4.2 Matrix Representation of Constitutive Equations

In the simple fluid concept it is assumed that constitutive variables like the stress tensor are fully determined by the history of deformation (axiom of determinism). Using the concept of fading memory, the history dependence of the material is then described by functional relations (Coleman and Noll, 1963). However, using this framework it is difficult to incorporate information about the micro-structure in the constitutive equation. Therefore, in recent polymer rheology as well as plasticity literature it is recognized advantageous to formulate constitutive equations using state variables e.g., the natural reference state concept of Besseling and van der Giessen (1994) in the field of plasticity, the Poisson-bracket approach of Beris and Edwards (1990) and the matrix model by Jongschaap *et al.* (1994) in polymer rheology. Here, the latter will be used to derive a constitutive equation for the rate-dependent yield behaviour of polymer glasses without strain hardening. To this extent we will first briefly introduce the matrix model, for a more elaborate discussion we refer to the original papers of Jongschaap (Jongschaap, 1990; Jongschaap *et al.*, 1994).

The notion of *state variables* plays a central role in the matrix model of Jongschaap. The current state of the material body $\mathcal{B}$ is completely determined by the momentaneous values of the external rate variables, $[\mathbf{F}, \dot{\mathbf{F}}, \ddot{\mathbf{F}}, \ldots, \dot{Q}]$. Although the body as a whole can be in a non-equilibrium state, it is assumed that there are subsystems which are in thermodynamic equilibrium. The internal (thermodynamic) state of these subsystems is described in the sense of equilibrium thermodynamics by the current value(s) of a (set of) state variable(s) $[X_1, X_2, \ldots, X_n]$. These may be scalar quantities like free volume, higher order tensorial quantities

like the stored elastic strain, or even distribution functions. Since state variables completely specify the state of the material body in the sense of *equilibrium* thermodynamics, it must in principle be possible to fix or control their value for an arbitrary time span by adjusting the external rate variables. Moreover, the state variables must appear in Gibbs' fundamental equation, since this equation completely describes the thermodynamic equilibrium state of the material body:

$$U = U(S, X_1, X_2, \ldots, X_n) \tag{2.20}$$

with the entropy per unit volume S. The rate of internal energy is obtained by differentiating Eq. (2.20) with respect to time:

$$\dot{U} = T\dot{S} + F_1\dot{X}_1 + F_2\dot{X}_2 + \cdots + F_n\dot{X}_n \tag{2.21}$$

Here, T is the absolute temperature $T = \partial U/\partial S$ and F_i are the associated forces defined as:

$$F_i = \frac{\partial U}{\partial X_i} = F_i(S, X_1, X_2, \ldots, X_n) \tag{2.22}$$

Note that all time derivatives in Eq. (2.21) are total differentials (path independent) in contrast to Eq. (2.17), which was derived from a conservation law. The sum $F_i\dot{X}_i$ is the rate of reversible storage of energy per unit volume.

Since entropy is not an easy quantity to control in practice, it can be eliminated from the list of independent variables by introducing the *Helmholtz free energy* $A = U - TS$:

$$\dot{A} = -S\dot{T} + F_1\dot{X}_1 + F_2\dot{X}_2 + \cdots + F_n\dot{X}_n \tag{2.23}$$

From this equation it can be seen that in an isothermal process, the rate of free energy $\dot{A}$ equals the rate of reversible storage of energy (Astarita and Marrucci, 1974).

The rate of entropy production Σ is defined as: $\Sigma = \dot{S} - \dot{Q}/T$ and can be obtained by eliminating $\dot{U}$ from Eqs. (2.17) and Eq. (2.21):

$$\Sigma = \frac{1}{T}\left(\mathbf{T} : \mathbf{L} - F_i\dot{X}_i\right) = \frac{\Delta}{T} \tag{2.24}$$

The quantity between the brackets is the difference between the total external power supply to the material body and the rate of reversible energy storage in the body and is denoted as the *rate of dissipation* Δ. By the second law of thermodynamics the absolute temperature is always positive and the rate of entropy production is greater than or equal to zero. Therefore, the rate of dissipation is always greater than or equal to zero.

Without loss of generality, we will for the moment assume that the internal variable which determines the internal state of the body is a second-order tensor $\mathbf{S}$

(sometimes called a "structure tensor") with an associated thermodynamic force $\mathbf{M} = \partial A/\partial \mathbf{S}$. In that case, for isothermal conditions, combining Eqs. (2.23) and (2.24), the rate of dissipation can be written as:

$$\Delta = \mathbf{T} : \mathbf{L} - \dot{A} = \mathbf{T} : \mathbf{L} - \frac{\partial A}{\partial \mathbf{S}} : \dot{\mathbf{S}} = \mathbf{T} : \mathbf{L} - \mathbf{M} : \dot{\mathbf{S}} \geq 0 \tag{2.25}$$

An important concept in the matrix model of Jongschaap is that of *macroscopic time reversal*, where it is examined to what extent the rate of the state variables $\dot{\mathbf{S}}$ and the stress tensor $\mathbf{T}$ are affected by a reversal of the macroscopic external velocity gradient $\mathbf{L}$. Here it should be noted that any function $f(\mathbf{L})$ can be decomposed in an even part f^+ and an odd part f^- according to:

$$f(\mathbf{L}) = f^+(\mathbf{L}) + f^-(\mathbf{L}) = \frac{1}{2}(f(\mathbf{L}) + f(-\mathbf{L})) + \frac{1}{2}(f(\mathbf{L}) - f(-\mathbf{L})) \tag{2.26}$$

By definition, the parity of the velocity gradient $\mathbf{L}$ itself is odd. Recognizing that state variables are even and (due to the second law of thermodynamics) the rate of dissipation is also even, it is possible to decompose Eq. (2.25) in an even part:

$$\Delta = \Delta^+ = \mathbf{T}^- : \mathbf{L} - \mathbf{M} : \dot{\mathbf{S}}^+ \tag{2.27}$$

and an odd part:

$$0 = \mathbf{T}^+ : \mathbf{L} - \mathbf{M} : \dot{\mathbf{S}}^- \tag{2.28}$$

Without loss of generality, the reversible part of $\dot{\mathbf{S}}$, $\dot{\mathbf{S}}^-$ can be written as:

$$\dot{\mathbf{S}}^- = \underline{\mathbf{\Lambda}} : \mathbf{L} \tag{2.29}$$

where the tensor $\underline{\mathbf{\Lambda}} = \underline{\mathbf{\Lambda}}(\mathbf{L}, \mathbf{M})$ is of rank four and even with respect to $\mathbf{L}$. A very general expression for the reversible part of the stress tensor $\mathbf{T}^R = \mathbf{T}^+$ is obtained by substitution of Eq. (2.29) in Eq. (2.28):

$$\mathbf{T}^+ = \mathbf{T}^R = \mathbf{M} : \underline{\mathbf{\Lambda}} = \underline{\mathbf{\Lambda}}^T : \mathbf{M} \tag{2.30}$$

A similar relation was first discussed by Grmela (1985) in his Poisson-bracket formulation of material behaviour.

To complete the matrix model, the fourth order tensors $\underline{\boldsymbol{\eta}}$ and $\underline{\boldsymbol{\beta}}$ are introduced to describe the dissipative parts of the stress tensor $\mathbf{T}^D$ and the time derivative of the state variable $\dot{\mathbf{S}}^D$:

$$\mathbf{T}^D = \mathbf{T}^- = \underline{\boldsymbol{\eta}}(\mathbf{M}, \mathbf{L}) : \mathbf{L} \quad \text{and} \quad \dot{\mathbf{S}}^D = \dot{\mathbf{S}}^+ = -\underline{\boldsymbol{\beta}}(\mathbf{M}, \mathbf{L}) : \mathbf{M} \tag{2.31}$$

The tensors $\underline{\boldsymbol{\eta}}$ and $\underline{\boldsymbol{\beta}}$ are (semi-) positive definite and even with respect to $\mathbf{L}$. Equations (2.29), (2.30) and (2.31) can be written in matrix notation, which concludes the generic matrix representation of constitutive equations:

$$\begin{bmatrix} \mathbf{T} \\ \dot{\mathbf{S}} \end{bmatrix} = \begin{bmatrix} \underline{\boldsymbol{\eta}} & -\underline{\mathbf{\Lambda}}^T \\ \underline{\mathbf{\Lambda}} & \underline{\boldsymbol{\beta}} \end{bmatrix} : \begin{bmatrix} \mathbf{L} \\ -\mathbf{M} \end{bmatrix} \tag{2.32}$$

2.5 Viscoelastic Behaviour

The matrix model of Jongschaap will now be applied to derive a general "single mode" viscoelastic relationship. To illustrate the method, the limiting case of complete (isotropic) elastic behaviour will be considered first.

2.5.1 Elastic Behaviour

In case of isotropic elastic behaviour it is assumed that the state variable determining the free energy is the left Cauchy-Green strain tensor $\mathbf{B}$. Because of isotropy, the free energy A can be expressed in the invariants of $\mathbf{B}$: $A = A(I_B, II_B, III_B)$. The thermodynamic force consequently equals:

$$\begin{aligned} \mathbf{M} = \frac{dA}{d\mathbf{B}} &= \frac{\partial A}{\partial I_B}\frac{dI_B}{d\mathbf{B}} + \frac{\partial A}{\partial II_B}\frac{dII_B}{d\mathbf{B}} + \frac{\partial A}{\partial III_B}\frac{dIII_B}{d\mathbf{B}} \\ &= \alpha_1\mathbf{I} + \alpha_2(\mathrm{tr}(\mathbf{B})\mathbf{I} - \mathbf{B}) + \alpha_3 \det(\mathbf{B})\mathbf{B}^{-1} \end{aligned} \tag{2.33}$$

with α_i the derivatives of the free energy (per unit volume) with respect to the invariants of $\mathbf{B}$.

From kinematics it follows that the Truesdell (upper convected) derivative $\overset{\triangledown}{\mathbf{B}}$ of $\mathbf{B}$ equals the null tensor $\mathbf{O}$:

$$\overset{\triangledown}{\mathbf{B}} = \dot{\mathbf{B}} - \mathbf{L}\cdot\mathbf{B} - \mathbf{B}\cdot\mathbf{L}^T = \mathbf{O} \tag{2.34}$$

This leads to the evolution equation for $\dot{\mathbf{B}}$:

$$\dot{\mathbf{B}} = \mathbf{L}\cdot\mathbf{B} + \mathbf{B}\cdot\mathbf{L}^T = \underline{\underline{\Lambda}} : \mathbf{L} \quad \text{with} \quad \Lambda_{ijkl} = \delta_{ik}B_{mj} + B_{im}\delta_{jk} \tag{2.35}$$

Since there is no dissipation, $\underline{\eta}$ and $\underline{\beta}$ vanish and with Eqs. (2.32), (2.33) and (2.35) the constitutive equation for isotropic elastic behaviour reduces to:

$$\left[\begin{array}{rcl} \mathbf{T} & = & \mathbf{M} : \underline{\underline{\Lambda}} = 2\left(\alpha_3 \det(\mathbf{B})\mathbf{I} + (\alpha_1 + \alpha_2\,\mathrm{tr}\,\mathbf{B})\mathbf{B} - \alpha_2\mathbf{B}\cdot\mathbf{B}\right) \\ \overset{\triangledown}{\mathbf{B}} & = & \mathbf{0} \end{array}\right. \tag{2.36}$$

which is the well known expression for Green elastic behaviour (Hunter, 1983).

The objective of this Chapter is to develop a three-dimensional expression for viscoelastic behaviour, where the volume response is purely elastic. Therefore, as a second example, the case of purely elastic behaviour will be considered where the volume deformation and the change of shape are uncoupled.

Because of the independent volume deformation it is assumed that the free energy is determined by two state variables, which can be derived from $\mathbf{B}$: the volume deformation factor $J = \det\mathbf{F} = \sqrt{\det\mathbf{B}}$ (for convenience $J\mathbf{I}$ will be

used, instead of J) and the left Cauchy-Green strain tensor at constant volume $\bar{\mathbf{B}} = J^{-2/3}\mathbf{B}$. In case of isotropic behaviour, the free energy will be a function of the invariants of $\bar{\mathbf{B}}$ and of J:

$$A = A(J, I_{\bar{B}}, II_{\bar{B}}) \quad (III_{\bar{B}} = \det \bar{\mathbf{B}} = 1) \tag{2.37}$$

Two conjugated thermodynamic forces can be distinguished now, one related to the volume deformation (N) and one related to the change of shape (M):

$$\mathbf{N} = \frac{\partial A}{\partial J\mathbf{I}} = \frac{1}{3}\left(\frac{\partial A}{\partial J}\right)\mathbf{I} \tag{2.38a}$$

$$\tilde{\mathbf{M}} = \frac{\partial A}{\partial \tilde{\mathbf{B}}} = \tilde{\alpha}_1\mathbf{I} + \tilde{\alpha}_2(\mathrm{tr}(\tilde{\mathbf{B}})\mathbf{I} - \tilde{\mathbf{B}}^T) \tag{2.38b}$$

From kinematics it follows that:

$$\dot{J}\mathbf{I} = J\,\mathrm{tr}(\mathbf{D})\mathbf{I} = J\mathbf{II} : \mathbf{L} \tag{2.39a}$$

$$\dot{\tilde{\mathbf{B}}} = \mathbf{L}^d \cdot \tilde{\mathbf{B}} + \tilde{\mathbf{B}} \cdot \left(\mathbf{L}^d\right)^T = \left(\underline{\mathbf{\Lambda}} - \frac{2}{3}\bar{\mathbf{B}}\mathbf{I}\right) : \mathbf{L} = \bar{\underline{\mathbf{\Lambda}}} : \mathbf{L} \tag{2.39b}$$

where the fourth-order tensor $\mathbf{II}$ is the dyadic product of the second-order unit tensor $\mathbf{I}$ with itself, and $\bar{\mathbf{B}}\mathbf{I}$ is the dyadic product of $\bar{\mathbf{B}}$ with $\mathbf{I}$.

The constitutive equation for elastic behaviour now becomes:

$$\left\{\begin{array}{l} \mathbf{T} = \mathbf{N} : J\underline{\mathbf{I}} + \tilde{\mathbf{M}} : \tilde{\underline{\mathbf{\Lambda}}} = \mathbf{T}^h + \mathbf{T}^d = \\ \qquad J\left(\dfrac{\partial A}{\partial J}\right)\mathbf{I} + 2\tilde{\alpha}_1\bar{\mathbf{B}}^d + 2\tilde{\alpha}_2\,\mathrm{tr}(\tilde{\mathbf{B}})\tilde{\mathbf{B}}^d + 2\tilde{\alpha}_2(\tilde{\mathbf{B}}\cdot\tilde{\mathbf{B}})^d \\ \dot{\tilde{\mathbf{B}}} = \mathbf{L}^d \cdot \tilde{\mathbf{B}} + \tilde{\mathbf{B}} \cdot \left(\mathbf{L}^d\right)^T \\ \dot{J}\mathbf{I} = J\,\mathrm{tr}(\mathbf{D})\mathbf{I} \end{array}\right. \tag{2.40}$$

Following Simo *et al.* (1985) and Rubin (1994), a formal separation of the volume effects from the shape deformation can now be achieved by assuming that there are two uncoupled contributions to the free energy, a "volumetric" part A^v and an "isochoric" (constant volume) part A^i:

$$A = A(J, I_{\bar{B}}, II_{\bar{B}}) = A^v(J) + A^i(I_{\bar{B}}, II_{\bar{B}}) \tag{2.41}$$

which results in:

$$\frac{\partial A}{\partial J} = \frac{\partial A^v}{\partial J}, \quad \tilde{\alpha}_1 = \tilde{\alpha}_1(\bar{\mathbf{B}}), \quad \tilde{\alpha}_2 = \tilde{\alpha}_2(\tilde{\mathbf{B}}) \tag{2.42}$$

As might be expected, the hydrostatic stress $\mathbf{T}^h$ is determined solely by the volume deformation, whereas the deviatoric stress $\mathbf{T}^d$ is governed by $\bar{\mathbf{B}}$.

2.5.2 Decomposition of the Rate-of Strain Tensor

In order to develop a basic viscoelastic constitutive equation for glassy polymers, the expression for elastic behaviour with a separated volume response, Eq. (2.40), will be used as a starting point. First it is noted that the evolution equation for $\bar{\mathbf{B}}$ may also be written as:

$$\overset{\circ}{\bar{\mathbf{B}}} = \dot{\bar{\mathbf{B}}} - \mathbf{W} \cdot \bar{\mathbf{B}} - \bar{\mathbf{B}} \cdot \mathbf{W}^T = \mathbf{D}^d \cdot \bar{\mathbf{B}} + \bar{\mathbf{B}} \cdot \mathbf{D}^d \tag{2.43}$$

where $\overset{\circ}{\bar{\mathbf{B}}}$ is the Jaumann rate of $\bar{\mathbf{B}}$.

In case of plastic deformation it is now assumed that the accumulation of elastic strain (at constant volume) is reduced because of the existence of a (deviatoric) plastic strain rate $\mathbf{D}_p$ (Leonov, 1976). Therefore, the evolution equation for $\bar{\mathbf{B}}$ is modified to:

$$\overset{\circ}{\bar{\mathbf{B}}}_e = (\mathbf{D}^d - \mathbf{D}_p) \cdot \bar{\mathbf{B}}_e + \bar{\mathbf{B}}_e \cdot (\mathbf{D}^d - \mathbf{D}_p) \tag{2.44}$$

Hence, there is no direct coupling anymore between the state variable $\bar{\mathbf{B}}_e$ and the external rate variables, as in the case of elastic deformation in the previous section. Therefore, kinematic arguments alone are not sufficient to solve the evolution equation for $\bar{\mathbf{B}}_e$ and a constitutive description of the plastic rate-of strain tensor $\mathbf{D}_p$ must be provided.

For materials in general (Krausz and Eyring, 1975) and polymers in specific (Ward, 1990), it is known that the plastic shear rate is often well modelled by using an Eyring-flow process. In the Eyring flow process it is assumed that the free energy barrier for molecular jump events becomes asymmetric upon the application of a (shear) stress.

The Eyring flow model can be depicted one-dimensionally as:

$$\dot{\gamma}_p = \frac{1}{\mathrm{A}} \sinh\left(\frac{\tau}{\tau_0}\right) \tag{2.45}$$

Here, τ is the shear stress and $\dot{\gamma}_p$ is the plastic rate of shear. The material constants (at constant temperature) A and τ_0 are related to the activation energy, ΔH, and the activation volume, V^*, respectively:

$$\begin{aligned} \mathrm{A} &= \mathrm{A}_0 \exp\left(\frac{\Delta H}{RT}\right) \\ \tau_0 &= \frac{RT}{V^*} \end{aligned} \tag{2.46}$$

with A_0 a pre-exponentional factor involving the fundamental vibration frequency, R the universal gas constant and T the absolute temperature.

By inversion of the Eyring equation, Eq. (2.45), a viscosity can be defined:

$$\dot{\gamma}_p = \frac{\tau}{\left(\frac{\tau_0 \operatorname{arcsinh}(A\dot{\gamma}_p)}{\dot{\gamma}_p}\right)} = \frac{\tau}{\eta(\dot{\gamma}_p)} \tag{2.47}$$

The Eyring flow equation, (2.47), is a special case of a one-dimensional non-Newtonian fluid relationship, which can be generalized into a three-dimensional form in a standard way (Bird *et al.*, 1987, Chapter 4):

$$\begin{aligned} \mathbf{D}_p &= \frac{\frac{1}{2}\mathbf{T}^d}{\tau_0 \operatorname{arcsinh}(A\dot{\gamma}_{eq})/\dot{\gamma}_{eq}} = \frac{\frac{1}{2}\mathbf{T}^d}{\eta(\dot{\gamma}_{eq})} \\ \dot{\gamma}_{eq} &= \sqrt{2\,\mathrm{tr}(\mathbf{D}_p \cdot \mathbf{D}_p)} \end{aligned} \tag{2.48}$$

The equivalent strain rate, $\dot{\gamma}_{eq}$, is defined such, that in case of a shear flow it reduces to the plastic shear rate $\dot{\gamma}_p$ (and than Eq. (2.48) reduces to Eq. (2.47)). Note that the plastic rate-of-strain tensor is parallel to the deviatoric Cauchy stress tensor, since plastic flow is assumed to be incompressible ($\mathrm{tr}\,\mathbf{D}_p = 0$). Complementary to the equivalent strain rate, an equivalent stress (τ_{eq}) can be defined, satisfying:

$$\dot{\gamma}_{eq} = \frac{1}{A}\sinh\left(\frac{\tau_{eq}}{\tau_0}\right) \quad , \quad \tau_{eq} = \sqrt{\frac{1}{2}\,\mathrm{tr}(\mathbf{T}^d \cdot \mathbf{T}^d)} \tag{2.49}$$

Substitution of Eq. (2.49) into Eq. (2.48), results in a three-dimensional Eyring equation, relating the plastic rate-of-strain tensor to the deviatoric part of the Cauchy-stress tensor:

$$\mathbf{D}_p = \frac{\mathbf{T}^d}{2\eta(\tau_{eq})} \quad , \quad \eta(\tau_{eq}) = A\tau_0 \frac{\left(\frac{\tau_{eq}}{\tau_0}\right)}{\sinh\left(\frac{\tau_{eq}}{\tau_0}\right)} = \eta_0 a_\sigma(\tau_{eq}) \tag{2.50}$$

with the so called *shift function* a_σ. The Eyring equation can be augmented in a straightforward way, to allow for pressure dependence and intrinsic softening effects, but this will not be considered here.

On a fitting level, the Eyring equation is almost indistinguishable from the Argon theory (Argon, 1973), used in the "BPA-model" (Boyce *et al.*, 1988), and the "full chain model" (Wu and van der Giessen, 1993), but conceptually there are differences (Ward, 1990). In contrast to the Argon theory, which regards yielding as a nucleation-controlled process, the Eyring approach implies that deformation mechanisms are essentially always present and that stress merely changes the rate of deformation. This is clearly expressed by the functional dependence of the Eyring viscosity on stress (Eq. (2.50). There is a linear region at low (equivalent)

stress ($\tau_{eq} \ll \tau_0$), where the viscosity is equal to the *zero-shear viscosity* $\eta_0 = A\tau_0$ and all the non-linear stress effects are incorporated into the shift function a_σ. Thus, according to the Eyring equation, deformation processes at very low stresses, as observed in linear viscoelastic measurements, are accelerated by stress. This point of view will be explored in more detail in Chapter 3.

A constitutive formulation for viscoelastic behaviour with an elastic volume response is now obtained by combining Eq. (2.40) for elastic behaviour with the new evolution equation for $\bar{\mathbf{B}}_e$, Eqs. (2.44) and Eq. (2.50), leading to:

$$\begin{cases} \mathbf{T} = J\left(\dfrac{dA}{dJ}\right)\mathbf{I} + 2\tilde{\alpha}_1\bar{\mathbf{B}}_e^{\,d} + 2\tilde{\alpha}_2\,\mathrm{tr}(\bar{\mathbf{B}}_e)\bar{\mathbf{B}}_e^{\,d} + 2\tilde{\alpha}_2(\bar{\mathbf{B}}_e\cdot\bar{\mathbf{B}}_e)^d \\ \overset{\circ}{\bar{\mathbf{B}}}_e = (\mathbf{D}^d - \mathbf{D}_p)\cdot\bar{\mathbf{B}}_e + \bar{\mathbf{B}}_e\cdot(\mathbf{D}^d - \mathbf{D}_p) \\ \dot{J}\mathbf{I} = J\,\mathrm{tr}(\mathbf{D})\mathbf{I} \\ \mathbf{D}_p = \dfrac{\mathbf{T}^d}{2\eta(\tau_{eq})} \end{cases} \tag{2.51}$$

It is assumed that the volume changes remain small ($J \approx 1$). According to Hooke's law, the hydrostatic-stress term $\mathbf{T}^h = J(dA/dJ)\mathbf{I}$ in Eq. (2.51) can then be written as: $\mathbf{T}^h = K(J-1)\mathbf{I}$, where K is the bulk modulus. Choosing $\tilde{\alpha}_2 = 0$ (only a linear dependence of $\mathbf{T}^d$ on $\bar{\mathbf{B}}_e$) and identifying $2\tilde{\alpha}_1$ to the shear modulus G, the constitutive formulation, Eq. (2.51), reduces to:

$$\mathbf{T} = K(J-1)\mathbf{I} + G\bar{\mathbf{B}}_e^{\,d} \tag{2.52a}$$

$$\overset{\circ}{\bar{\mathbf{B}}}_e = (\mathbf{D}^d - \mathbf{D}_p)\cdot\bar{\mathbf{B}}_e + \bar{\mathbf{B}}_e\cdot(\mathbf{D}^d - \mathbf{D}_p) \tag{2.52b}$$

$$\dot{J}\mathbf{I} = J\,\mathrm{tr}(\mathbf{D})\mathbf{I} \tag{2.52c}$$

$$\mathbf{D}_p = \frac{\mathbf{T}^d}{2\eta(\tau_{eq})} \tag{2.52d}$$

$$\eta(\tau_{eq}) = A\tau_0\frac{\left(\dfrac{\tau_{eq}}{\tau_0}\right)}{\sinh\left(\dfrac{\tau_{eq}}{\tau_0}\right)} \tag{2.52e}$$

Although derived in a different way, this model is very similar to compressible Leonov models as discussed by Rubin (1987, 1994) and Baaijens (1991).

2.5.3 Results

Some features of the "compressible Leonov model", which was derived in the previous section, are demonstrated in this section, using polycarbonate as a model polymer.

Material Parameters

The material parameters required by the compressible Leonov model are the linear elastic constants K and G from Hooke's law and two non-linearity parameters from the Eyring viscosity function: A and τ_0. The elastic constants were obtained by measuring the Young's modulus E and the Poisson constant ν in a tensile test, at low stresses and strains, which resulted in $E = 2335$ [MPa] and $\nu = 0.41$ [-]. The shear modulus is related to E and ν by Hooke's law: $G = E/2(1+\nu) = 830$ [MPa].

At the yield point, the plastic strain rate is approximately equal to the total strain rate. Therefore, according to the Leonov model, at the yield point, a material behaves as a generalized Newtonian fluid.

$$\mathbf{T} = -p\mathbf{I} + 2\eta\mathbf{D}_p = -p\mathbf{I} + 2\eta\mathbf{D} \tag{2.53}$$

Because of the incompressibility constraint, the hydrostatic stress p depends only on the boundary conditions. The yield point is defined by the moment the stress remains constant at a constant applied strain rate and is, therefore, completely determined by the viscosity function (Eq. (2.48)):

$$\eta = \frac{\tau_0}{\dot{\gamma}_{eq}} \operatorname{arcsinh}(\mathrm{A}\dot{\gamma}_{eq}) \ , \quad \dot{\gamma}_{eq} = \sqrt{2(\mathbf{D}_p \cdot \mathbf{D}_p)} \tag{2.54}$$

If the yield point σ_y is measured in a tensile experiment at a (Henky) strain rate $\dot{\epsilon}$ in the z-direction, we have from Eq. (2.53):

$$\begin{bmatrix} 0 & 0 & 0 \\ 0 & 0 & 0 \\ 0 & 0 & \sigma_y \end{bmatrix} = \begin{bmatrix} -p & 0 & 0 \\ 0 & -p & 0 \\ 0 & 0 & -p \end{bmatrix} + 2\eta(\dot{\gamma}_{eq}) \begin{bmatrix} -\frac{1}{2}\dot{\epsilon} & 0 & 0 \\ 0 & -\frac{1}{2}\dot{\epsilon} & 0 \\ 0 & 0 & \dot{\epsilon} \end{bmatrix} \tag{2.55}$$

From this equation it can be seen that the equivalent plastic strain rate becomes $\dot{\gamma}_{eq} = 2\dot{\epsilon}^2$. The yield stress as a function of strain rate, therefore, equals:

$$\sigma_y = \sigma_{zz} - \sigma_{xx} = \tau_0\sqrt{3}\operatorname{arcsinh}(\mathrm{A}\dot{\epsilon}\sqrt{3}) \tag{2.56}$$

If the argument of the hyperbolic sine function is large, it can be approximated by an exponential function and Eq. (2.56) may be transformed to:

$$\sigma_y = \tau_0\sqrt{3}\ln(2\mathrm{A}\sqrt{3}) + \tau_0\sqrt{3}\ln\dot{\epsilon} \tag{2.57}$$

From the last equation it follows that the Eyring parameters from the Leonov model can be determined by linear regression, plotting the yield stress versus the logarithm of the strain rate. This is called an *Eyring plot*. Note that Eq. (2.57) depends on the mode of deformation, for example, in shear, the generalized Newtonian flow equation, Eq. (2.53), relates the shear-yield stress τ_y to the applied shear rate $\dot{\gamma}$:

$$\tau_y = \tau_0\ln(2\mathrm{A}) + \tau_0\ln\dot{\gamma} \tag{2.58}$$

In a planar extension test, the generalized Newtonian flow rule reduces to:

$$\sigma_y^{pl} = 2\tau_0 \ln(4A) + 2\tau_0 \ln \dot{\varepsilon}^{pl} \tag{2.59}$$

where σ_y^{pl} is the yield stress in planar extension at a planar extension rate $\dot{\varepsilon}^{pl}$.

Eyring plots for polycarbonate in various deformation modes are depicted in Figure (2.1). The solid lines in this figure are the best fit of a single set of Eyring parameters: $\tau_0 = 0.9$ [MPa] and $A = 1.75 \cdot 10^{20}$ [s]. From this figure it is clear

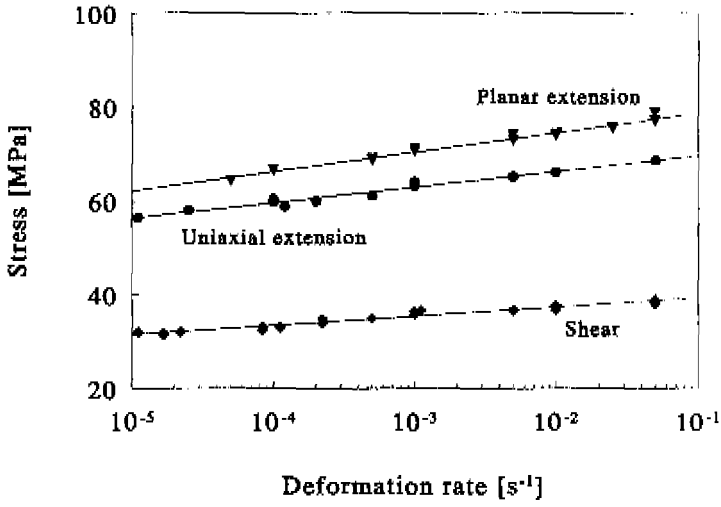

Figure 2.1 *Eyring plot for polycarbonate constructed from yield points in various deformation modes. The solid lines are a best fit using a single set of Eyring parameters.*

that at the yield point polycarbonate behaves like a generalized Newtonian fluid.

Having determined all the material constants, it is now possible to calculate any response from the compressible Leonov model. First, a standard uniaxial tensile test will be considered, in which a tensile bar is elongated in the x direction at two different rates-of deformation. The tensile bar is stress free in the radial and tangential direction (see Figure 2.2a). As second deformation mode, a plane-stress shear test, also called "laboratory shear", is chosen. The upset of a plane-stress shear test is shown in Figure 2.2b, the shear strain $\gamma_{xy} = \tan(\phi)$.

The response of the Leonov model, Eq. (2.52), for these two deformation modes, is given in Figure 2.3. In this figure it can be seen that the Leonov model predicts a sharp instead of a gradual transition from elastic to plastic behaviour, which is very similar to that of an elastic-perfectly plastic material with a rate-dependent Von Mises yield criterion. This similarity originates from

the proportionality of the equivalent stress τ_{eq} with the Von Mises equivalent stress τ_{vm} ($\tau_{eq} = \tau_{vm} 1/3\sqrt{3}$).

2.5.4 Comparison with Other Models

A common way to describe viscoelastic behaviour are the so-called *generalized Maxwell models*, often depicted as a number of springs and dashpots in series. In a Maxwell model it is assumed that the velocity gradient is decomposed in an elastic and a plastic part:

$$\mathbf{L} = \mathbf{L}_e + \mathbf{L}_p = (\mathbf{D}_e + \mathbf{W}_e) + (\mathbf{D}_p + \mathbf{W}_p) \tag{2.60}$$

For the kinematic interpretation of $\mathbf{L}_e$ and $\mathbf{L}_p$, usually a so-called unloaded state or "natural reference state" is introduced (Besseling and van der Giessen, 1994).

In case of isotropic materials, the orientation of the unloaded state is irrelevant and the plastic spin $\mathbf{W}_p$ is set equal to the null tensor. Furthermore, it is an experimental fact that, to a good approximation, polymers, like most other materials, show negligible volume deformation during plastic flow, i.e. $\mathrm{tr}\,\mathbf{D}_p = 0$. Therefore, the (deviatoric) plastic rate-of-strain tensor $\mathbf{D}_p$ is assumed to be parallel to the deviatoric Cauchy-stress tensor:

$$\mathbf{T}^d = 2\eta(I_T, \tau_{eq})\mathbf{D}_p \tag{2.61}$$

This equation reflects that the viscosity may be pressure dependent although the volume response is purely elastic.

The elastic part of the deformation is usually modelled by a rate formulation of Hooke's law for isotropic materials. This results in an isotropic relationship between an objective time derivative of the Cauchy-stress tensor and the elastic rate-of-strain tensor:

$$\overset{\diamond}{\mathbf{T}} = \lambda\,\mathrm{tr}(\mathbf{D}_e)\mathbf{I} + 2\mu\mathbf{D}_e = \underline{\mathcal{L}}^e : \mathbf{D}_e \tag{2.62}$$

Here, $\diamond$ denotes an objective rate, λ and μ are the Lamé constants and $\underline{\mathcal{L}}^e$ is a tensor of rank four.

Combining Eqs. (2.60), (2.61) and (2.62), leads to a standard viscoelastic rate equation:

$$\begin{cases} \overset{\diamond}{\mathbf{T}} = \underline{\mathcal{L}}^e : (\mathbf{D} - \mathbf{D}_p) \\ \mathbf{D}_p = \dfrac{\mathbf{T}^d}{2\eta(I_T, \tau_{eq})} \end{cases} \tag{2.63}$$

The subject of objective rates is a controversial one in continuum mechanics. By far the most common choice in plasticity theory is the Jaumann rate or corotational derivative, which is the time derivative with respect to a co-rotating

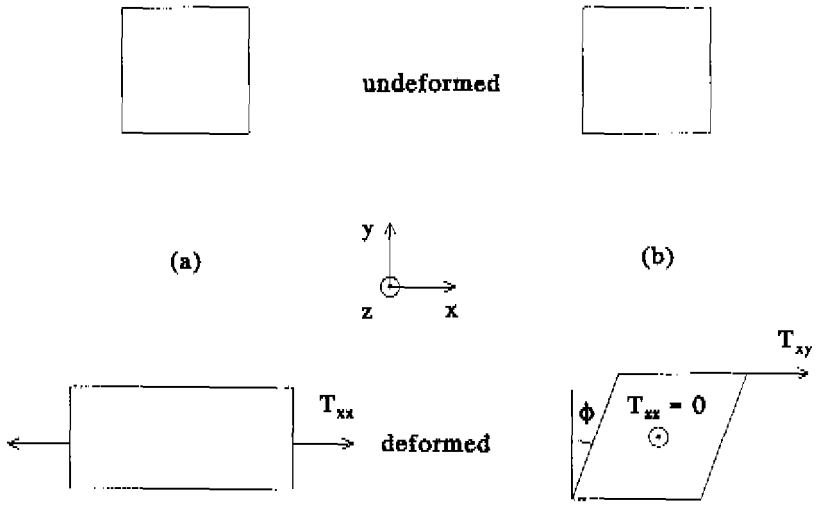

Figure 2.2 *Schematic drawing of (a) the uniaxial tensile test and (b) the plane-stress shear test, the shear strain* $\gamma = \tan(\phi)$.

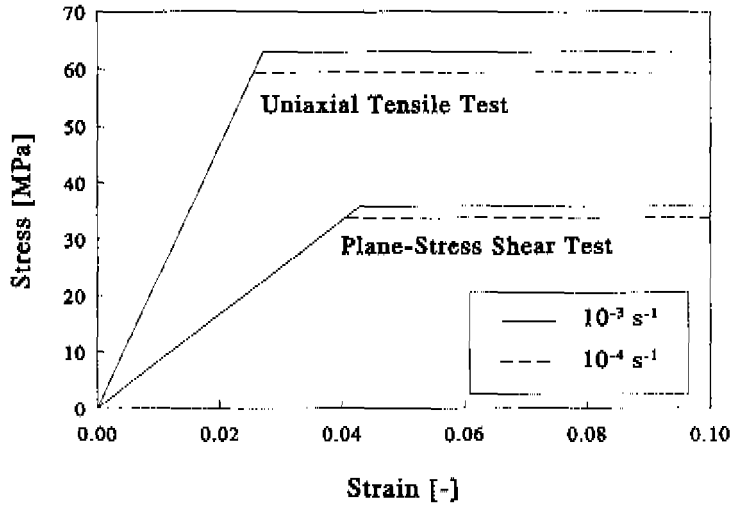

Figure 2.3 *Calculated response from the Leonov model for polycarbonate in uniaxial-tensile and plane-stress shear deformation, at two strain rates*

reference frame (Neale, 1981). Applying the Jaumann derivative in Eq. (2.63) results in the so called *corotational Maxwell model*:

$$\frac{\eta(I_T,\tau_{eq})}{G}\mathring{\mathbf{T}} + \mathbf{T}^d = 2\eta(I_T,\tau_{eq})\mathbf{D} + \lambda\left(\frac{\eta(I_T,\tau_{eq})}{G}\right)\mathrm{tr}(\mathbf{D}) \tag{2.64}$$

Another well known rate is the Truesdell or upper-convected time derivative. As already mentioned above, this is the time derivative with respect to a co-deforming reference frame (Bird *et al.*, 1987, Chapter 9). Using the Truesdell derivative in Eq. (2.63) results in what will be denoted as the "Truesdell-rate model":

$$\frac{\eta(I_T,\tau_{eq})}{G}\overset{\triangledown}{\mathbf{T}} + \mathbf{T}^d = 2\eta(I_T,\tau_{eq})\mathbf{D} + \lambda\left(\frac{\eta(I_T,\tau_{eq})}{G}\right)\mathrm{tr}(\mathbf{D}) \tag{2.65}$$

It can be shown that integration of the Truesdell-rate formulation of Hooke's law results in correct hyperelastic behaviour, whereas integration of the Jaumann rate results in a hypoelastic law (van Wijngaarden, 1988; Sansour and Bednarczyk, 1993) (in contrast to a hypoelastic relation, a hyperelastic law is a constitutive equation for elastic behaviour, which can be derived from a strain-energy potential). Therefore, if large elastic deformations occur like in polymer flow, the Truesdell-rate is more attractive from a Physics point of view. This was for instance shown by Beris and Edwards (1990), who found that their Poisson-bracket formulation of continuum mechanics could only accommodate the upper-convected time derivative (and its counterpart, the lower-convected derivative).

From the Truesdell-rate model, Eq. (2.65), and the corotational Maxwell model, Eq. (2.64), only the latter is approximately equal to the compressible Leonov model, Eq. (2.52), in the limit of small elastic strains. This can be shown by taking the Jaumann derivative of the expression for the stress tensor in the Leonov formulation, Eq. (2.52a):

$$\mathring{\mathbf{T}} = K\dot{J}\mathbf{I} + G\mathring{\bar{\mathbf{B}}}_e - \frac{G}{3}\mathrm{tr}(\dot{\bar{\mathbf{B}}}_e)\mathbf{I} \tag{2.66}$$

Substitution of the evolution equations for $\bar{\mathbf{B}}_e$ and J, Eqs. (2.52b) and (2.52d) at small isochoric-elastic and volume strains ($\bar{\mathbf{B}}_e \approx \mathbf{I}$ and $J \approx 1$), then results in the corotational Maxwell model:

$$\mathring{\mathbf{T}} = K\,\mathrm{tr}(\mathbf{D})\mathbf{I} + 2G(\mathbf{D}^d - \mathbf{D}_p) = \underline{\mathcal{L}}^e : (\mathbf{D} - \mathbf{D}_p) \tag{2.67}$$

However, taking the Truesdell derivative of Eq. (2.52a), results in:

$$\overset{\triangledown}{\mathbf{T}} = K\dot{J}\mathbf{I} - 2K(J-1)\mathbf{D} + G\overset{\triangledown}{\bar{\mathbf{B}}}_e - \frac{G}{3}\mathrm{tr}(\dot{\bar{\mathbf{B}}}_e)\mathbf{I} \tag{2.68}$$

Again substituting the evolution equations for $\bar{\mathbf{B}}_e$ and J at small elastic strains, now results in:

$$\begin{aligned} \overset{\nabla}{\mathbf{T}} &= 2G(\mathbf{D}^d - \mathbf{D}_p) + K\,\mathrm{tr}(\mathbf{D})\mathbf{I} - 2K(J-1)\mathbf{D} \\ &= \underline{\mathcal{L}}^e : (\mathbf{D} - \mathbf{D}_p) - 2K(J-1)\mathbf{D} \end{aligned} \tag{2.69}$$

In this expression an extra term appears, compared to the Truesdell-rate model, Eq. (2.65), which can not be neglected when the elastic strain rate tensor $\mathbf{D}_e$ is small ($\mathbf{D} \approx \mathbf{D}_p$). In contrast to the Jaumann derivative, the Truesdell derivative of a deviatoric tensor, in general, is not deviatoric. Therefore, the Truesdell derivative fails to preserve the (physically meaningful) distinction between the hydrostatic part and the deviatoric part of the Cauchy-stress tensor (Sansour and Bednarczyk, 1993).

It is possible, however, to reduce the compressible Leonov model, Eq. (2.52), at small elastic strains, to a slightly modified Truesdell-rate model. For this purpose, an extra-stress tensor $\mathbf{T}_E$ is defined, of which the deviatoric part is equal to the deviatoric part of the Cauchy-stress tensor:

$$\mathbf{T}_E = G(\bar{\mathbf{B}}_e - \mathbf{I}) \quad ; \quad \mathbf{T}_E^d = \mathbf{T}^d \tag{2.70}$$

Taking the Truesdell derivative of this expression, followed by substitution of the flow rule for $\mathbf{D}_p$, Eq. (2.61), and the evolution laws for $\bar{\mathbf{B}}_e$ and J, Eqs. (2.52b) and (2.52d), at small elastic strains, results in:

$$\left\{ \begin{array}{c} \mathbf{T} = K(J-1)\mathbf{I} + \mathbf{T}_E^d \\ \dfrac{\eta(I_T, \tau_{eq})}{G} \overset{\nabla}{\mathbf{T}}_E + \mathbf{T}_E^d = 2\eta(I_T, \tau_{eq})\mathbf{D} \\ \dot{J} = \mathrm{tr}(\mathbf{D}) \end{array} \right. \tag{2.71}$$

Apart from the stress dependence of the viscosity, the Truesdell-rate equation for the extra-stress tensor $\mathbf{T}_E$, Eq. (2.71), corresponds to the upper-convected Maxwell model, well known from polymer rheology (Larson, 1988, Chapter 1). In the next section, this model, to be denoted as the UCM-model, will be evaluated as well. Note that the corotational Maxwell model, Eq. (2.64), can be written in a similar form as Eq. (2.71), using only the Cauchy-stress tensor, due to the fortunate fact that the Jaumann derivative of a deviatoric tensor is always deviatoric:

$$\left\{ \begin{array}{c} \mathbf{T} = \mathbf{T}^d + K(J-1)\mathbf{I} \\ \dfrac{\eta(I_T, \tau_{eq})}{G} \overset{\nabla}{\mathbf{T}} + \mathbf{T}^d = 2\eta(I_T, \tau_{eq})\mathbf{D} \\ \dot{J} = \mathrm{tr}(\mathbf{D}) \end{array} \right. \tag{2.72}$$

The performance of the compressible Leonov model and the "standard" rate equations involving the Truesdell and the Jaumann derivative are mutually compared and evaluated by means of two simple homogeneous deformation tests, using polycarbonate as a model polymer. The material parameters are $G = 830$ MPa, $K = 4600$ MPa (which is equivalent to $E = 2335$ MPa and $\nu = 0.41$ [-]), $A = 1.75 \cdot 10^{21}$ s^{-1} and $\tau_0 = 0.89$ MPa. First a standard uniaxial tensile test will be considered, in which a tensile bar, stress-free in the radial and the tangential direction, is elongated in the x-direction at a deformation rate of 10^{-3} s^{-1}. (see Figure 2.4).

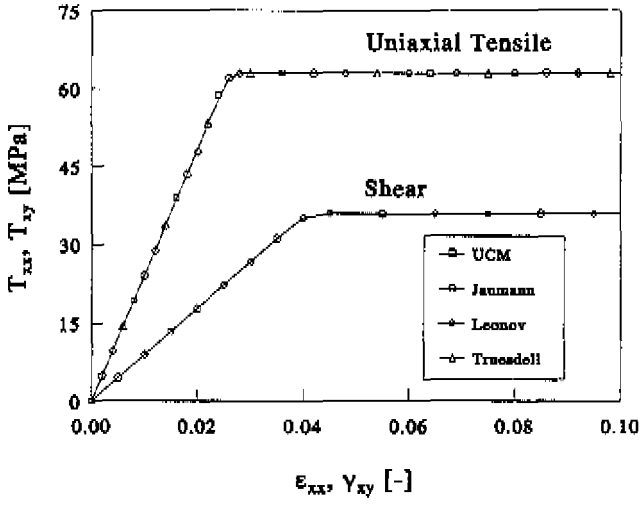

Figure 2.4 *Stress-strain curves for a uniaxial tensile test ($\mathbf{T}_{xx}$ vs. ε_{xx}) and a plane-stress shear test ($\mathbf{T}_{xy}$ vs. γ_{xy}), both at a rate of deformation of 10^{-3} s^{-1}.*

The calculated axial Cauchy-stress versus logarithmic-strain curves for all four models are virtually indistinguishable, as can be seen in Figure 2.4. Moreover, as might be expected from these single mode models, they all show a sharp instead of a gradual transition from elastic to plastic behaviour.

The calculated volume response as a function of logarithmic strain, is depicted in Figure 2.5. All four models show a correct volume response in the elastic region, according to Hooke's law. However, the Truesdell-rate model displays a volume decrease during plastic flow, which is not in accordance with the assumption of incompressible flow during plastic deformation.

Second, a plane-stress shear test is calculated. The Truesdell-rate model is not considered anymore because of its anomalous volume decrease in a tensile test. Virtually the same behaviour is obtained for all three models, Figure (2.4).

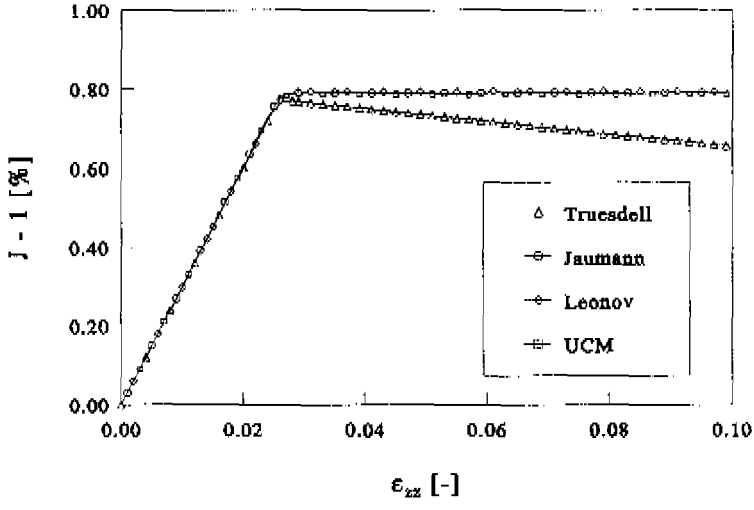

Figure 2.5 *Relative volume deformation as a function of logarithmic strain for a uniaxial tensile test at a rate of deformation of* $10^{-3}\ s^{-1}$.

However the calculated normal stress in the y direction, T_{yy}, differs markedly for the three models considered, as is depicted in Figure (2.6). In contrast to the corotational Maxwell model, both the compressible Leonov model and the UCM model display "correct" neo-Hookean behaviour in the elastic region, where the normal stress in the y direction is a quadratic function of the shear strain. This is to be expected, since integration of the Jaumann-rate version of Hooke's law does not result in hyperelastic behaviour. In contrast, at higher strains, the UCM model predicts zero normal stress in the y direction, whereas shear flow of a polymeric substance normally results in negative normal stresses (Bird *et al.*, 1987, Chapter 3), as it is displayed by the corotational Maxwell model and the compressible Leonov model. The Leonov model provides a smooth transition from Neo-Hookean behaviour in the elastic region, to the more realistic response of the corotational Maxwell element during yielding.

It is interesting to note that the first normal stress difference, $N1$ ($N1 = \mathbf{T}_{xx} - \mathbf{T}_{yy}$), is virtually equal for all three models considered, as can be concluded from Figure (2.7). Apparently, at small elastic strains, all three models differ mainly in the hydrostatic-stress contribution, resulting in different absolute values of the normal stresses themselves. This can also be derived from the calculated volume response, see Figure 2.8, recalling that in these models, the relative volume change is directly related to the hydrostatic stress.

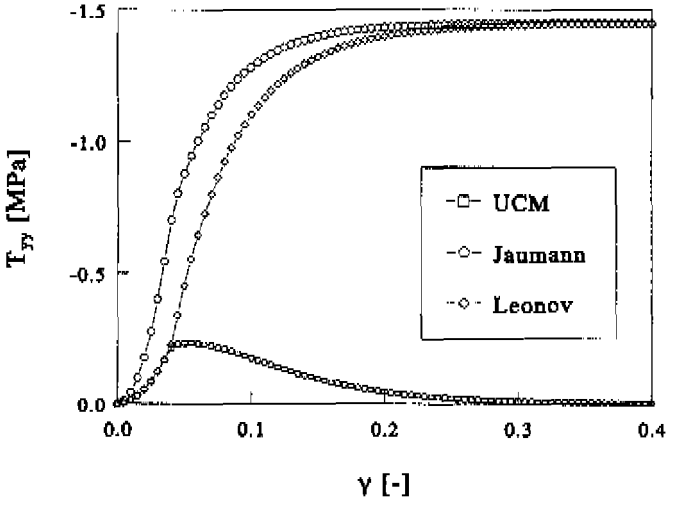

Figure 2.6 *Normal stress in the y direction as a function of shear strain at a deformation rate of* $10^{-3}\ s^{-1}$.

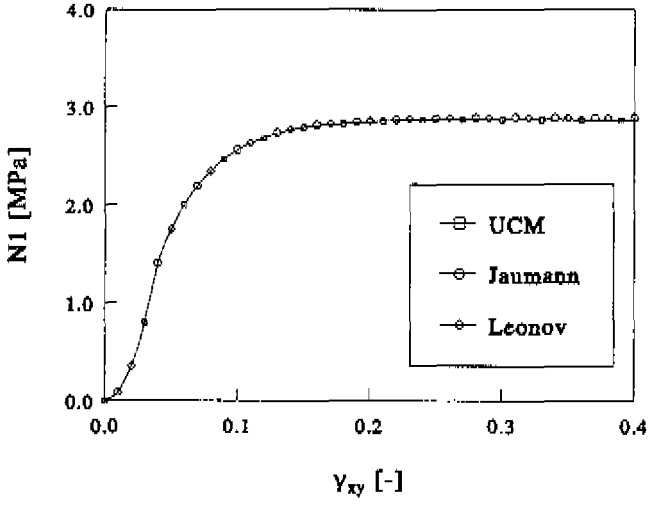

Figure 2.7 *First normal stress difference* $N1$ ($N1 = \mathbf{T}_{xx} - \mathbf{T}_{yy}$) *as a function of shear strain at a deformation rate of* $10^{-3}\ s^{-1}$.

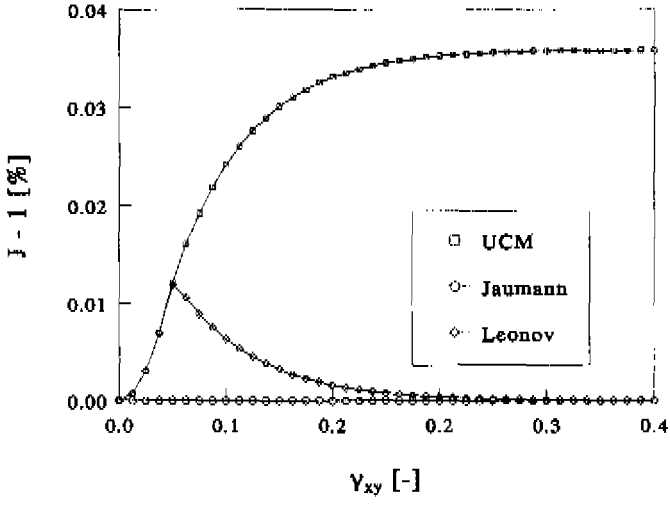

Figure 2.8 *Relative volume deformation as a function of shear strain for a plane-stress shear test at a rate of deformation of* $10^{-3}\ s^{-1}$.

2.6 Discussion and Conclusions

In this Chapter a so-called "compressible Leonov model" has been introduced which can be depicted as a single Maxwell model employing a relaxation time dependent on an equivalent stress proportional to the Von Mises stress. The model has been derived using a generic formalism for the development of thermodynamically consistent constitutive equations. It was assumed that the free energy of the system at constant temperature, which is a measure for the amount of stored energy, is determined by two state variables, the isochoric elastic strain and the volume strain. The plastic strain rate was constitutively described by stress-activated Eyring flow.

A comparison has been made between the Leonov model and two standard constitutive equations for the description of relaxation behaviour, the Truesdell-rate and the corotational Maxwell model. It was concluded that neither of these two standard models is able to describe plastic deformation accompanied by large elastic deformations, as it can occur during strain-hardening of glassy polymers. Integration of the corotational Maxwell model is known to result in hypoelastic elastic behaviour, whereas integration of the Truesdell model results in a volume decrease during plastic flow in a tensile test. Based upon the Leonov model, a slightly modified Truesdell-rate model was proposed, the so-called upper-convected Maxwell model (UCM-model), for which the volume remains constant

during plastic flow in a tensile experiment.

In a plane-stress shear test, the UCM-model, the corotational Maxwell model and the Leonov model only seem to differ in their volume response. The corotational Maxwell model shows no volume response at all, which is somewhat unrealistic for a plane-stress configuration. Contrary, the compressible Leonov model and the UCM model display a volume increase in the elastic region, but the volume does not remain constant after yielding as in the tensile test. It is doubtful, whether experimental data can shed any light on these results. In principle, the normal stress in the y direction can be measured experimentally up to the yield point. After the yield point however, shear bands will develop, prohibiting a straightforward interpretation of the data. Furthermore, even if it would be possible to extract useful data after the yield point, the effects mentioned would probably be overwhelmed by the strain-hardening response, which will be discussed in Chapter 5. Since the models considered here are all "single mode" models, even the response in the elastic region is not be predicted realistically. Therefore, a theoretical and experimental study of the full non-linear viscoelastic response up to the yield point of polycarbonate, will be discussed in the next Chapter.

Chapter 3

Finite Nonlinear Viscoelastic Behaviour

3.1 Introduction

In the previous Chapter, the compressible Leonov model was introduced to describe the yield behaviour of polymer glasses (and other materials). A single Leonov *mode* is a Maxwell model employing a relaxation time that is dependent on an equivalent stress proportional to the Von Mises stress. Furthermore, a Leonov mode correctly separates the (elastic) hydrostatic and (viscoelastic) deviatoric stress response and accounts for the geometrical complexities associated with simultaneous elastic and plastic deformations.

However, the use of a single stress-dependent relaxation time cannot account for the (non)linear viscoelastic response at small and moderate strains. Moreover, using a single relaxation time results in an abrupt transition from elastic to viscous behaviour that is rarely seen in practice. Therefore, a description employing a spectrum of relaxation times would be more appropriate. If the additional assumption is made that all relaxation times depend in the same way on the total stress, one arrives at the principle of time-stress superposition, equivalent to time-temperature superposition, where it is assumed that all relaxation times depend in the same way on the (total) temperature. Time-stress superposition implies that the nonlinear effect of stress is to alter the intrinsic time-scale of the material, hence it is sometimes referred to as a "stress clock" (Bernstein and Shokooh, 1980).

Other choices are possible as well. Valanis (1971) assumed that strain instead of stress accelerates relaxation processes in a material. However, using the total strain as a variable implies that the material under consideration is a solid and since all materials ultimately flow, it is better to use a fluid point of view (Bernstein and Shokooh, 1980). Shay, Jr. and Caruthers (1986) considered a volume clock to describe nonlinear viscoelastic behaviour and yielding. However, in this way, they were unable to recover Von Mises like yield behaviour that is observed experimentally. Furthermore, volume recovery measurements by McKenna *et al.*

(1994) suggest that the structural state of a glass (its volume) is decoupled from the mechanical stress field. Hasan and Boyce (1995) used a spectrum of activation energies to describe the distributed nature of local plastic transformations. However, using a spectrum of activation energies results in thermo-rheological complex behaviour which is not always observed in practice.

The concept of time-stress superposition has been used frequently to describe nonlinear viscoelastic behaviour. It was incorporated in the Boltzmann integral by Schapery (1969) using the concept of a reduced time (Leaderman, 1943). Bernstein and Shokooh (1980) showed that the introduction of special stress-clock functions can transform a viscoelastic relation (in their case the class of BKZ-equations (Larson, 1988)) into an elastic-perfectly plastic constitutive equation. In this Chapter, time-stress superposition is used to obtain a compressible three-dimensional constitutive equation which provides a unified description of finite nonlinear viscoelastic behaviour and yield. The constitutive relation will be verified experimentally using polycarbonate as a model polymer.

It is well known that the viscoelastic response of polymers changes with time, a thermo-reversible process called physical aging (Struik, 1978). In this Chapter, we will limit ourselves to samples which all have the same age, exceeding by far the longest time in the experiments. Therefore, to a first approximation, aging will not be taken into account. Some aspects of aging in relation to mechanical behaviour will be discussed in Chapter 6.

3.2 Theory

3.2.1 Single Mode Approach

In Chapter 2 an elasto-viscoplastic equation for polymer glasses (and other materials) was introduced, the so-called compressible Leonov model (Leonov, 1976; Tervoort *et al.*, 1994). In this model a formal decoupling of the volume response and the isochoric "shape" response was achieved by assuming that the free energy of the system is determined by two state variables: the relative volume deformation, $J = \det(\mathbf{F})$, where $\mathbf{F}$ is the deformation gradient and the isochoric Cauchy-Green strain tensor, $\check{\mathbf{B}}_e$, ($\det(\check{\mathbf{B}}_e) = 1$) (see also Rubin (1987, 1994) and Baaijens (1991)). Using a formalism developed to derive thermodynamically consistent constitutive equations (Jongschaap *et al.*, 1994), it was shown that the hydrostatic stress is coupled to the volume deformation, whereas the deviatoric stress is determined by the isochoric (constant volume) elastic strain. Furthermore it was assumed that the volume deformation remained elastic whereas the accumulation of isochoric-elastic strain was reduced because of a plastic strain rate $\mathbf{D}_p$. At small volume deformations ($J \approx 1$) the compressible Leonov model reduces to

(see Eq. (2.52)):

$$\begin{cases} \mathbf{T} = K(J-1)\mathbf{I} + G\bar{\mathbf{B}}_e^d \\ \overset{\circ}{\bar{\mathbf{B}}}_e = (\mathbf{D} - \mathbf{D}_p)\cdot\bar{\mathbf{B}}_e + \bar{\mathbf{B}}_e\cdot(\mathbf{D} - \mathbf{D}_p) \\ \dot{J} = J\,\mathrm{tr}(\mathbf{D}) \end{cases} \tag{3.1}$$

Here, K is the bulk modulus, G the shear modulus, the superscript "d" denotes the deviatoric part and $\overset{\circ}{\bar{\mathbf{B}}}_e$ is the Jaumann or co-rotational derivative of $\bar{\mathbf{B}}_e$:

$$\overset{\circ}{\bar{\mathbf{B}}}_e = \dot{\bar{\mathbf{B}}}_e - \mathbf{W}\cdot\bar{\mathbf{B}}_e - \bar{\mathbf{B}}_e\cdot\mathbf{W} \tag{3.2}$$

with the vorticity tensor $\mathbf{W}$. The plastic strain rate $\mathbf{D}_p$, which reduces the accumulation of isochoric-elastic strain, was constitutively described by the Eyring equation (see Eq. (2.50)). The Eyring equation for plastic flow is a semi-empirical relation which describes stress-activated flow of structural units in a material, like segments in case of a polymer. It is depicted three-dimensionally as (Tervoort *et al.*, 1994):

$$\begin{cases} \mathbf{D}_p = \dfrac{\mathbf{T}^d}{2\eta(\tau_{eq})} \\ \eta(\tau_{eq}) = A\tau_0 \dfrac{\left(\frac{\tau_{eq}}{\tau_0}\right)}{\sinh\left(\frac{\tau_{eq}}{\tau_0}\right)} = \eta_0 \mathrm{a}_\sigma(\tau_{eq}) \\ \tau_{eq} = \sqrt{\dfrac{1}{2}\,\mathrm{tr}(\mathbf{T}^d\cdot\mathbf{T}^d)} \end{cases} \tag{3.3}$$

Here, τ_{eq} is an equivalent stress, proportional to the Von Mises stress. The material constants (at constant temperature) A and τ_0 are related to the activation energy, ΔH and the activation volume, V^*, respectively:

$$A = A_0 \exp\left(\frac{\Delta H}{RT}\right), \quad \tau_0 = \frac{RT}{V^*} \tag{3.4}$$

with A_0 a pre-exponential factor involving the fundamental vibration frequency, R the gas constant and T the absolute temperature. The product $A\tau_0$ is the zero-shear viscosity η_0. The shift function $\mathrm{a}_\sigma\,(\tau_{eq})$ is, in fact, a dimensionless viscosity which is equal to one when $\tau_{eq} < \tau_0$ and rapidly decreases to zero when $\tau_{eq} \geq \tau_0$.

From Eqs. (3.1) and (3.3) it can be seen that the deviatoric stress response as described by the compressible Leonov model (to be called: "a single Leonov mode") can be depicted as a single Maxwell model employing a nonlinear relaxation time $\lambda = \eta/G$:

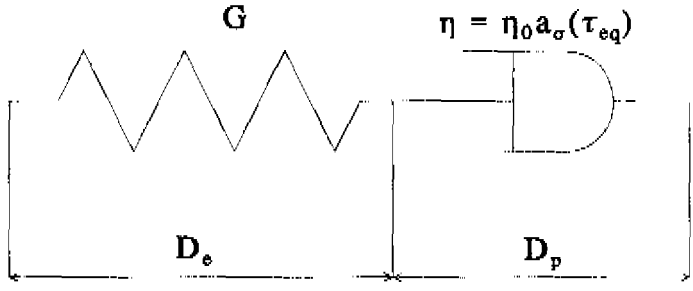

Figure 3.1 *Graphical representation of the deviatoric stress response of a single Leonov mode.*

In the Eyring approach it is assumed that deformation processes are essentially always present and that stress, like temperature, merely changes the rate of deformation. This is reflected by the functional dependence of the relaxation time on stress (Eqs. (3.1) and (3.3)). At low equivalent stress ($\tau_{eq} \ll \tau_0$) there is a linear region where the relaxation time is constant, $\lambda = \lambda_0 = \eta_0/G$. At higher stress ($\tau_{eq} \geq \tau_0$) the relaxation time decreases rapidly as described by the shift function $a_\sigma(\tau_{eq})$. Thus the intrinsic time scale of the material ("the internal clock") is changed by the application of stress, hence the name "stress-clock" material (Bernstein and Shokooh, 1980). The nonlinear effect of stress can be observed most clearly in a constant stress experiment, like the creep test. For a creep experiment at a very low (equivalent-) stress level ($\tau_{eq} < \tau_0$) the compliance curve of a single Leonov mode is determined by the linear relaxation time λ_0 as can be seen in Figure 3.2, that shows the compliance curves versus time, with the equivalent stress as a parameter.

For creep tests performed at higher stress levels ($\tau_{eq} \geq \tau_0$) the relaxation time is reduced by a factor $a_\sigma(\tau_{eq})$. On a logarithmic time axis this results in a horizontal shift of the compliance curve (hence the name "shift function"). A single Leonov mode is not capable of predicting realistic compliance curves, since it is dominated by a single relaxation time, see Figure 3.2.

A set of typical tensile curves at various strain rates, calculated from a single Leonov mode is depicted in Figure 3.3.

As with the creep test, a single Leonov mode is not able to offer a realistic description of the experimental curve, as it only accounts correctly for the initial modulus and the (strain-rate dependent) "yield stress". This is not surprising since both are essentially the material parameters supplied to the model. There exists, however, a serious discrepancy between calculated and experimental curves before and after the (experimental) yield point (the maximum in the tensile curve), which shows a more gradual transition from elastic to yield behaviour and the yield

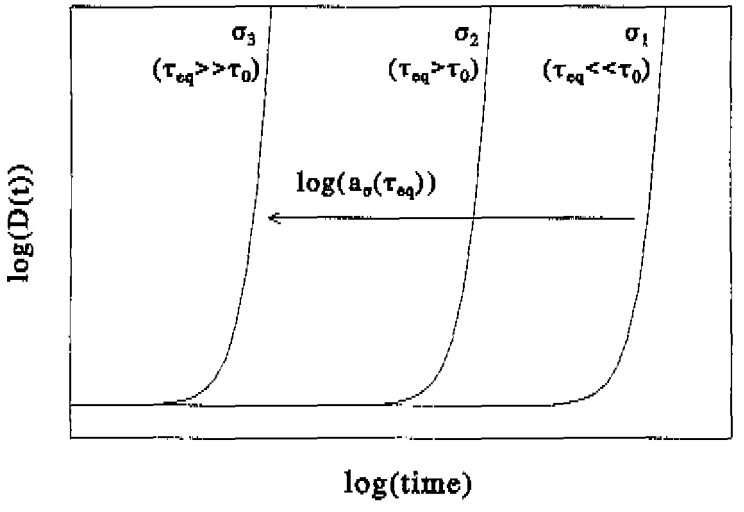

Figure 3.2 *Compliance curves for a single Leonov mode at various stress levels.*

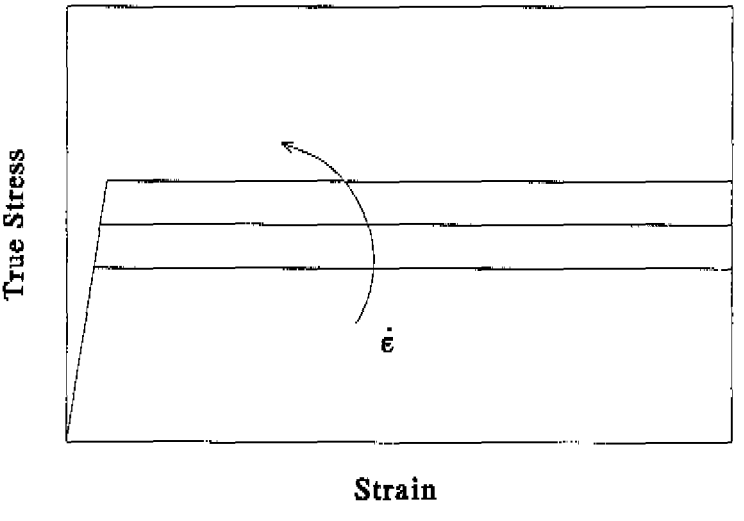

Figure 3.3 *Calculated tensile curves for a single Leonov mode at various strain rates.*

point is, therefore, generally found at a higher strain. Inhomogeneous deformation and possible strain softening account for the discrepancy after the "yield point". In contrast, before the "yield point" the deformation is fairly homogeneous and the deviation between model predictions and the experimental curves must be due to another course. It will be shown that a quantitative description of a tensile test, and in fact the complete three-dimensional nonlinear viscoelastic behaviour of polymer glasses, can be obtained by using a spectrum of stress-dependent relaxation times, rather than one.

It is to be noted that the inability of a single Leonov mode to describe accurately the nonlinear viscoelastic response of a polymer glass is inherent to all models which employ only one stress-dependent relaxation time (Boyce *et al.*, 1988; Wu and van der Giessen, 1993).

3.2.2 Multi Mode Approach

From polymer physics it is well known that time-dependent behaviour of amorphous polymers can result from a wide variety of molecular transitions. The most important of these is the glass transition (α-transition) which is associated to main chain segmental motion. Many polymers also exhibit so-called secondary transitions (β-transitions) originating from the motions of side groups, end groups, or restricted motion of the main chain (Ward, 1990).

The time dependence, resulting from a specific molecular transition, is generally mathematically represented by a spectrum of relaxation times. In contrast, it is usually assumed that the activation of a molecular transition by temperature is determined by a single parameter, the activation energy ΔH. This implies that all the relaxation times, due to a specific molecular transition, depend in an identical way on temperature, resulting in the well known time-temperature superposition principle (thermo-rheological simple behaviour). According to this principle, the influence of temperature on viscoelastic properties, whose time dependence is determined by (a set of) relaxation time(s), can be described by a so-called reduced time t^* (Leaderman, 1943):

$$t^* = \int_0^t \frac{dt'}{a_T} \tag{3.5}$$

Dividing the real time t by a shift factor a_T results, on a logarithmic time axis, in a horizontal shift by a factor $\log(a_T)$, where a_T is the ratio of the relaxation times at temperatures T and T_0.

In practice, experimental verification of the applicability of time-temperature superposition consists of two parts (Ferry, 1980): First it is attempted to construct a smooth master curve of a viscoelastic quantity, like the creep compliance, at a certain reference temperature. This is done by shifting curves measured at different temperatures horizontally along the logarithmic time axis. Second, if a

smooth master curve is obtained, a plot of the resulting shift factors as a function of temperature must obey a "familiar" relation, e.g. the Arrhenius equation or the WLF-equation.

According to the Eyring approach, besides activation by temperature, a molecular transition can also be activated by stress (to be more precise: by the equivalent stress τ_{eq}). Again it is commonly assumed that stress activation is described by a single parameter, the activation volume V^*. Indeed, determination of the activation energy and volume is often used for the identification of certain molecular transitions (Ward, 1990). It is, therefore, logical to assume that, like in the case of activation by temperature, all relaxation times are the same function of the *total equivalent stress*. This leads to the principle of time-stress superposition, which states that the nonlinear effect of stress can be described by using a reduced time, like in the case of temperature. It implies that, if a discrete spectrum of Leonov modes is used as an approximation of the relaxation-time spectrum, all modes should be shifted by the same factor $a_\sigma(\tau_{eq})$, where τ_{eq} is the *total equivalent stress*. Furthermore, it implies that the experimental verification of the applicability of time-temperature superposition, as described above could also be used to justify time-stress superposition. Data obtained for constant stress levels must shift to a smooth master curve and the resulting shift factors, as a function of equivalent stress, must obey a "familiar" relation like the Eyring equation, Eq. (3.3). In essence, for polymer glasses, time-stress superposition implies that yielding can be regarded as a stress induced glass transition.

3.3 Experimental

Experiments were carried out on test specimens produced according to ASTM D 638 from extruded sheets of Makrolon (bisphenol A polycarbonate, Bayer), 2 mm thick. Polycarbonate was selected as a model polymer since, at room temperature, it exhibits only one active relaxation mechanism of interest; the glass transition. At room temperature the β-transition, which is situated at -100 °C to -50 °C, is only relevant for very fast processes.

Stress relaxation experiments were performed on a Frank 81565 tensile tester, whereas creep and constant strain rate experiments were performed on a Zwick Rel servo-hydraulic tensile tester (20 kN). In all cases the extension was measured using an Instron (2620-602) strain gauge extensometer with a measure length of 50 mm and a range of $\pm$ 2.5 mm. The radial strain was measured using an Instron (2640-008) transverse extensometer. The relative accuracy in the force and strain measurements was 1%.

Stress relaxation experiments, with loading times not exceeding 10^4 s, were performed at strains of 0.5% to 3%. Creep experiments, with loading times not exceeding 10^3 s, were performed in dead weight loading at loads of 10 to 55 MPa. The strains and loads in the stress relaxation and creep experiments were applied

within 1 s. Tensile test experiments were performed at constant strain rates up to 10^{-2} s^{-1}. Each experiment was performed on a new sample at room temperature. All test samples had the same age, which exceeded by far the longest time in the experiments.

3.4 Results

In Section 3.2 it was argued that the deformation behaviour of glassy polymers is determined by the linear relaxation time spectrum which is shifted to shorter times when stress is applied. In this section, the admissibility of this time-stress superposition principle will be verified experimentally using polycarbonate as a model polymer. Subsequently the linear relaxation time spectrum will be determined in order to complete the multi-mode Leonov model for polycarbonate. Finally, the model will be verified using constant strain rate experiments and stress relaxation experiments (in tensile deformation).

3.4.1 Admissibility of Time-Stress Superposition

In order to verify, experimentally, the admissibility of time-stress superposition for polycarbonate, it was first attempted to construct a smooth master curve from a number of creep tests at different stress levels as described in Section 3.2.2. The results of the creep tests are depicted in Figure 3.4. The curves were shifted

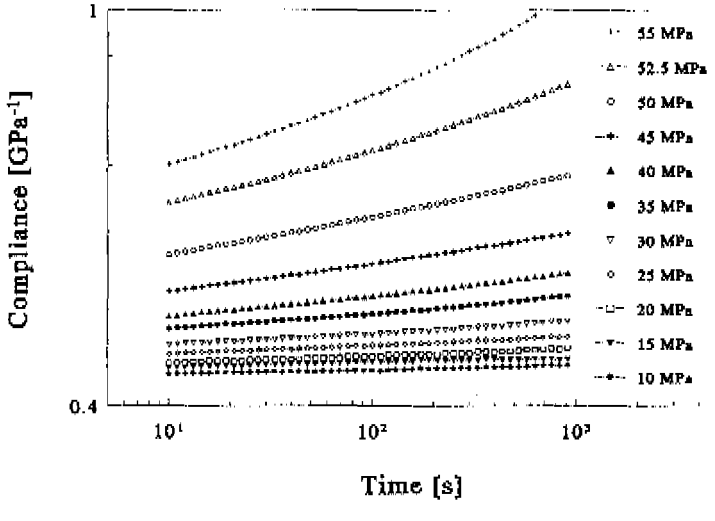

Figure 3.4 *Creep compliance of polycarbonate at various loads at 20 °C.*

horizontally along the logarithmic time axis with respect to the 10 MPa reference curve. The resulting master curve is depicted in Figure 3.5.

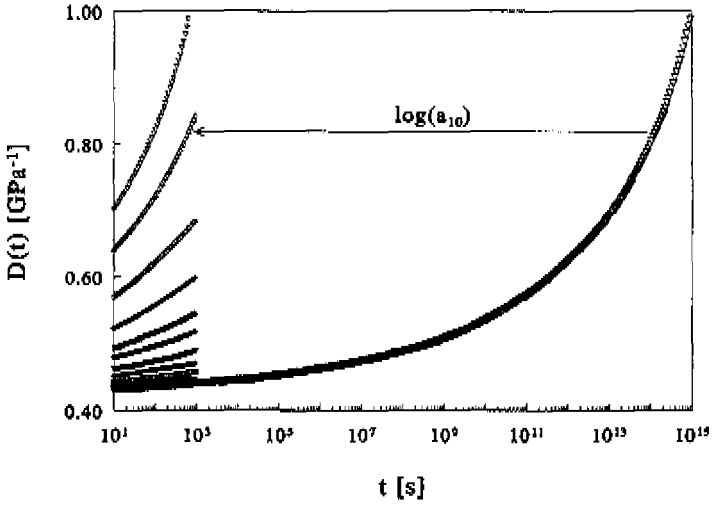

Figure 3.5 *Construction of the master curve of the creep compliance at a reference stress of 10 MPa.*

From Figure 3.5 it is clear that a smooth compliance master curve can be constructed by horizontal shifting of the creep tests at different stresses. It must be emphasized that the compliance master curve at 10 MPa is a "virtual" curve that will strongly deviate from an experimental creep test on the same time scale, due to aging effects.

The logarithm of the shift factors $\log(a_{10})$, are tabulated in Tabel 3.1 as a function of the creep load:

σ_0 [MPa]	10	15	20	25	30	35	40	45	50	52.5	55
$\log(a_{10})$ [-]	0	-1.5	-2.6	-3.9	-5	-6.5	-7.4	-8.6	-10	-11.4	-12.2

Table 3.1 *Shift factors resulting from the construction of the 10 MPa master compliance curve.*

The second part of the experimental verification of time-stress superposition consists of fitting the shift data from Tabel 3.1 with the Eyring equation, Eq. (3.3), see Figure 3.6. It is clear that the creep data are determined by one Eyring shift

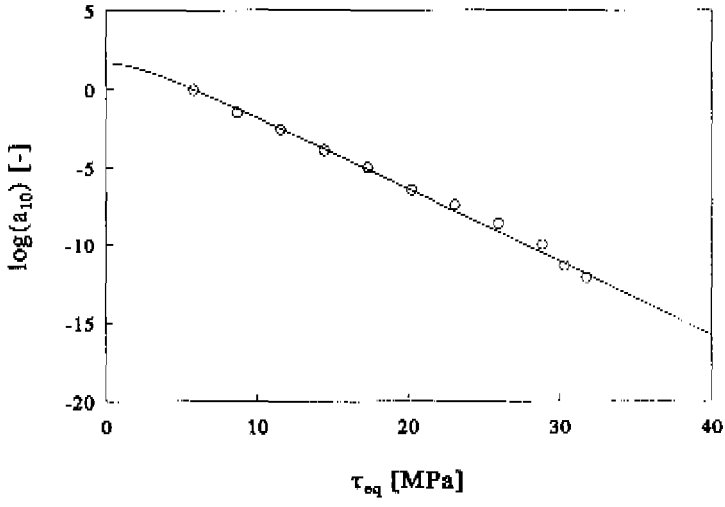

Figure 3.6 *Logarithm of the shift factors with respect to 10 MPa obtained from the creep tests as a function of equivalent stress. The solid line is a fit using the Eyring shift function (Eq. (3.3)).*

function only. Therefore, the second condition is also met and we may assume that time-stress superposition may be applied.

3.4.2 Material Parameters

Now it is verified experimentally that time-stress superposition applies to polycarbonate, the multi-mode Leonov model for polycarbonate can be completed by determining the material parameters.

The Eyring Parameters

The Eyring viscosity function, Eq. (3.3), which describes the nonlinearity in the stress response, is determined by two parameters, the zero-shear viscosity η_0 and the nonlinearity parameter τ_0, which may be determined by using an Eyring plot (see Chapter 2, Section 2.5.3). In order to make such a Eyring plot, we need to extract viscosity data from the creep tests at different stress levels (Figure 3.4). In principle, this should be done by measuring the plateau-creep rate ($\dot{\varepsilon}_{pl}$) of each creep experiment. The plateau-creep rate is determined by the constancy of the creep rate at an imposed (constant) creep load σ_0 and, therefore, defines a viscosity $\eta^e_{pl} = \sigma_0/\dot{\varepsilon}_{pl}$. Note that this is an extensional viscosity (as denoted by

the superscript "e") since the creep data were obtained from tensile experiments. In terms of the Leonov model, the plateau-creep viscosity η^e_{pl} is equal to the sum of the viscosities $\eta^e_i = \eta^e_{0i} a_\sigma$ of all the separate Leonov modes:

$$\eta^e_{pl} = \frac{\sigma_0}{\dot{\varepsilon}_{pl}} = \sum_i \eta^e_{0i} a_\sigma(\tau^{pl}_{eq}) \tag{3.6}$$

where τ^{pl}_{eq} is the equivalent stress associated with the creep load σ_0. The plateau-creep rate is usually obtained from a *Sherby-Dorn plot*, which is a graph of the creep rate versus creep strain.

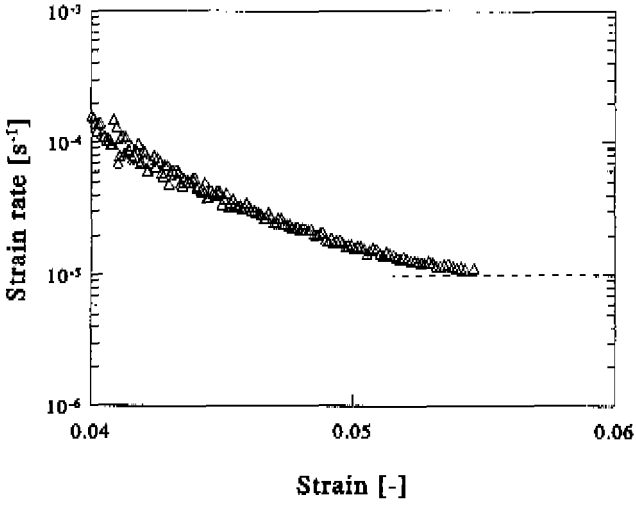

Figure 3.7 *Sherby-Dorn plot for the determination of the plateau creep rate at 55 MPa.*

Due to the limited experimental time window, a plateau-creep rate was observed only at the highest creep load of 55 MPa. From the Sherby-Dorn plot, the value of the plateau-creep rate was estimated to be $\dot{\varepsilon}_{pl} = 10^{-5}$ s^{-1}, leading to a plateau-creep viscosity of $\eta^e_{pl} = 55 \cdot 10^5$ MPa·s^{-1} (see Figure 3.7). For all the other creep tests, a constant creep rate could not be established experimentally. However, according to Eq. (3.6), the ratio of the plateau-creep viscosities at two different stress levels τ^1_{eq} and τ^2_{eq}, is equal to the ratio of the shift factors at those stress levels:

$$\frac{\eta^e_{pl}(\tau^1_{eq})}{\eta^e_{pl}(\tau^2_{eq})} = \frac{a_\sigma(\tau^1_{eq})}{a_\sigma(\tau^2_{eq})} \tag{3.7}$$

Therefore, the value of the plateau-creep viscosity at 55 MPa may be used to convert the plot of shift factors (Figure 3.6) to a graph of viscosity as a function of equivalent stress (Figure (3.8)).

In order to obtain an accurate estimation of both the activation volume (τ_0) and the zero-shear viscosity η_0, it is necessary to have viscosity data up to the (equivalent) "yield stress". Therefore, yield data obtained by tensile testing at different strain rates were included in Figure 3.8. Note that a "yield point" also defines a viscosity since it is determined by the moment the stress becomes constant at an imposed constant strain rate. Since it is irrelevant whether this steady-state situation is achieved at an imposed stress or imposed strain rate, the "yield viscosity" is also equal to the sum of the viscosities of all the separate Leonov modes:

$$\eta_y^e = \sum_i \eta_{0i}^e a_\sigma(\tau_{eq}^y) \tag{3.8}$$

where τ_{eq}^y is the equivalent yield stress.

The results of the tensile tests at different strain rates are shown in Tabel (3.2). A plot of all the viscosity data is depicted in Figure 3.8. The solid line is a best fit using a single Eyring viscosity function. From this figure it is clear that both yield and creep are determined by the same Eyring process. The best fit resulted in a value for $\tau_0 = 0.89$ MPa and for $\eta_0^e = 4.6561 \cdot 10^{20}$ MPa·s.

$\dot{\varepsilon}$ [s^{-1}]	$1.4 \cdot 10^{-4}$	$1.5 \cdot 10^{-4}$	$1.4 \cdot 10^{-3}$	$1.4 \cdot 10^{-3}$	$1.4 \cdot 10^{-3}$	$1.6 \cdot 10^{-2}$	$1.4 \cdot 10^{-2}$
σ_y [MPa]	61.7	59.9	63.6	63.1	63.1	65.3	66.6
η_y [MPa·s]	$4.5 \cdot 10^5$	$4.1 \cdot 10^5$	$4.6 \cdot 10^4$	$4.5 \cdot 10^4$	$4.5 \cdot 10^4$	$4.2 \cdot 10^3$	$4.7 \cdot 10^3$
τ_{eq}^y [MPa]	35.6	34.6	36.7	36.4	36.4	37.7	38.5

Table 3.2 *Viscosities from yield points at different strain rates as a function of equivalent stress.*

Linear Viscoelastic Parameters

In the limit of small stresses and strains, the multi-mode Leonov model reduces to a generalized Maxwell model (in shear). In order to find the linear Leonov (Maxwell) parameters, we start from the the 10 MPa compliance master curve, which was obtained through application of the time-stress superposition principle (Section 3.4.1). This compliance curve is complete towards the long time limit, since the plateau creep regime was established. However, the 10 MPa compliance master curve does not constitute the true linear compliance curve. The value of the nonlinearity parameter τ_0 indicates that, above an equivalent stress of 0.89 MPa, polycarbonate already behaves in a nonlinear way. Therefore, the true linear compliance curve could only be obtained indirectly by shifting the

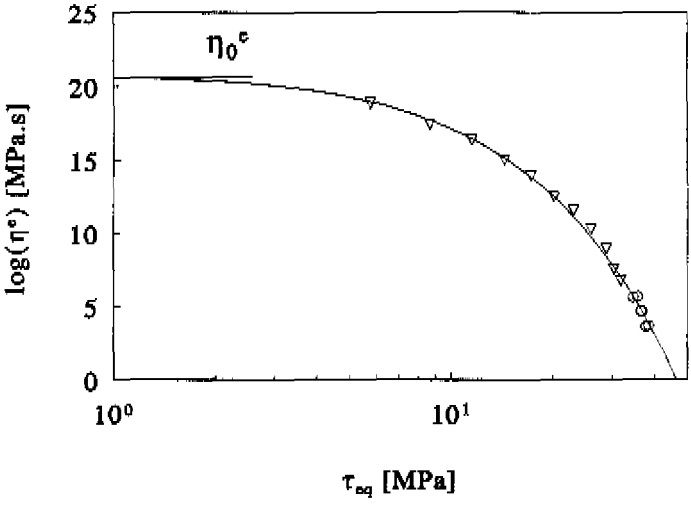

Figure 3.8 *A plot of the elongational viscosity as a function of equivalent stress, obtained from creep data (▽) and yield data (○). The solid line is a fit using a single Eyring function.*

10 MPa master curve horizontally by a factor $a_\sigma(\tau_{eq}^{10\ MPa})$. The resulting linear compliance curve is depicted in Figure 3.9. Also plotted in Figure 3.9 is the single mode approximation of the linear compliance curve, which is obtained by only taking into account the glassy compliance D_g and the total zero-shear viscosity η_0^e. The solid line in Figure 3.9 is a fit using a generalized Kelvin-Voigt model (see Appendix A):

$$D(t) = D_g + \sum_{i=1}^{n} D_i(1 - e^{-\frac{t}{\lambda_i}}) + \frac{t}{\eta_0^e} \tag{3.9}$$

with $D_g = 1/E_g$, where the initial ("glassy") Young's modulus was measured to be: $E_g = 2335$ MPa. The fit was obtained using CONTIN, a constrained regularization program developed to invert ill-posed linear integral equations (Provencher, 1982a, 1982b). Using an equidistant grid of relaxation times, eighteen modes were necessary to obtain a accurate description of the linear compliance curve. No further attempts were made at this stage of the research to reduce the number of modes.

In order to obtain the linear Leonov parameters, the linear tensile compliance curve D(t) must be converted to the linear shear relaxation modulus curve G(t). This was done by invoking the correspondence principle (Tschoegl, 1989),

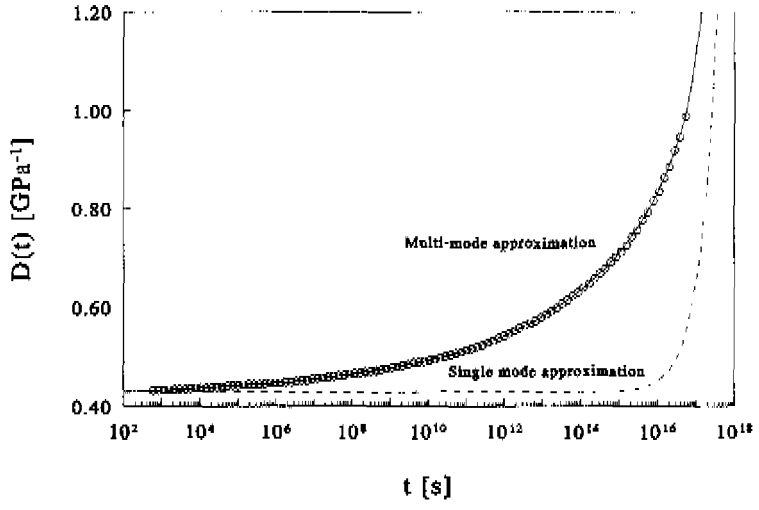

Figure 3.9 *The linear compliance curve $D(t)$ (∘). The solid line is a fit using a generalized Kelvin-Voigt model, for comparison the single mode approximation of the yield behaviour is added (dashed line).*

assuming a constant bulk modulus $K = 4300$ MPa (which corresponds to the experimentally determined initial Poisson ratio of polycarbonate $\nu = 0.41$ [-]), see Appendix A. The resulting shear relaxation modulus is depicted in Figure 3.10, the eighteen shear moduli and relaxation times are tabulated in Tabel 3.3. It must be emphasized that these linear parameters bear no physical meaning, only the relaxation modulus $G(t)$ itself is a material function.

3.4.3 Model Verification

In Section 3.2.2 it was argued that the finite nonlinear viscoelastic behaviour of polymer glasses is determined by the linear relaxation time spectrum which is shifted to shorter times when stress is applied. In the previous Section 3.4.2, the linear relaxation time spectrum for a model polymer, polycarbonate, was approximated using eighteen Leonov modes, all subdued to the same stress dependence. In this Section, this multi mode Leonov constitutive equation of polycarbonate will be verified by constant strain rate experiments (homogeneous uniaxial tensile tests) and stress relaxation experiments.

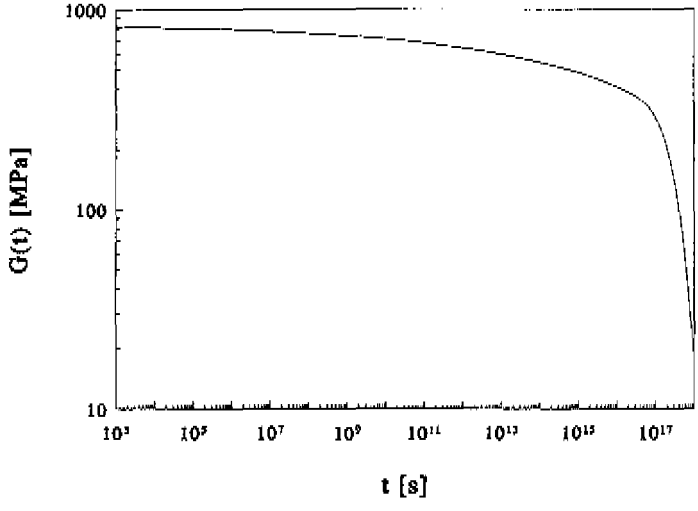

Figure 3.10 *The linear shear relaxation modulus $G(t)$ calculated from the linear tensile compliance curve $D(t)$ as described in Appendix A.*

Uniaxial Tensile Test

The first verification experiment considered, is a standard uniaxial tensile test at various constant strain rates (constant crosshead speed). Figure 3.11 shows a comparison between the experimental data (open symbols) and the numerical predictions (solid line). It is clear that, in contrast to a single mode Leonov model (see Figure 3.3), the multi mode Leonov model provides an quantitative description of the strain rate dependent "yield behaviour" of polycarbonate.

In the multi-mode Leonov model, polycarbonate is essentially regarded as a highly nonlinear fluid. It is, therefore, instructive to divide both stress and strain data in Figure 3.11 by the constant applied strain rates and make a plot of the extensional viscosity versus time, as is common practice in rheology, see Figure 3.12.

During the tensile test the lateral contraction was measured as well. Figure 3.13 shows a comparison between the experimental data (open symbols) and the numerical predictions (solid line) of the radial strain versus axial strain. The dashed line is the prediction for an elastic solid with a (constant) Poisson ratio equal to the initial Poisson ratio of polycarbonate $\nu = 0.41$.

From Figure 3.13 it is clear that the multi mode Leonov model also provides a quantitative description of the strain rate dependent volume behaviour during tensile testing of polycarbonate up to the "yield point".

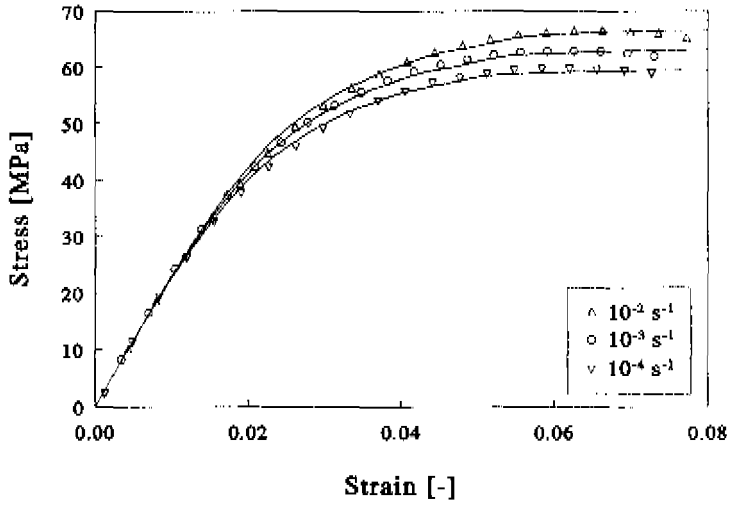

Figure 3.11 *Uniaxial tensile experiments at various strain rates (open symbols), compared to model predictions (solid lines).*

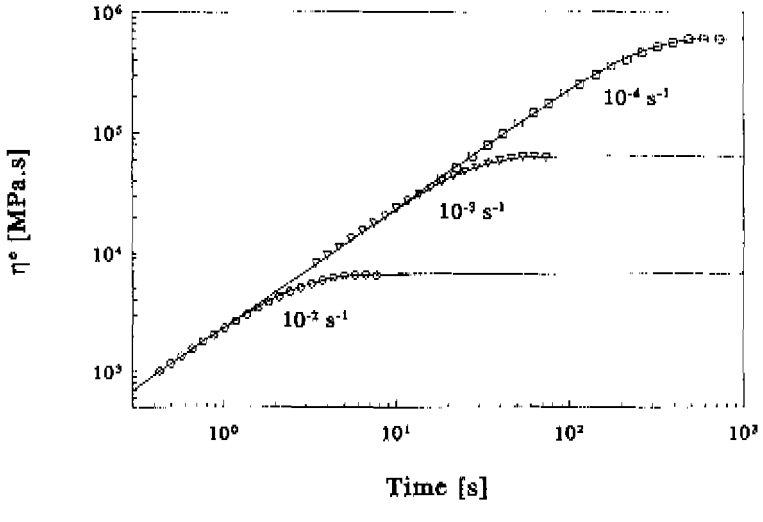

Figure 3.12 *Extensional viscosity build-up measured at various (Hencky) strain rates (symbols), compared to model predictions (solid lines).*

i	λ_i [s]	G_i [MPa]	$\eta_{0,i} = \lambda_{0,i} \cdot G_i$ [MPa·s]
1	0.7080e+04	0.2254e+02	0.1596e+06
2	0.3548e+06	0.9810e+01	0.3481e+07
3	0.2512e+07	0.1096e+02	0.2753e+08
4	0.1778e+08	0.1354e+02	0.2407e+09
5	0.1259e+09	0.1633e+02	0.2056e+10
6	0.8913e+09	0.1687e+02	0.1503e+11
7	0.6310e+10	0.2125e+02	0.1341e+12
8	0.4467e+11	0.2331e+02	0.1041e+13
9	0.3162e+12	0.3336e+02	0.1055e+14
10	0.2239e+13	0.3642e+02	0.8153e+14
11	0.1585e+14	0.4226e+02	0.6698e+15
12	0.1122e+15	0.4532e+02	0.5085e+16
13	0.7943e+15	0.5148e+02	0.4089e+17
14	0.5623e+16	0.7140e+02	0.4015e+18
15	0.3981e+17	0.5088e+01	0.2026e+18
16	0.2818e+18	0.3992e+03	0.1125e+21
17	0.1995e+19	0.6563e+01	0.1310e+20
18	0.1413e+20	0.2049e+01	0.2894e+20

Table 3.3 *Linear Leonov parameters obtained by fitting the linear relaxation modulus*

Stress Relaxation

In order to verify the description potential of the nonlinear viscoelastic behaviour of polycarbonate, offered by the multi-mode Leonov model, nonlinear relaxation experiments were performed. The results of experimental data and numerical calculations at various strain levels are depicted in Figure 3.14.

Note that all the stress relaxation experiments displayed in Figure 3.14 are essentially nonlinear, since the equivalent stress levels are well above the value of the nonlinearity parameter $\tau_0 = 0.89$ MPa. In contrast, visually, the response up to one per cent strain appears to be quite linear, which illustrates that conclusions about true linear behaviour can only be drawn with great precaution. This becomes evident when describing these nonlinear stress-relaxation experiments. In an ideal stress relaxation experiment, it is assumed that loading takes place instantaneously. In practice, however, loading always occurs over a finite time. In case of true linear behaviour the difference in response between instantaneous and ramp-like loading is negligible after ten times the loading time (Struik, 1978). In contrast, due to the nonlinear behaviour, it was found that, in order to obtain a good agreement between experimental data and calculations, as displayed in Figure 3.14, it was necessary to take into account the exact loading program as

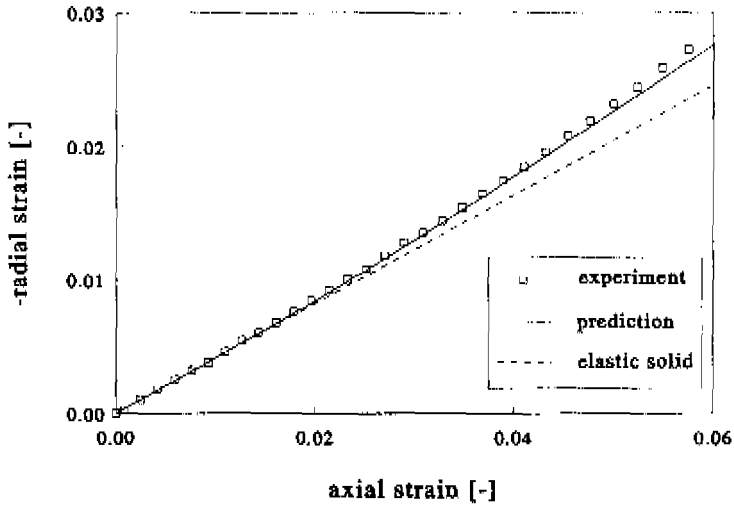

Figure 3.13 *Calculated radial strain during a constant strain rate tensile test (solid line, $\dot{\epsilon} = 10^{-3}\ s^{-1}$), compared to experimental data.*

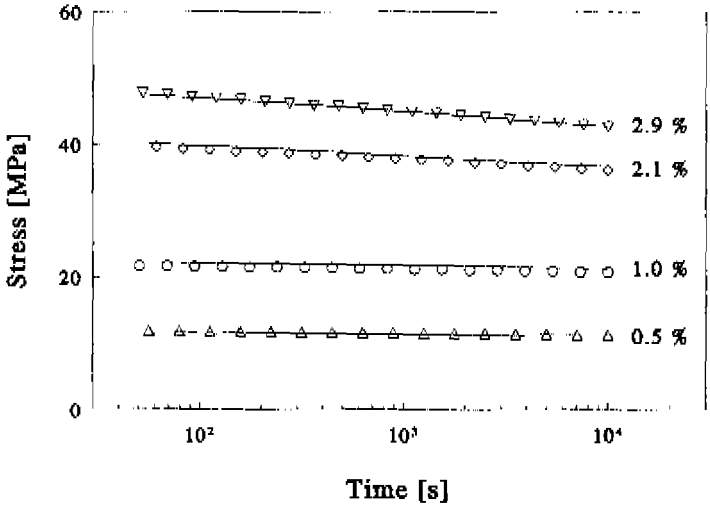

Figure 3.14 *Stress relaxation experiments measured at various strain levels (symbols), compared to model predictions (solid lines).*

used in the experiment. Assuming an instantaneous loading program in the calculations, resulted in differences with the experiments which persisted much longer than ten times the experimental loading time. This kind of "hidden" nonlinear behaviour could be of importance when considering the influence of a short stress pulse on creep behaviour (Struik, 1978) as was also mentioned by McKenna *et al.* (1994).

Shear Test

Another possible verification experiment would be a plane-stress shear test also called "laboratory shear" (see Figure 3.15, the shear strain $\gamma = \tan(\theta)$). The predicted shear stress τ versus shear strain γ data are depicted in Figure 3.15. Note that the "yield points" in tensile and in shear deformation compare very well to a (strain rate dependent) Von Mises criterion. This is due to the fact that the equivalent stress τ_{eq}, which determines the nonlinear response, is proportional to the Von Mises equivalent stress. Unfortunately, at present, we are not able to measure the shear stress response experimentally, nor could we find accurate data in the literature for samples having the same thermal history as our samples.

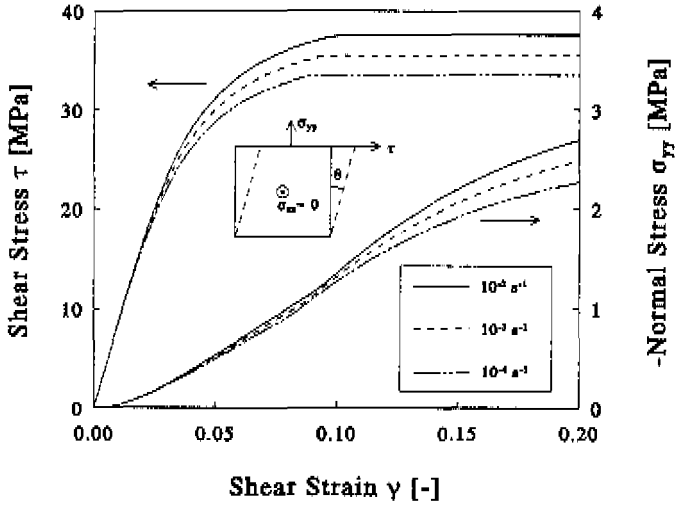

Figure 3.15 *Calculated plane-stress shear test experiments, at various shear strain rates. The left axis is the shear stress and the right axis is the normal stress in the y direction.*

3.5 Discussion and Conclusions

The present research shows that the finite three-dimensional nonlinear viscoelastic behaviour (including yielding) of polycarbonate is completely determined by the (in good approximation constant) bulk modulus, the linear shear relaxation time spectrum and one nonlinearity parameter, which describes how the spectrum is shifted to shorter times upon loading. The nonlinearity parameter (related to the activation volume) and the linear relaxation time spectrum can be determined on basis of creep experiments and constant strain rate experiments using time-stress superposition. Polycarbonate was selected as a model system, since it exhibits only one relaxation mechanism of interest at room temperature (the glass transition). A quantitative three-dimensional constitutive equation for polycarbonate as a model polymer was obtained by approximating the relaxation time spectrum by eighteen Leonov modes. A single Leonov mode is a Maxwell model employing a relaxation time which is dependent on an equivalent stress proportional to the Von Mises equivalent stress. Furthermore, a Leonov mode correctly separates the hydrostatic and deviatoric stress response and accounts for the geometrical complexities associated with simultaneous (large) elastic and plastic deformations.

The present research establishes the linear shear relaxation time spectrum as the key quantity determining the nonlinear viscoelastic behaviour of glassy polymers. Deviatoric stress (and temperature) merely distort the time scale. It should be noted that mechanical properties in general, and viscoelastic behaviour especially, are also profoundly influenced by physical aging (Struik, 1978). It is now well established that, under influence of aging, the creep compliance curve shifts toward longer times, which can be quantified by an aging-time shift factor as defined by Struik (1978). However, all samples used in this study had the same age, which by far exceeded the longest time in the experiment. Therefore, to a first approximation, aging was not taken into account (which will cause the model to be less accurate for differently aged samples). As opposed to aging, it has also been observed that plastic deformation beyond the "yield point" can result in a decrease of the viscosity, leading to intrinsic strain softening and a decrease of the yield stress. This phenomenon is called "rejuvenation" and is thought to be the result of mechanically "deaging" the sample by plastic deformation (Hasan *et al.*, 1993; Struik, 1978). Until now here, however, only the response up to the "yield point" is considered and rejuvenation is not taken into account. Furthermore, the good agreement between experiments and predictions for the stress-relaxation experiments, as well as the applicability of time-stress superposition, suggest that, up to the "yield stress", rejuvenation effects (Struik, 1978; Hasan *et al.*, 1993) are not important (for monotone loading paths and for short loading times relative to the age of the material). In Chapter 6, aging and rejuvenation will be addressed in more detail.

In this Chapter, it was shown that glassy polymers behave essentially as highly nonlinear fluids. In the next Chapter, we will discuss some of the consequences of this nonlinear behaviour with respect to inhomogeneous behaviour.

Chapter 4

Localisation Phenomena

4.1 Introduction

In the previous chapters a detailed constitutive equation was presented, which describes the nonlinear viscoelastic behaviour of polymer glasses up to the "yield" point. In Chapter 5 this description will be extended to include the strain-hardening regime. An important consequence of the highly nonlinear behaviour of polymers in general, and polymer glasses specifically, is their sensitivity to strain localisation, which will be the topic of this Chapter.

Strain localisation, defined loosely as amplification of non-homogeneous behaviour due to small fluctuations of the stress- or strain field, manifests itself in glassy polymers in the form of shear bands and crazes. Shear bands are localized yield zones which can be diffuse or sharp and which grow at constant volume. Crazes can be envisaged as micro-cracks bridged by fibrillar material. Craze growth is accompanied by an increase in volume.

Understanding the initiation and evolution of these strain inhomogeneities is the key to the design of *macroscopic* tough polymeric materials (van der Sanden *et al.*, 1993) and detailed finite element calculations are now used to examine the influence of specific morphologies on the strength of polymeric systems (Huang *et al.*, 1993). Initiation and growth of shear bands results from the combined action of nonlinear material behaviour and the applied boundary conditions, and is now understood qualitatively (Boyce and Arruda, 1990; Wu and van der Giessen, 1994). It appears that strain localisation is inherently related to yielding. The inhomogeneous response is enhanced by intrinsic strain softening, although in some loading conditions the nonlinear yield behaviour itself can already result in the formation of shear bands (Wu and van der Giessen, 1995). Craze initiation is more complex and less well understood. Crazing is a dilatational process and, therefore, most craze-initiation criteria usually involve the hydrostatic stress or strain (Ward, 1990, Chapter 12). In this Chapter, however, it will be shown experimentally that the yield process is the rate-determining step in craze initiation.

4.2 Theory

4.2.1 Craze-Initiation Criteria

Macroscopic brittle fracture of glassy polymers is normally preceded by the formation of *crazes*, small crack-like defects, bridged by fibrillar material. Unlike real cracks, crazes have load bearing capacity and when viewed on a microscopic level, they display large plastic deformations. Therefore, crazes are the most important source of fracture toughness in brittle glassy polymers, even though the volume fraction crazes during fracture is generally low. It is, therefore, not surprising that a vast amount of research has been done on all aspects of crazing: craze nucleation, growth and failure, the micro-structure of crazes, the influence of molecular parameters, etc., and a number of excellent reviews are available (Kramer (1983); Kramer and Berger (1990) and Kinloch and Young (1985), Chapter 5).

Craze initiation has received relatively little attention. It is generally accepted that craze initiation is enhanced by both the hydrostatic and the deviatoric stress state, and, consequently, craze-initiation criteria normally involve both the first and the second invariant of the stress tensor (Ward, 1990). Unfortunately, two factors complicate the search for a macroscopic craze criterion. First, it is well known that crazes always initiate on surface grooves or small imperfections in the polymer, where the exact state-of stress (and strain) are unknown. Second, especially at low stresses, there can be a considerable time lag between load application and the occurrence of the first visible craze, which indicates that craze initiation is a time-dependent phenomenon. Therefore, a meaningful craze criterion can probably only be defined on a local scale, in a well defined micro-structure, where the state-of stress is known (Kambour, 1986). Such a local criterion would still be very useful in numerical aided design of morphologies where shear yielding prevails crazing.

Figure 4.1 depicts some of the microscopic events that are likely to be involved in craze nucleation (Kramer, 1983). First, plastic deformation starts at a local stress concentration. The nonlinear nature of the yield process and the strain softening character of polymer glasses will result in a localisation of deformation as the plastic strain increases. Since the material at some distance of the local deformation zone is relatively undeformed, lateral stresses will develop. At this stage two things can happen. First, the strain-hardening response of the material can stabilize the strain-localisation process and the micro-shear band will spread out. Second, it has been shown (Argon and Hannoosh, 1977) that the hydrostatic stress required to plastically expand a micro-porous region, is greatly reduced if the material is in a state of flow. Therefore, if the lateral stresses become high enough, the material in the deformation zone will cavitate, and craze nucleation has been accomplished.

It is difficult to predict which of the events in Figure 4.1 will be the rate-determining step in craze nucleation. In one of the most detailed studies on craze

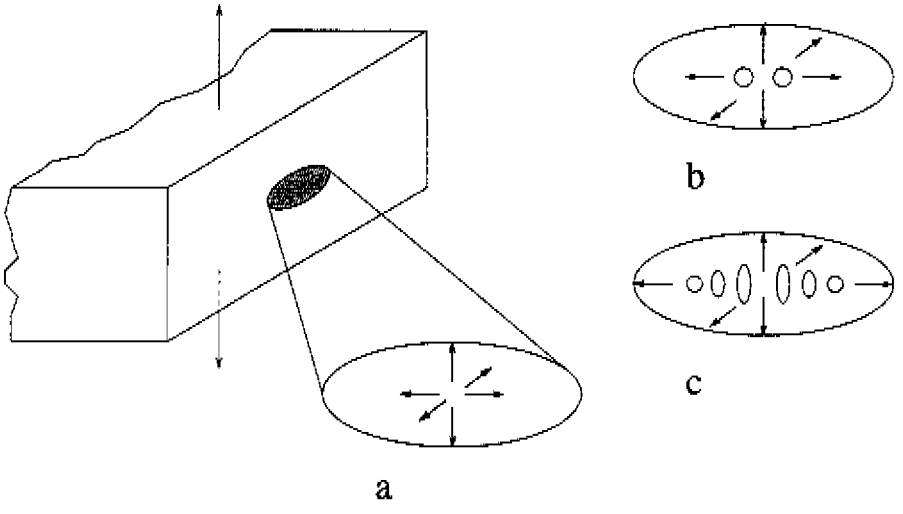

Figure 4.1 *Schematic drawing of microscopic events involved in craze nucleation:* **a** *Formation of a localized surface plastic zone and buildup of lateral stresses.* **b** *Cavitation of the plastic zone.* **c** *deformation of the polymer ligaments between voids and coalescence of individual voids to form a void network (after Kramer, 1983).*

initiation, Argon and Hannoosh (1977), it was argued that nucleation of voids is a thermally activated process. The activation-free energy for pore formation consists out of two terms: the formation of a slip patch, which is started and arrested by molecular inhomogeneities, followed by the formation of a stable round cavity by plastic expansion of micro-porous regions inside the slip patch. This model was criticized by Kramer (1983), because it ignores both surface-tension and chain-entanglement effects. Furthermore, in the study by Argon and Hannoosh (1977) the true kinetics of craze initiation were obscured by the considerable time lag between the void formation and visible occurrence of the first craze. The void-initiation time could only be estimated indirectly by assuming a power-law relation between the equivalent stress- and strain during the plastic expansion of the initial void until it is large enough to reflect light.

In order to avoid the difficulties associated with the unknown state-of stress, Dekkers (1985) studied craze initiation around a well-adhering glass bead. Linear elastic finite-element calculations were used to determine the local state-of stress- and strain. Comparing these calculations with the spatial arrangement of crazes around the glass beads, it was concluded that the major principle stress and the dilatation were the most likely candidates for a craze-initiation criterion. In this study, the kinetics of craze initiation were not considered. Moreover, the assump-

tion of linear elastic behaviour up to the point of craze initiation is questionable.

The concept of a local, time-independent craze-initiation criterion is appealing and could be very useful in finite element calculations on a microscopic level. Unfortunately, a direct experimental verification of the existence of such a criterion on a macroscopic level is not possible. However, defining a local time-independent craze-initiation criterion implies that the rate-determining step in craze-initiation is either the initiation of strain localisation, or the evolution of the localized plastic zone up to the point of voiding. In the next section, it will be argued that the rate dependence of the initiation of strain localisation in glassy polymers is determined by the nonlinear yield behaviour. Therefore, if strain localisation, leading to the formation of a slip patch, is the rate-determining step in craze initiation, then the kinetics of craze initiation and the nonlinear yield behaviour should be identical. The latter statement is accessible to direct (macroscopic) experimental verification, as it will be shown in Section 4.4.

4.2.2 Strain Localisation in Polymer Glasses

Strain localisation in polymer glasses is the result of the combined action of nonlinear material response, comprising the nonlinear yield behaviour, intrinsic strain softening and strain hardening, and the applied boundary conditions. The *initiation* of strain localisation, however, is only determined by the yield process and the applied boundary conditions. Moreover, the rate dependence (the "kinetics") of the yield behaviour is fully described by the Eyring process (Chapter 2, Eq. (2.52)), and is not influenced by strain hardening or strain softening. A rigorous justification of these statements would require a full stability analysis of the nonlinear flow problem (Rice, 1977; Anand *et al.*, 1987). Here, however, a more qualitative argument will be used to illustrate the influence of the constitutive behaviour on strain localisation (Bowden, 1970). To start, it will be assumed that, at the yield point, the material behaviour can be approximated by a Kelvin-Voigt model, representing the nonlinear flow behaviour and the strain-hardening response in shear (see Figure 4.2), which results from a rubber-elastic response of the "entanglement" network, see Chapter 5.

At the yield point, to a good approximation, the total strain rate is equal to the plastic strain rate. According to Figure 4.2, the relation between the shear-flow stress τ and the plastic strain rate $\dot{\gamma}_p$ becomes:

$$\dot{\gamma}_p = \frac{\tau - G_r \gamma_p}{\eta((\tau - G_r \gamma_p), \gamma_p)} \tag{4.1}$$

where G_r is the "rubbery" strain-hardening modulus (see Chapter 5).

All the nonlinear flow characteristics (the "kinetics" of the yield process) are

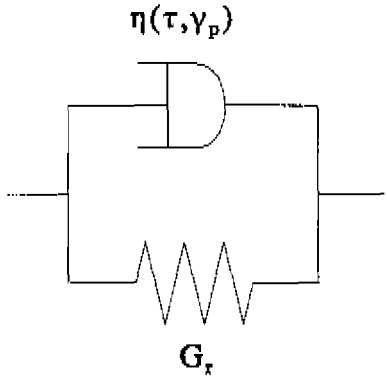

Figure 4.2 *Schematic drawing of the mechanical behaviour of a polymer glass at the yield point. The dashpot depicts the nonlinear flow behaviour, which depends on stress and plastic strain, and the (neo-Hookean) spring with shear modulus G represents the entropic strain hardening.*

incorporated in the viscosity function η (Figure 4.2):

$$\eta = \eta_0 a_\sigma a_\gamma \tag{4.2a}$$

$$a_\sigma(\tau) = \frac{\left(\frac{\tau}{\tau_0}\right)}{\sinh\left(\frac{\tau}{\tau_0}\right)} \tag{4.2b}$$

$$a_\gamma = \exp(-D) \tag{4.2c}$$

$$\dot{D} = h\left(1 - \frac{D}{D_\infty}\right)\dot{\gamma}_p \tag{4.2d}$$

The function $a_\sigma(\tau)$ is the Eyring-shift factor, which describes stress activated flow, as discussed in Chapters 2 and 3. The last two relations, Eqs. (4.2c) and (4.2d), present a phenomenological description of intrinsic strain softening, using a scalar internal variable, D, which is related to the number density of shear transformation sites (areas of increased mobility due to a high free volume) (Hasan *et al.*, 1993). The constants D_∞ and h are essentially fitting parameters. The shift factor a_γ can be expressed as a function of the plastic strain γ_p by integration of Eqs. (4.2c) and (4.2d):

$$a_\gamma = \exp\left[-D_\infty\left(1 - \exp\left[-\frac{h}{D_\infty}\gamma_p\right]\right)\right] \tag{4.3}$$

In Chapter 6, the subject of intrinsic strain softening will be discussed in more detail.

At high stress levels, the hyperbolic sine function in Eq. (4.2b) can be approximated by an exponential. Using Eqs. (4.1) and (4.2), the plastic strain rate can then be written as:

$$\ln \dot{\gamma}_p = \ln\left(\frac{\tau_0}{2\eta_0 a_\gamma}\right) + \frac{\tau - G_r\gamma_p}{\tau_0} \tag{4.4}$$

The nonlinear character of the Eyring process is depicted in an Eyring plot of the yield stress versus the logarithm of the plastic strain rate (Figure 4.3). From this plot, it is clear that the Eyring process can trigger inhomogeneous behaviour. A small fluctuation of the stress field will result in a large deviation of the local plastic strain rate, depending on the value of the activation volume (which determines the slope τ_0, see Figure 4.3). Dependent on the specific boundary conditions, this can lead to strain localisation.

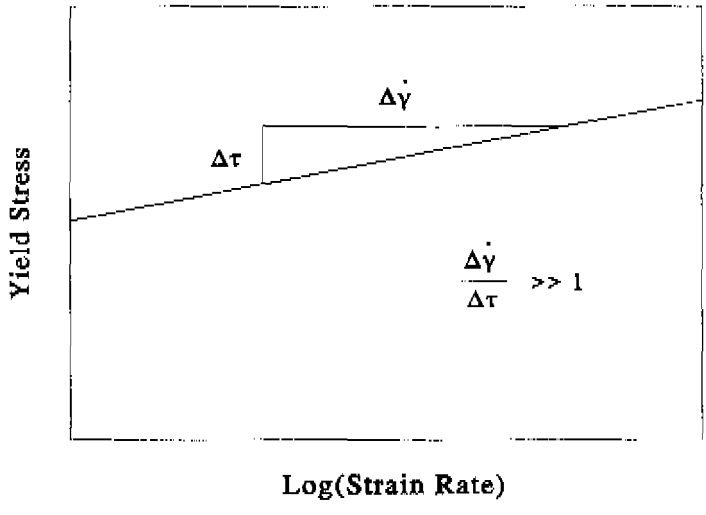

Figure 4.3 *A graphical representation of the nonlinear yield behaviour as described by the Eyring process. A small fluctuation in the stress results in a large deviation of the plastic strain rate (logarithmic x-axis!).*

Crazing, as an extreme form of strain localisation, is not determined by the Eyring process alone. Figure 4.4 depicts a combined Eyring plot of several polymers. From this Figure it can be seen, that polymers sensitive to crazing, like polystyrene, can have a smaller activation volume (larger τ_0) than polymers like

polycarbonate, which are insensitive to crazing and generally fail through shearing. Intrinsic strain softening and the strain hardening, amplify respectively sta-

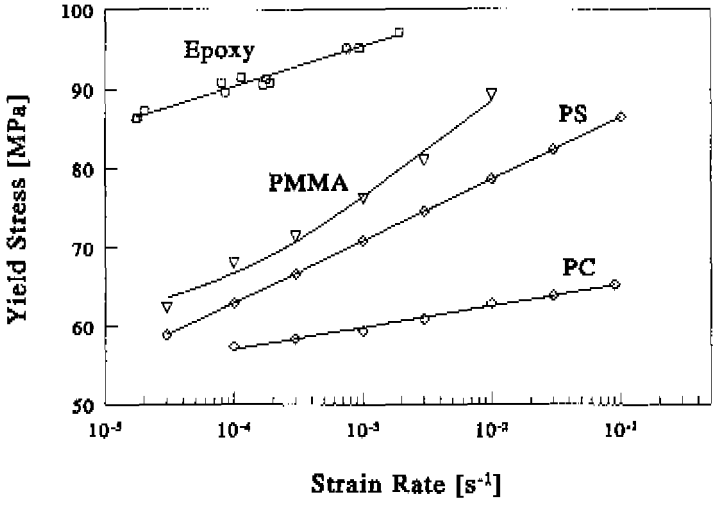

Figure 4.4 *A combined Eyring plot for several well known polymers. The polystyrene data are a prediction, using Eq.* (4.13).

bilize small stress fluctuations. This is depicted in Figures 4.5 and 4.6, where some typical values of the material constants in Eq. (4.4) for polycarbonate were used (Timmermans *et al.*, 1995), to show the effect of strain softening- and hardening on the plastic strain as a function of time, at different stress levels.

As is clear from this Figure, the plastic strain as a function of time increases dramatically if the material displays strain softening behaviour. Dependent on the balance between strain hardening and strain softening, and the specific boundary conditions, this will promote strain localisation. Particularly, elimination of strain softening will result in a more homogeneous deformation behaviour, as was also mentioned by Argon and Hannoosh (1977). This concept will be used in Chapter 5, where the strain-hardening behaviour is investigated by means of large homogeneous deformations, obtained via elimination of strain softening.

From Eq. (4.1) it can also been seen that the value of the strain-hardening modulus G_r determines the level at which the plastic strain stabilizes. A high value of G_r promotes homogeneous behaviour. Moreover, a high strain-hardening modulus is indicative of a dense entanglement network. In Chapter 3, it was shown that the yield point can be envisaged as a stress-induced glass transition. Therefore, a plastically expanding zone is effectively a rubber. From rubber-cavitation theories, (Gent and Wang, 1995) it is known that dense networks have

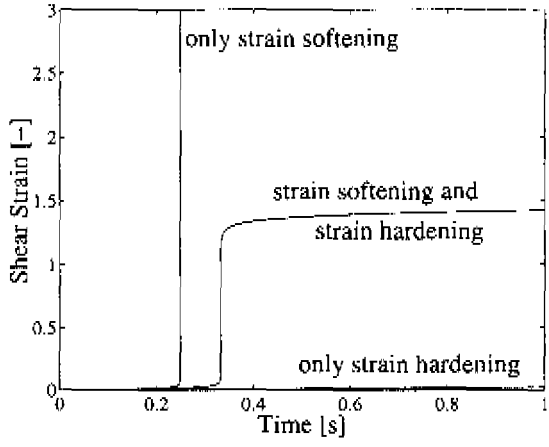

Figure 4.5 *Plastic strain as a function of time, according to Eqs. (4.1) and (4.2), at a shear stress $\tau = 40$ MPa. Parameters used for polycarbonate: $D_\infty = 43$ [-] and $h = 120$ [-] (Timmermans et al., 1995), $G_r = 26$ MPa (Chapter 5), $\tau_0 = 0.888$ MPa and $\eta_0 = 4.656 \cdot 10^{20}$ MPa-s (Chapter 3).*

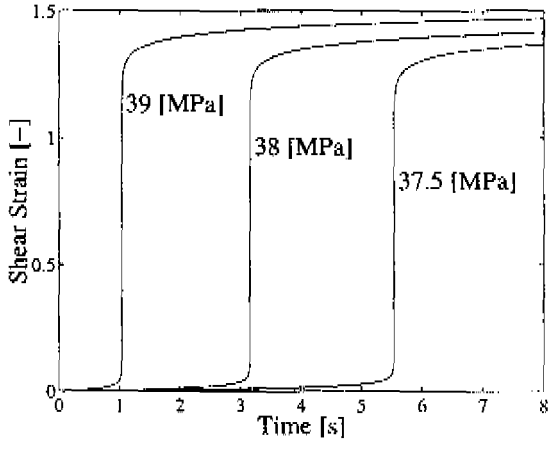

Figure 4.6 *Plastic strain as a function of time, according to Eqs. (4.1) and (4.2), at different constant shear stress. Parameters as in Figure 4.5.*

a higher cavitation stress. As a consequence, a high strain-hardening modulus will inhibit voiding of the slip patch. An alternative point of view is that the cavitation stress is higher, because the covalent-bond contribution to the surface energy of a glassy polymer increases with entanglement density (Kramer, 1983). Therefore, due to its dense entanglement network, polycarbonate is not very sensitive to crazing, despite its rather strong strain-softening response and its small activation volume.

Using Eq. (4.4), the sensitivity of the local plastic strain rate to deviations in the stress field, can be expressed as:

$$\frac{d(\ln \dot{\gamma}_p)}{d\tau} = \frac{1}{\tau_0} \tag{4.5}$$

Thus, the kinetics of the yield process, responsible for the *initiation* of strain localisation, is fully described by the Eyring process and, in particular, independent of strain hardening- and softening. This will be verified experimentally in Chapters 5 and 6. Consequently, if the initiation of strain localisation is the rate-determining step in craze initiation, the kinetics of craze initiation should be described by the same Eyring parameters as the yield process.

4.3 Experimental

The polystyrene grade (Styron 638^{TM}), used in this study, was specially selected for its extreme brittle behaviour, creating a situation where the craze-initiation stress is approximately equal to the macroscopic breaking stress. The strain rate dependence of the craze-initiation stress was studied using biaxial flexure (ball-ring test, (de Smet *et al.*, 1992)). In these tests the maximum stress region is limited to a very small volume, thus minimizing the influence of surface flaws and other defects on the experimentally determined strength. The biaxial flexure tests were performed on 3 mm thick polystyrene disks with a diameter of 45 mm. The support (ring) consisted of thrust bearing of 30 mm diameter with balls of 3 mm radius. The load was applied in the centre of the disk with a 3 mm radius ball. As the loading path was linear, the nominal fracture stress σ_f, and the corresponding strain rate $\dot{\epsilon}$ were evaluated according to linear elastic theory (Roark and Young, 1984):

$$\sigma_f = \frac{3(1+\nu)F_f}{4\pi d^2}\left[1 + 2\ln\left(\frac{a}{b}\right) + \left(\frac{1-\nu}{1+\nu}\right)\left(\frac{a^2}{R^2}\right)\left(1 - \frac{b^2}{2a^2}\right)\right] \tag{4.6a}$$

$$\dot{\epsilon} = \frac{1}{t}\left(\frac{1-\nu}{E}\right)\sigma_f \tag{4.6b}$$

where a is the support radius, b the effective contact radius, R the specimen radius, d the specimen thickness, E Young's modulus, F_f the force at fracture,

t the loading time and ν Poisson's ratio. The effective contact radius b can be calculated from the contact radius according to Hertz, c (Westergaard, 1952, page 163):

$$b = \sqrt{1.6c^2 + t^2} - 0.675t \tag{4.7}$$

To study the strain rate dependence and pressure sensitivity of the yield behaviour of polystyrene two other test methods were employed:

1. Tensile tests under a superimposed hydrostatic pressure (500 MPa), performed on polystyrene specimens with dimensions: $35 \times 10 \times 2$ mm. The experiments were performed with kind permission at the IRC of Polymer Science & Technology (University of Leeds). The experimental set-up at the IRC has been described extensively by Sweeney *et al.* (1988).

2. Planar compression tests, performed on polystyrene specimens with a gauge length of $40 \times 12 \times 3$ mm. The specimens were supported by two Teflon covered steel plates to create a plane strain condition.

All specimen were produced by compression moulding and were carefully polished to minimize the effect of surface defects.

4.4 Results

Uniaxial tensile tests under superimposed hydrostatic pressure, and planar compression tests were performed, in order to suppress crazing (Matsushige *et al.*, 1975). The yield stresses obtained from these tests and the results of the fracture tests are depicted in Figure 4.7.

A convenient way to verify whether the rate dependence of the yield and fracture process (craze initiation) are identical, is to compare the results of Figure 4.7 in a single Eyring plot. Because different loading geometries are involved, the state-of stress and the strain rate at the yield- and fracture points must be expressed in terms of *equivalent* stress and strain rate, respectively. The resulting Eyring plot is depicted in Figure 4.8.

The pressure-modified Eyring relation (Ward, 1990, Chapter 11) in terms of equivalent quantities, is given by (compare to Eqs. (2.45) and (2.46)):

$$\dot{\gamma}_{eq} = \frac{1}{A} \sinh\left(\frac{\tau_{eq}}{\tau_0}\right) \exp\left(\frac{-P}{\omega_0}\right) \tag{4.8}$$

which at high stress leads to:

$$\tau_{eq} = \tau_{eq}^0 + \tau_0 \ln \dot{\gamma}_{eq} + \mu P \tag{4.9}$$

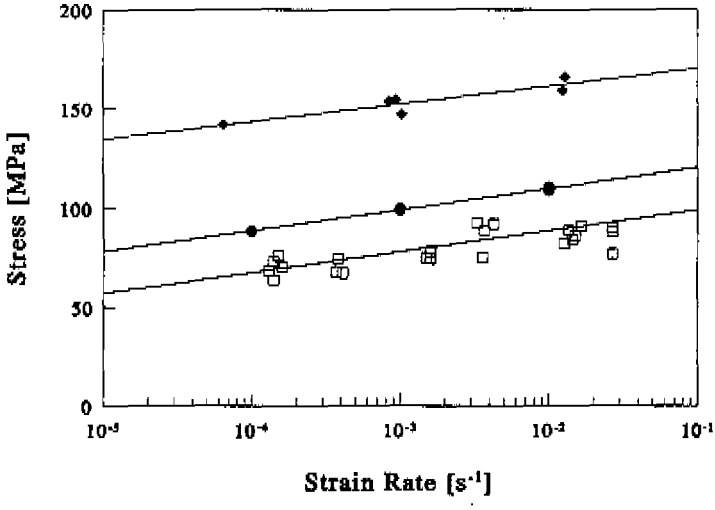

Figure 4.7 *Combined plot of yield stress (closed symbols) and fracture stress (open symbols) as a function of deformation rate. Yield stress from planar compression tests (•) and uniaxial tensile tests under superimposed hydrostatic pressure (♦). Fracture stress from ball-ring tests (□). The solid lines are visual fits.*

where $\tau_{eq}^0 = \ln(2A)$ is a constant, P the hydrostatic pressure, and $\mu = \tau_0/\omega_0$, with ω_0 related to the pressure activation volume. In general loading situations, the hydrostatic pressure P and the equivalent (yield) stress τ_{eq}, are not independent. For example, in case of uniaxial extension under a superimposed pressure P_0, τ_{eq} and P are equal to:

$$\tau_{eq} = \sqrt{\frac{1}{2} II_{T^d}} = \frac{1}{3}\sqrt{3}\sigma \tag{4.10}$$

$$P = P_0 - \frac{1}{3}\sigma \tag{4.11}$$

Therefore, P can be written as a function of τ_{eq}:

$$P = P_0 + \alpha\tau_{eq} \tag{4.12}$$

with $\alpha = -\frac{1}{3}\sqrt{3}$. For other loading geometries, the coefficient α can be calculated in a similar way, see Table 4.1.

Introduction of the coefficient α, Eq. (4.12), into the Eyring flow equation, Eq. (4.9), leads to:

$$\tau_{eq} = \frac{\tau_{eq}^0 + \tau_0 \ln \dot{\gamma}_{eq} + \mu P_0}{1 - \mu\alpha} \tag{4.13}$$

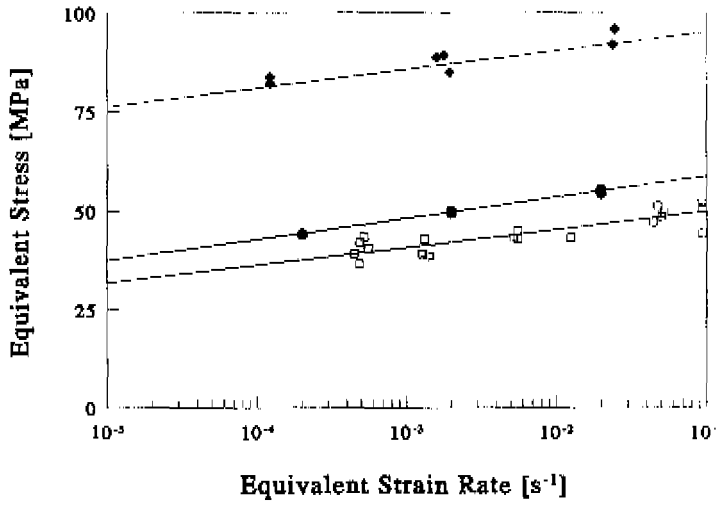

Figure 4.8 *Equivalent stress versus equivalent strain rate for polystyrene (Styron 638^{TM}) in various loading geometries. Open symbols: crazing; closed symbols: yielding (see Figure 4.7). The solid lines are a best fit of all data according to Eq.* (4.13)*, using a single set of Eyring parameters.*

Loading geometry	Geometry factor α
Uniaxial extension	$-\frac{1}{3}\sqrt{3}$
Biaxial extension	$-\frac{2}{3}\sqrt{3}$
Planar compression	$\frac{1}{2}\sqrt{2}$

Table 4.1 *Geometry factor α for the different loading geometries in Figure 4.8.*

This equation facilitates a direct interpretation of the experimental data, presented in Figure 4.8. The drawn lines in this figure, are a best fit of all data using a single set of Eyring parameters: $\tau_{eq}^{0} = 60.0$ MPa, $\tau_0 = 2.2$ MPa and $\mu = 0.09$ [-]. From Figure 4.8 it is clear that this single set of parameters accurately describes both yield and craze initiation. In our opinion, this is a strong indication that the rate-determining step in craze initiation is the formation of a localised plastic zone. The evolution and cavitation of these patches are either relatively fast or even time-independent processes.

4.5 Discussion and Conclusions

In this Chapter, it was illustrated how the combined action of nonlinear plastic flow behaviour, as described in Chapters 2 and 3, strain hardening and intrinsic strain softening, can give rise to strain localisation. It was argued that the *initiation* of strain localisation is only determined by the yield process. The aim of this Chapter was to investigate whether craze initiation can be envisaged as a plastic localisation process, followed by (time-independent) cavitation of the deformed zones. An extremely brittle polystyrene grade was selected as a model material, to ensure that, during a fracture test, the time between craze-initiation and macroscopic fracture is negligible small. A ball-ring test and a three-point bending test were used to minimize the effect of inhomogeneities on the fracture process. The strain rate dependence of the yield process was determined using plane-strain compression tests and uniaxial tensile tests under superimposed hydrostatic pressure. Expressing the results of these tests in equivalent quantities, it was shown that both fracture and yield have the same strain rate dependence, which is described by one Eyring process. This is a strong indication that the occurrence of small deformation zones ("slip patches") is indeed the rate-determining step in craze initiation. The evolution of these micro-shear bands is determined by the combined action of constitutive behaviour, as described in this thesis, and the local boundary conditions. Given a certain micro-structure, the evolution of these slip patches could in principle be calculated using finite element methods, employing the detailed constitutive equation discussed in this thesis. This offers possibilities for defining a local craze-initiation criterion, by comparing these detailed finite element calculations (instead of linear elastic calculations as in Dekkers (1985)) with experimental craze studies. Such a local craze-initiation criterion is essential in computer-aided design of new heterogeneous polymer systems, where the morphology is optimized in such a way that shear yielding prevails crazing.

Chapter 5

Strain-Hardening Behaviour

5.1 Introduction

A characteristic feature of polymer systems is their composite structure on a molecular level, consisting out of covalent bonded chains, held together by secondary forces. Stress-activated segmental motion is responsible for the nonlinear viscoelastic behaviour, as discussed in Chapters 2 and 3. In particular, it was argued in Chapter 3, that the yield point can be viewed upon as a stress-induced glass transition. The primary bonds survive the segmental jump process, and give rise to steric hindrance ("chains cannot mutually cross"), which results in strain-hardening behaviour, the topic of this Chapter. This reinforcing effect of the covalent chains, prevents segmental motion from leading to fatal fracture like in low molecular weight glasses. Instead, the deformation is spread throughout the material, and leads to crazing or shear bands (see Chapter 4). For this reason, polymers are intrinsically very tough materials, with a critical energy release rate which is orders of magnitude larger than the (Van der Waals) surface energy.

The steric hindrance between the polymer chains is also of prime importance for the flow behaviour of polymer melts, where all the secondary bonds are broken by thermal energy. It is well known, that, above a certain molecular weight and on a restricted time scale, a polymer melt behaves like a rubbery solid (Larson, 1988, Chapter 4). Comparing this behaviour to that of a real (chemically cross-linked) rubber, leads to the definition of *entanglements*. Entanglements are envisaged as physical knots, which can not unravel on the time scale of the experiment. The molecular weight between these entanglements is calculated from the "stiffness" (plateau modulus) of the melt, using the classical theory of rubber elasticity. In this way, the molecular weight between entanglements, M_e, provides a scalar measure of the diffuse steric hindrance between the covalent chains.

It is, therefore, not surprising that the concept of entanglements play an important role in the large-strain deformation behaviour of polymer solids as well. For example, it is now widely accepted, that strain-hardening in glassy poly-

mers originates from the rubber-elastic response of the entanglement network. Moreover, it is often assumed, that the entanglement network, like a chemically cross-linked network, has a limited extensibility. This leads to the concept of a *maximum draw ratio* λ_{max} (Allison and Ward, 1967), which can be estimated from the maximum extensibility of a single strand in the entanglement network. It was shown by Donald and Kramer (1982b, 1982a) that this maximum draw ratio of the entanglement network correlates remarkably well with the extension ratio of craze fibrils and within shear bands.

Haward and Thackray (1968) were the first to incorporate these two features of strain-hardening behaviour, a rubber-elastic response and finite extensibility, into a constitutive equation. This one-dimensional equation was extended to the three-dimensional "BPA model" by Boyce *et al.* (1988), who used the "three-chain model" (James and Guth, 1943; Wang and Guth, 1952) to describe the strain-hardening response. The BPA model was later refined with respect to strain hardening by introducing better representations of the spatial distribution of molecular chains, leading to the "eight-chain model" (Arruda and Boyce, 1993b), and the "full-chain model" (Wu and van der Giessen, 1993).

Although finite extensibility is relevant for a *chemically* cross-linked rubber, it seems less obvious that it also applies to a (thermoplastic) glassy polymer, which can ultimately flow. In fact, for a number of polymers, the upswing in strain-hardening response, associated with finite extensibility, was not observed experimentally, G'Sell *et al.* (1992). In this Chapter, the large strain behaviour of polycarbonate will be studied experimentally, in order to determine the dependence of strain hardening on the state-of deformation. Predeformation above the glass-transition temperature and mechanical preconditioning are used to ensure homogeneous behaviour.

5.2 Theory

5.2.1 Strain-Hardening Behaviour

A typical stress-strain curve of a glassy polymer below the glass-transition temperature is depicted in Figure 5.1. Haward and Thackray (1968) captured this behaviour in a constitutive equation, assuming that the isothermal deformation behaviour of a glassy polymer below the glass-transition temperature can be decomposed in an elastic region, followed by rate-dependent yielding, due to stress-activated segmental motion and a (rubber) elastic strain-hardening part, due to orientation of the entanglement network (see Figure 5.1).

It is now generally accepted that the strain-hardening response in (glassy) polymers originates from the rubber elastic response of the entanglement network, although quantitative agreement seems to be lacking (Haward, 1993). Therefore, first some of the rubber elastic network models, which are used to describe strain-

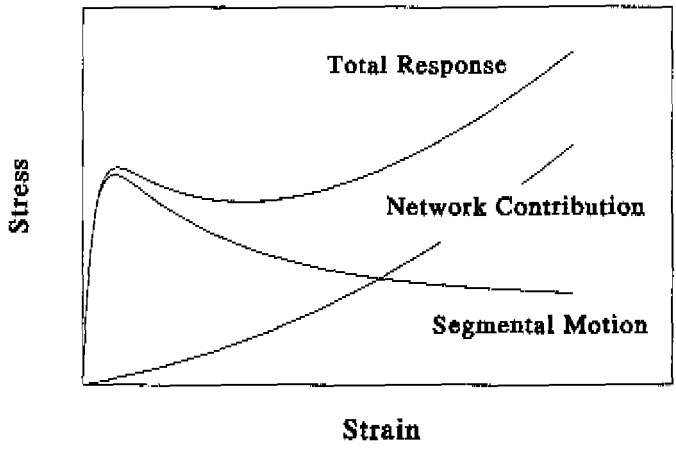

Figure 5.1 *a. Schematic decomposition of a (simplified) stress-strain curve of a glassy polymer, showing an initial elastic region, followed by (rate-dependent) yield behaviour (including strain-softening), and strain-hardening behaviour.*

hardening, will be reviewed.

5.2.2 Rubber Elastic Network Models

In the classical theory of rubber elasticity it is assumed that the internal energy remains constant upon isochoric deformations. Therefore, at isothermal conditions, the thermodynamic force, Eq. (2.38b), is only dependent on changes in entropy:

$$\mathbf{M} = \left(\frac{dA}{d\bar{\bar{\mathbf{B}}}}\right)_T = \left(\frac{dU}{d\bar{\bar{\mathbf{B}}}}\right)_T - T\left(\frac{dS}{d\bar{\bar{\mathbf{B}}}}\right)_T = -T\left(\frac{dS}{d\bar{\bar{\mathbf{B}}}}\right)_T \tag{5.1}$$

The change in entropy is a consequence of the distortion of the molecular network and can be calculated from statistical mechanical arguments (Treloar, 1975). The most simple expression follows from the so-called "Gaussian network approximation", where it is assumed that the end-to-end distance vectors of a chain between two cross-links, are described by a Gaussian distribution function (James and Guth, 1943). In this case, the entropy will depend on deformation as:

$$S = -\frac{1}{2}nk(I_{\bar{B}} - 3) \tag{5.2}$$

where n is the number of (randomly oriented) chains per unit volume in the network, and k is Boltzmann's constant. Using the evolution equation for the

isochoric elastic strain, Eq. (2.39b), and the expression for the Cauchy-stress tensor, Eq. (2.30), the Gaussian network approximation leads to neo-Hookean behaviour:

$$\mathbf{T}^d = G\,\tilde{\mathbf{B}}^d \tag{5.3}$$

with the shear modulus $G = nkT$.

A more accurate expression for the configurational entropy of a stretched molecular chain, taking into account the effect of finite extensibility, was first derived by Kuhn and Grün (1942). Considering a single ideal chain, containing N links of length l, having a root-mean-square distance $\sqrt{< r_0^2 >} = \sqrt{N}\,l$ and a maximum draw ratio $\lambda_{max} = \sqrt{N}$, they derived an expression for the Helmholtz-free energy as a function of draw ratio λ:

$$A = nkT\left(\frac{\lambda}{\sqrt{N}}\beta + \ln\left[\frac{\beta}{\sinh\beta}\right]\right) - A_0 \tag{5.4}$$

$$\beta = \mathcal{L}^{-1}\left(\frac{\lambda}{\sqrt{N}}\right) \tag{5.5}$$

where A_0 is an arbitrary constant and $\mathcal{L}(\beta)$ is the Langevin function defined by:

$$\mathcal{L}(\beta) = \coth\beta - \frac{1}{\beta} \tag{5.6}$$

A useful expression is the first Padé approximant of the inverse Langevin function (Cohen, 1991):

$$\mathcal{L}^{-1}(x) \approx x\frac{3 - x^2}{1 - x^2} \tag{5.7}$$

For elastic behaviour, at isothermal conditions, the total power input $\sigma\dot{\varepsilon}$, with $\dot{\varepsilon} = \dot{\lambda}/\lambda$, is equal to the rate-of-elastic energy storage $\dot{A} = (\partial A/\partial\lambda)\dot{\lambda}$. Hence, the stress-strain relation becomes:

$$\sigma = \lambda\left(\frac{\partial A}{\partial\lambda}\right)_T = kT\sqrt{N}\lambda\mathcal{L}^{-1}\left(\frac{\lambda}{\sqrt{N}}\right) \tag{5.8}$$

In this equation, the stress becomes infinitely large, as the draw ratio λ approaches its limiting value $\lambda_{max} = \sqrt{N}$. Invoking the affine deformation scheme, Wu and van der Giessen (1993) extended this one dimensional equation to describe three-dimensional behaviour, by calculating the exact spatial distribution of the molecular chains. This so called "full chain" model, though mathematically exact, has the disadvantage that it can not be solved analytically. Three-dimensional extensions of Eq. (5.8) that lead to analytical expressions, were obtained by sampling the orientational distribution function only in a discrete number of directions, like the "three-chain" model of James and Guth (1943) (see also Wang and Guth (1952)),

and the "eight-chain" model of Arruda and Boyce (1993b). The "four chain" model of Flory and Rehner, Jr. (1943) also approximates the real distribution of orientations, but does not lead to an analytical equation.

The three-chain model was obtained by assuming that Eq. (5.8) can be used to calculate the principle stresses σ_i from the principle stretches λ_i:

$$\sigma_i = \frac{1}{3} nkT\sqrt{N}\lambda_i \mathcal{L}^{-1}\left(\frac{\lambda_i}{\sqrt{N}}\right) \tag{5.9}$$

with $n/3$ chains per unit volume in each of the principle stretch directions.

In the eight-chain model, Eq. (5.4) is assumed to hold, multiplied by the number of chains per unit volume, n, and using an average chain-stretch parameter λ_{chain}:

$$\lambda_{chain} = \frac{1}{\sqrt{3}}\sqrt{\lambda_1^2 + \lambda_2^2 + \lambda_3^2} = \frac{1}{\sqrt{3}}\sqrt{I_{\bar{B}}} \tag{5.10}$$

Here, it should be noted that $\sqrt{I_{\bar{B}}/3}$ equals the average change in length of a line element at a point P, averaged over all possible orientations (Macosko, 1994, Chapter 1). The thermodynamic force for the eight-chain model becomes:

$$\mathbf{M} = \frac{\partial A}{\partial \tilde{\mathbf{B}}} = \left(\frac{\partial A}{\partial \lambda_{chain}}\right)\left(\frac{\partial \lambda_{chain}}{\partial I_{\bar{B}}}\right)\left(\frac{\partial I_{\bar{B}}}{\partial \tilde{\mathbf{B}}}\right) \tag{5.11}$$

where:

$$\left(\frac{\partial A}{\partial \lambda_{chain}}\right) = nkT\sqrt{N}\mathcal{L}^{-1}\left(\frac{\lambda_{chain}}{\sqrt{N}}\right) \tag{5.12}$$

$$\left(\frac{\partial \lambda_{chain}}{\partial I_{\bar{B}}}\right) = \frac{1}{6}\sqrt{3} I_{\bar{B}}^{-\frac{1}{2}} = \frac{1}{6\lambda_{chain}} \tag{5.13}$$

$$\left(\frac{\partial I_{\bar{B}}}{\partial \tilde{\mathbf{B}}}\right) = \mathbf{I} \tag{5.14}$$

The constitutive relation for the eight-chain model then follows from the the evolution equation for $\tilde{\mathbf{B}}$, Eq. (2.39b), and substitution of Eqs. (5.11)-(5.14) in the general expression for the stress tensor, Eq. (2.30)[1]:

$$\mathbf{T}^d = \frac{1}{3} nkT\sqrt{N}\mathcal{L}^{-1}\left(\frac{\lambda_{chain}}{\sqrt{N}}\right)\frac{1}{\lambda_{chain}}\tilde{\mathbf{B}}^d = G(I_{\bar{\mathbf{B}}})\bar{\mathbf{B}}^d \tag{5.15}$$

Note that the eight-chain model can be envisaged as a neo-Hookean relation, employing a shear modulus which is dependent on the first invariant of $\tilde{\mathbf{B}}$.

[1] In the original derivation (Arruda and Boyce, 1993b), the total -instead of the isochoric strain was used, under the assumption of incompressible behaviour. This leads to a relation between the extra stress tensor and the Green-Lagrange strain tensor, and is, therefore, slightly different from Eq. ((5.15)). This applies also to the other rubber-elastic models in this Chapter.

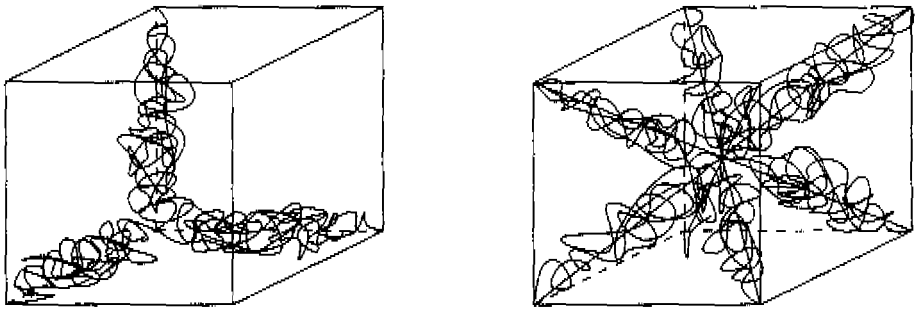

Figure 5.2 *Schematic drawing of (a) the three-chain model and (b) the eight-chain model.*

A schematic view of the three-chain model and the eight-chain model is given in Figure 5.2. From this figure it is clear that the three-chain model samples only the principle strain directions, while the eight-chain model samples none of the principle strain directions. Therefore, the three-chain model will overestimate the network stiffness, whereas the eight-chain model underestimates the network response. Since the response of the full-chain model is always between the upper and lower bound provided by the three and eight-chain model, Wu and van der Giessen (1992) proposed a simple mixing rule:

$$\sigma_i^{full-ch} = (1-\rho)\sigma_i^{3-ch} + \rho\sigma_i^{8-ch} \tag{5.16}$$

$$\rho = 0.85\frac{\lambda_{max}}{\sqrt{N}} \tag{5.17}$$

where σ_i are the principle stresses and λ_{max} is the maximum principle stretch.

It should be noted that Eq. (5.8), which is the starting point of all non-Gaussian network theories, was criticized by Flory (Flory, 1988, Chapter 8) for a number of reasons. First, from statistical mechanics point of view, Eq. (5.8) is only correct in the limit of a large number of segments N and at small chain stretch ($\lambda/\sqrt{N} \approx 1$). It can be shown that, especially at small N, the Gaussian distribution function is, in fact, a better approximation of the exact distribution function than the Langevin expression over most of the range-of deformation, except at very high chain stretch. Second, Flory noted that, in a number of cases, the stress-upswing in uniaxial extension could also be due to strain-induced crystallization. Therefore, it is probably better to regard Eq. (5.8) as an empirical relation, which can be used to incorporate finite extensibility.

When considering the state-of deformation dependence, it should be realized that, in a geometrical sense, all possible isochoric deformations are bounded by uniaxial extension and uniaxial compression (which is equivalent to biaxial extension). This is quantified by the difference between the first and the second invariant of the isochoric elastic strain, $I_{\bar{B}} - II_{\bar{B}}$, which is called the *alignment strength* (Larson, 1988, Chapter 7). A deformation for which $I_{\bar{B}}$ is larger than $II_{\bar{B}}$ is called strongly aligning, when $I_{\bar{B}} = II_{\bar{B}}$, the deformation is neutrally aligning, and for $I_{\bar{B}} < II_{\bar{B}}$, the deformation is weakly aligning (see Figure 5.3).

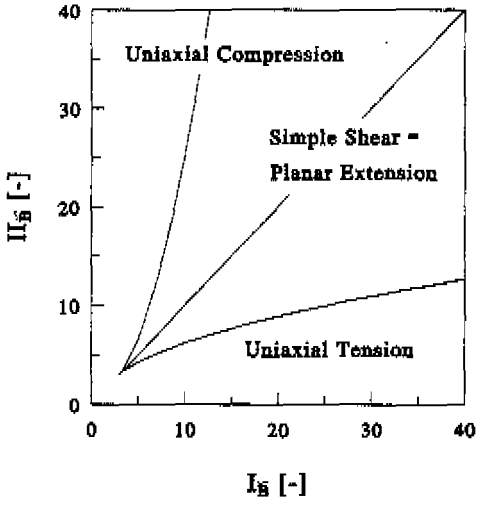

Figure 5.3 *A plot of $I_{\bar{B}}$ versus $II_{\bar{B}}$ for all possible isochoric deformations ($III_{\bar{B}} = 1$) (from Treloar (1975)).*

All network models introduced in this section converge to simple neo-Hookean behaviour at small chain stretch (see for example Eq. (5.15) in case of the eight-chain model). Since the bulk modulus of a rubber is several orders of magnitude larger than its shear modulus, in general, deformation of a rubber proceeds at nearly constant volume (except for pure volume deformations). Therefore, to a good approximation, the isochoric-elastic strain tensor $\bar{\mathbf{B}}$ is equal to the left Cauchy-Green strain tensor $\mathbf{B}$. In case of uniaxial extension in the x-direction, $\mathbf{B}$ equals:

$$\mathbf{B} = \begin{pmatrix} \lambda^2 & 0 & 0 \\ 0 & \frac{1}{\lambda} & 0 \\ 0 & 0 & \frac{1}{\lambda} \end{pmatrix} \tag{5.18}$$

According to neo-Hookean behaviour, the deviatoric stress-strain relation then becomes:

$$\begin{aligned}\mathbf{T}^d &= \begin{pmatrix} \frac{2}{3}\sigma & 0 & 0 \\ 0 & -\frac{1}{3}\sigma & 0 \\ 0 & 0 & -\frac{1}{3}\sigma \end{pmatrix} \\ &= G \begin{pmatrix} \frac{2}{3}\left(\lambda^2 - \frac{1}{\lambda}\right) & 0 & 0 \\ 0 & -\frac{1}{3}\left(\lambda^2 - \frac{1}{\lambda}\right) & 0 \\ 0 & 0 & -\frac{1}{3}\left(\lambda^2 - \frac{1}{\lambda}\right) \end{pmatrix}\end{aligned} \tag{5.19}$$

Therefore, the tensile stress $\sigma = \mathbf{T}^d_{xx} - \mathbf{T}^d_{yy}$ equals:

$$\sigma = G\left(\lambda^2 - \frac{1}{\lambda}\right) \tag{5.20}$$

From this last equation it is clear that even neo-Hookean behaviour, which has no finite extensibility, results in a (quadratic) upswing of the stress in a $\sigma - \lambda$ plot. The effect of finite extensibility is revealed more clearly in a graph of the stress versus $\lambda^2 - 1/\lambda$. In this case, neo-Hookean behaviour will yield a straight line and the effect of finite extensibility will manifest itself as a deviation from this straight line.

All network models with finite extensibility discussed so far have two adjustable parameters: the number of segments N, which determines the maximum chain stretch and the number of chains per unit volume n, which, given N, determines the initial modulus (at constant temperature). The Gaussian-network approximation leads to neo-Hookean behaviour with only one parameter: the initial modulus. The response of these various network models in uniaxial and planar extension, is depicted in Figures 5.4 and 5.5, using the three-chain, eight-chain, and full-chain parameters reported by Arruda (1992) and Wu and van der Giessen (1993) for the strain-hardening behaviour of polycarbonate in uniaxial compression (see Table 5.1).

	three-chain	eight-chain	full-chain	Gaussian chain
nkT [MPa]	17.0	12.7	12.7	19.5
N [-]	3.5	2.25	2.8	-

Table 5.1 *Network parameters required by the different rubber-elasticity models to describe the strain-hardening behaviour of polycarbonate in uniaxial compression (Arruda, 1992; Wu and van der Giessen, 1993).*

The value of the shear modulus of the Gaussian-chain model in Table 5.1 was

chosen to coincide with the initial shear modulus of the eight-chain model, G_8:

$$G_8 = \frac{1}{3} nkT \frac{3 - \frac{1}{N}}{1 - \frac{1}{N}} \tag{5.21}$$

using the Padé approximation of the inverse Langevin function (Eq. (5.7)).

5.3 Experimental

The most straightforward way to verify the strain-hardening response of polymer glasses experimentally, is to apply large homogeneous deformations. However, it was shown in Chapter 4 that most polymer systems, and especially polymer glasses are prone to inhomogeneous deformation. G'Sell *et al.* (1992) developed an experimental technique in which locally a constant strain rate could be applied to an axis-symmetric hour-glass shaped sample, by means of video-controlled tensile testing (a digital closed loop system). Arruda and Boyce (1993a) argued that the deformation in uniaxial -and planar compression will remain homogeneous, since, contrary to a tensile test, there is no area-reduction. This seems to be a rather strong assumption, since the development of shear bands in compression has been observed for a number of polymers (see Bowden, 1970). On the other hand, finite element calculations of Wu and van der Giessen (1994) have shown that the effect of shear band formation on the global stress-strain behaviour is not very large.

In this study, thermal and mechanical treatments will be used to ensure homogeneous deformation. In Chapter 4 it was shown that strain localisation in polymer glasses is initiated by the nonlinear yield behaviour. Strain hardening and intrinsic-strain softening respectively stabilize and amplify non-homogeneous behaviour. Unfortunately, the stress dependence of the yield process is a material property and, therefore, it can not be eliminated as a cause for inhomogeneous deformation behaviour below the glass-transition temperature. However, by raising the temperature above the glass-transition temperature, thermal agitation overwhelms stress-activated flow, and the material will deform homogeneously like a rubber. Freezing in orientation applied above the glass-transition temperature by quenching to room temperature, will result in anisotropic yield behaviour, from which information about the strain hardening behaviour can be retrieved.

Another way to promote homogeneous behaviour, is to eliminate intrinsic-strain softening by means of mechanical conditioning, as was discussed in Chapter 4 (Argon and Hannoosh, 1977). Large plastic deformations rejuvenate the material up to a saturation level which is maintained when the stress is released. As a result, subsequent testing will not lead to strain softening. In the next sections, these methods will be discussed in more detail.

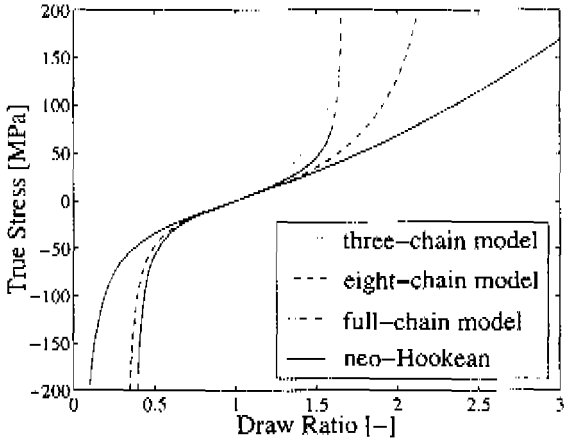

Figure 5.4 *Comparison of the different network models in their description of the strain-hardening response of polycarbonate in uniaxial deformation. Network parameters according to Table 5.1.*

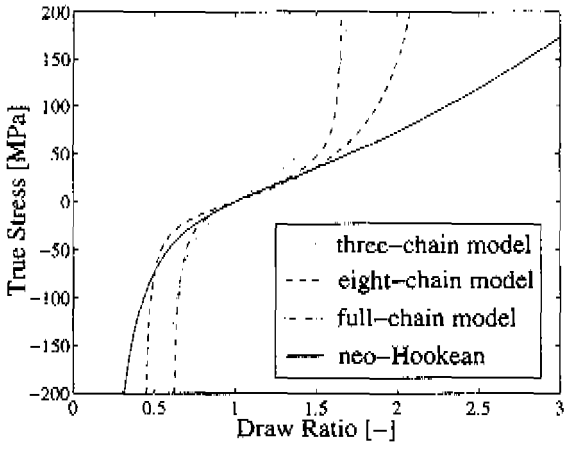

Figure 5.5 *Comparison of the different network models in their description of the strain-hardening response of polycarbonate in planar extension (equivalent to simple shear). Network parameters according to Table 5.1.*

5.3.1 Predeformation Above the Glass-Transition Temperature

Dumb-bell shaped specimen were cut from an extruded sheet of Makrolon (bisphenol A polycarbonate, Bayer), 2 mm thick, according to ASTM D368 type III. To prevent degradation during predeformation at 160 °C, the material was dried at 80 °C for about three days. Before predeformation above the glass-transition temperature, the samples were brought 15 °C above T_g for 15 minutes, to ensure the same testing conditions for all samples (T_g = 150 °C). Uniaxial predeformation was imposed using a FRANK 81565 tensile tester at a constant strain rate of 500 mm/min at 163 °C. In this way a range of predeformed samples were obtained up to a draw ratio of $\lambda = 1.85$, for which the deformation was visually homogeneous.

After predeformation, the oven was opened to enable rapid cooling to room temperature, in order to freeze in the applied orientation. To verify the amount of predeformation, markers were used on some of the samples. After determination of the amount of predeformation, these specimen were brought back to the oven at 180 °C for 15 minutes, to allow for shrinkage in order to measure the effective draw ratio. All samples showed complete recovery.

Planar predeformed sheets were kindly provided by the university of Leeds (IRC of Polymer Science & Technology). On these sheets, the planar predeformation was imposed at a constant strain rate of 500 mm/min at 163 °C. From these sheets, small dumb-bell shaped samples were cut at different angles with the main principle-strain axis (see Figure 5.6)

To determine the anisotropic yield behaviour, the uniaxially predeformed samples were tested on a FRANK 81565 tensile tester at four different strain rates, from 10^{-4} to 10^{-1} s^{-1}. The dumb-bell shaped samples, cut in different orientations from the planar predeformed sheets, were tested on a ZWICK 1432 tensile tester at three rates of strain: $10^{-4}, 10^{-3}$ and 10^{-2} s^{-1}. All tests were performed at room temperature (21 °C).

5.3.2 Predeformation Below the Glass-Transition Temperature

A way to enable large homogeneous deformations below the glass transition temperature, is to rejuvenate the material through mechanical conditioning at room temperature.

For this purpose, dog-bone shaped, axis-symmetrical tensile bars (see Figure 5.7), manufactured from extruded polycarbonate (bisphenol A, Bayer) rod, were subjected to large strain torsion at room temperature. The torsion was applied manually, by clamping the sample in a universal lathe and turning one side to and fro over 720 degrees, with a line on the sample as a reference. After predeformation some of the samples were heated to 180 °C, but no motion due to residual stress was observed. This indicates that, with respect to the strain-hardening response, the samples were returned to their isotropic state. A disadvantage of

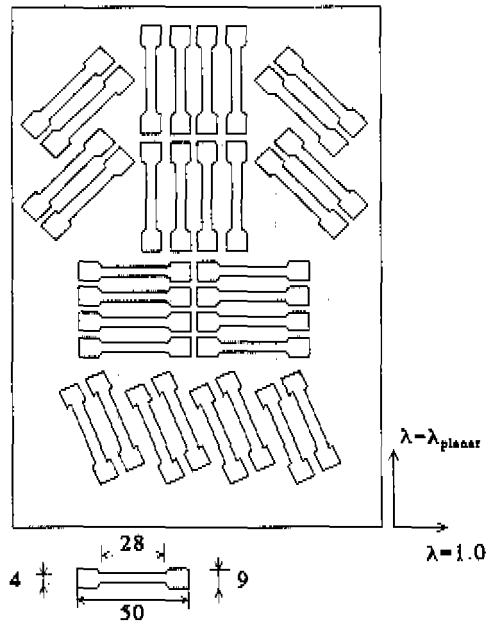

Figure 5.6 *Schematic representation of the production of small dumb-bell shaped samples from a planar predeformed sheet.*

the method is that the predeformation is not homogeneously distributed and that the central fibre of the sample will not deform (and, therefore, not rejuvenate) at all.

Immediately after rejuvenation, the samples were tested uniaxially on a ZWICK Rel 1852 servo-hydraulic tensile tester (20 kN). In all cases the extension was measured using an INSTRON (2620-602) strain gauge extensometer with a measure length of 50 mm and a range of ±2.5 mm. The relative accuracy in force and strain measurements was 1%. The tensile tests were performed at several temperatures between room temperature and the glass transition temperature, at constant strain rates. The torsion experiments were performed on a custom-made torsion-rig, at a rotation speed of 1 rad/s.

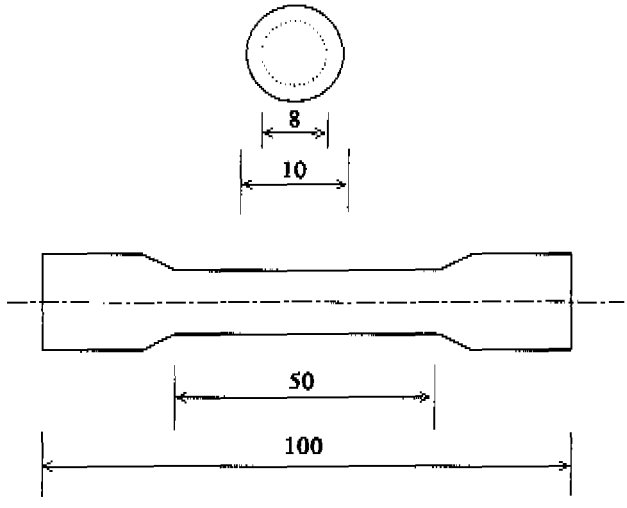

Figure 5.7 *Tensile bar used for mechanical conditioning below the glass transition temperature.*

5.4 Results and Discussions

5.4.1 Characterisation of the Untreated Material

For polymer glasses, it is normally assumed that the strain hardening response and the yield behaviour (Chapter 3) are two separate processes, which add up to the total stress-strain relation (see Figure 5.1). Therefore, the nonlinear flow behaviour (activation volume) should not be influenced by predeformation or strain hardening (see Chapter 4, Section 4.2.1). To verify this assumption, first the yield behaviour of the untreated material was determined. This untreated material was subjected to the same temperature history as the material predeformed above the glass-transition temperature.

In Chapter 3 it was shown that a full characterization of the nonlinear flow behaviour of a polymer glass comprises the combination of creep tests at different stress levels and yield stresses at different strain rates, combined in a single Eyring plot (see Figure 3.8). This Chapter, however, focuses on the strain-hardening behaviour and only yield stresses at different strain rates were used to determine the nonlinear-stress dependence, described by the Eyring parameter τ_0. An Eyring plot of the yield stress versus the logarithm of strain rate, is depicted in Figure 5.8.

The best fit of the yield data in Figure 5.8 results in a value for the Eyring parameter $\tau_0 = 1.59$ MPa. This value differs considerably from the value $\tau_0 =$

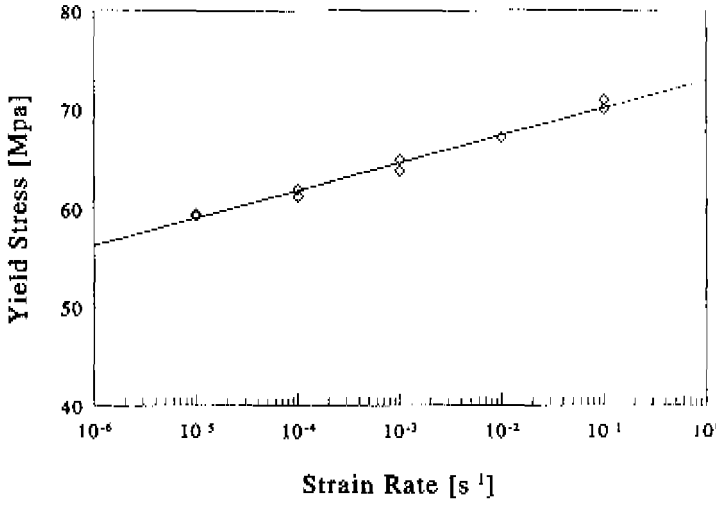

Figure 5.8 *Eyring plot of the yield stress as a function of logarithmic strain rate for untreated polycarbonate. The solid line is a best fit.*

0.89 MPa determined in Chapter 3, which is due to the narrow range of equivalent stress covered, (compared to Figure 3.8) using only yield-stress data.

5.4.2 Predeformation Above the Glass-Transition Temperature

By deforming the sample above the glass-transition temperature it is possible to separate the nonlinear viscoelastic response and the elastic strain-hardening behaviour, since the temperature treatment erases residual viscoelastic (memory) effects. Samples, predeformed above the glass-transition, should have the same activation volume as untreated material. This was verified for a series of tensile bars, predeformed uniaxially above the glass-transition temperature at five different levels of extension. Eyring plots of the yield stress as a function of logarithmic strain rate, at various levels of predeformation are depicted in Figure 5.9. The solid lines in this figure are a fit using the same value of the Eyring parameter τ_0 as the untreated material. An excellent agreement was obtained, indicating that the activation volume is indeed independent of the strain-hardening response.

A disadvantage of predeformation above the glass-transition temperature, is that large homogeneous deformations below the glass-transition temperature cannot be obtained, since the heat treatment will restore the intrinsic-strain softening behaviour. Therefore, information about the strain-hardening behaviour can only be obtained indirectly from the anisotropic yield behaviour. In principle, using a

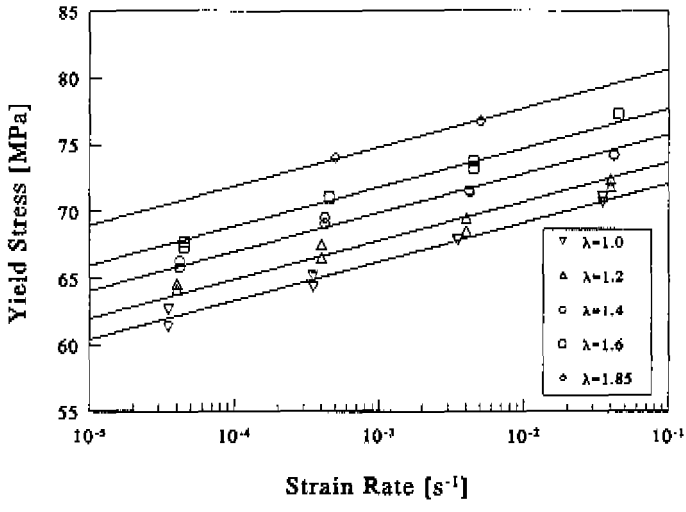

Figure 5.9 *Eyring plots of polycarbonate in uniaxial tension at various levels of predeformation.*

three-dimensional constitutive equation with one of the network models from the previous section to describe the strain-hardening behaviour, the development of this anisotropy, as well as the effect on the stress-strain curve upon reloading, can be calculated numerically (see Boyce and Arruda, 1990).

A useful approximation to determine the effect of orientational hardening on the yield point alone, is to assume that, at the yield point, the initial elastic strain rate is zero, and that the material response is adequately described by a Kelvin-Voigt model (see Figure 5.10). At low stress and at low temperature, the viscosity in the dashpot (Figure 5.10) is very high. At high stress and/or at high temperature, the viscosity can be low enough to facilitate homogeneous deformation of the entanglement network, characterized by the rubbery modulus G_r. If the material is homogeneously deformed above the glass-transition temperature, quenching to room temperature will freeze-in the predeformed situation. After releasing the sample, the deviatoric network stress will be balanced by the deviatoric viscous stress. In other words, the high viscosity at room temperature and at low stress, prevents the material from returning to its original state.

The representation by a Kelvin-Voigt model implies that the total deviatoric stress is decomposed in a network stress and a viscous stress:

$$\mathbf{T}^d = G_s \tilde{\mathbf{B}}_p^d + 2\eta(II_{T_v^d})\mathbf{D}_p \tag{5.22}$$

Here, $\tilde{\mathbf{B}}_p$ is the "plastic" predeformation applied above the glass-transition tem-

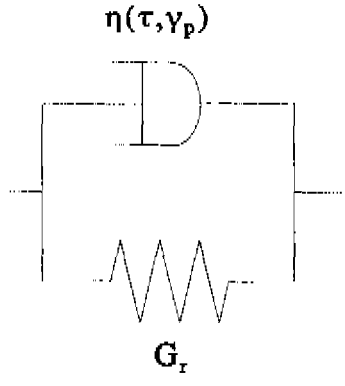

Figure 5.10 *Schematic representation of the deviatoric stress response at the yield point.*

perature, and $\mathbf{T}_v^d$ is the deviatoric stress acting over the dashpot. The "yield point" of this Kelvin-Voigt model is determined by a critical value of the second invariant of $\mathbf{T}_v^d$. In other words, the dashpot "yields" according to a Von Mises criterion. The critical value of $II_{T_v^d}$, therefore, equals $1/3\sigma_0$, with σ_0 the uniaxial yield stress of the untreated isotropic material ($\bar{\mathbf{B}}_p^d = \mathbf{0}$).

Uniaxial Predeformation

In case of uniaxial predeformation, the frozen-in deformation is described by:

$$\bar{\mathbf{B}}_p = \begin{pmatrix} \lambda_p^2 & 0 & 0 \\ 0 & \frac{1}{\lambda_p} & 0 \\ 0 & 0 & \frac{1}{\lambda_p} \end{pmatrix} \tag{5.23}$$

where λ_p is the uniaxial draw ratio.

At the moment the predeformed sample "yields" at a stress σ_y, upon uniaxial reloading at room temperature, the deviatoric viscous stress equals:

$$\begin{aligned} \mathbf{T}_v^d &= \mathbf{T}^d - G\bar{\mathbf{B}}_p^d \\ &= \frac{1}{3}\begin{pmatrix} 2\left(\sigma_y - G\left[\lambda_p^2 - \frac{1}{\lambda_p}\right]\right) & 0 & 0 \\ 0 & -\left(\sigma_y - G\left[\lambda_p^2 - \frac{1}{\lambda_p}\right]\right) & 0 \\ 0 & 0 & -\left(\sigma_y - G\left[\lambda_p^2 - \frac{1}{\lambda_p}\right]\right) \end{pmatrix} \end{aligned} \tag{5.24}$$

A relation between the yield stress of the predeformed material -and the untreated isotropic material, respectively σ_y and σ_0, can now be obtained from the critical condition for yield:

$$II_{T^d_y} = \frac{1}{3}\sigma_0 \tag{5.25}$$

This quadratic equation in σ_y has two solutions, one for the case of yielding in tension, and one for yielding in compression:

$$\sigma_y = \sigma_0 + G\left(\lambda_p^2 - \frac{1}{\lambda_p}\right) \tag{5.26a}$$

$$\sigma_y = -\sigma_0 + G\left(\lambda_p^2 - \frac{1}{\lambda_p}\right) \tag{5.26b}$$

According to Eq. (5.26), the strain-hardening modulus G can be obtained from a plot of the yield stress as a function of predeformation. This is depicted in Figure 5.11, where it is shown that the yield stress as a function of $(\lambda_p^2 - 1/\lambda_p)$ reveals a straight line, indicative of neo-Hookean behaviour with a constant shear modulus $G = 3$ MPa. Apparently, there is no effect of finite extensibility up to a draw ratio of $\lambda_p = 1.85$ [-] (applied above the glass-transition temperature). This is not in accordance with the uniaxial and plane -strain compression data for polycarbonate of Arruda (1992), see Figure 5.4, which would predict a strong upswing in the stress, accompanied by a higher initial modulus.

Planar Predeformation

As in the case of uniaxial predeformation, samples, subjected to planar predeformation above the glass-transition temperature, should have the same activation volume as the untreated material. This was verified for a series of tensile bars, cut at four different directions from a sheet, planarly predeformed above the glass-transition temperature at two different levels of extension (see Figure 5.6). Eyring plots of the yield stress as a function of logarithmic strain rate, at various levels of predeformation and at different levels of orientation are depicted in Figures 5.12 and 5.13. The solid lines in this figure are a fit using the same value of the Eyring parameter τ_0 as the untreated material. A good agreement is obtained, indicating that the activation volume is indeed independent of the strain-hardening response.

In case of planar predeformation, the frozen-in deformation is described by:

$$\bar{\mathbf{B}}_p = \begin{pmatrix} \lambda_p^2 & 0 & 0 \\ 0 & 1 & 0 \\ 0 & 0 & \frac{1}{\lambda_p^2} \end{pmatrix} \tag{5.27}$$

where λ_p is the planar draw ratio (see Figure 5.6).

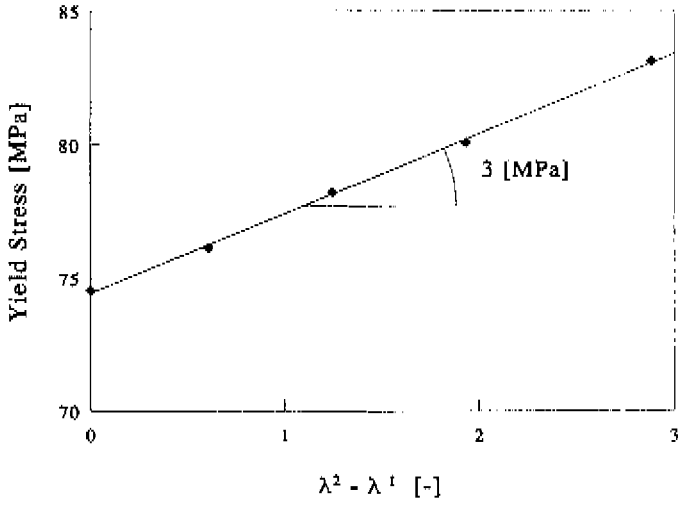

Figure 5.11 *The yield stress as a function of uniaxial predeformation above the glass-transition temperature.*

To examen the anisotropy in yield behaviour introduced by planar predeformation, samples, cut in different orientations with respect to the drawing direction (see Figure 5.6), were subjected to uniaxial tensile experiments at room temperature. During these uniaxial tensile experiments, the deviatoric "viscous" stress equals:

$$\mathbf{T}_v^d = \mathbf{T}^d - G\mathbf{R} \cdot \mathbf{B}_p^d \cdot \mathbf{R}^T \tag{5.28}$$

with the rotation tensor $\mathbf{R}$:

$$\mathbf{R} = \begin{pmatrix} \cos\theta & -\sin\theta & 0 \\ \sin\theta & \cos\theta & 0 \\ 0 & 0 & 1 \end{pmatrix} \tag{5.29}$$

The uniaxial "yield stress" σ_y of a tensile bar, cut at an angle θ with respect to the planar draw direction, is again determined by the critical value of the second invariant of the deviatoric "viscous-stress tensor", Eq. (5.25). Like in the case of uniaxial predeformation, this criterion results in a relation between σ_y and the isotropic yield stress σ_0, which is quadratic in σ_y and has two solutions, one in

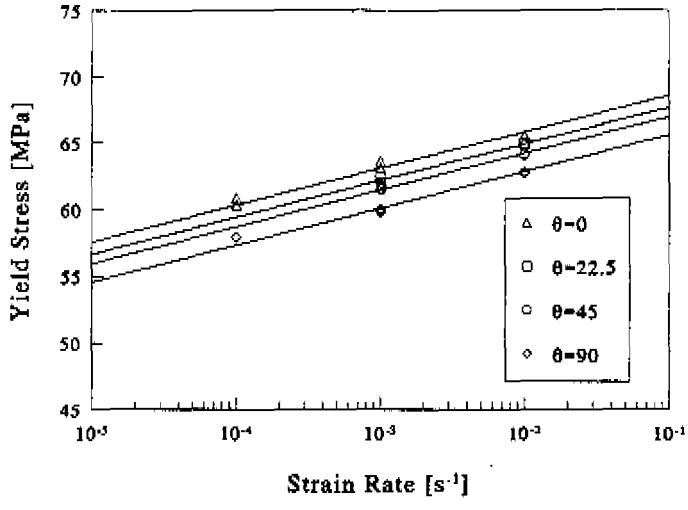

Figure 5.12 *Yield stress versus strain rate for planarly predeformed samples (λ_p = 1.23), at different orientations with respect to the predrawing direction.*

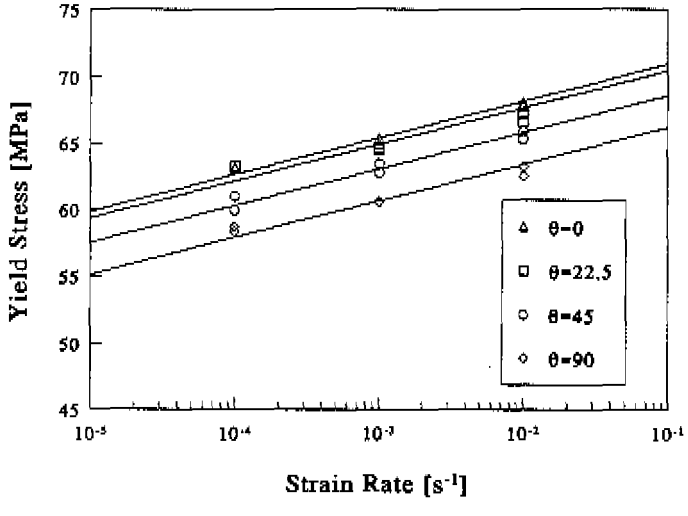

Figure 5.13 *Yield stress versus strain rate for planarly predeformed samples (λ_p = 1.5), at different orientations with respect to the predrawing direction.*

tension and one in compression :

$$\sigma_y = \frac{1}{2\lambda^4}\left[\frac{1}{2}G\lambda^2\left(\lambda^2-1\right)\left(\lambda^2+3\lambda^2\cos(2\alpha)+2\right)+\left(4\lambda^4\left(-G^2+G^2\lambda^2+G^2\lambda^6-G^2\lambda^8+\lambda^4\sigma_0^2\right)+\frac{1}{4}G^2\lambda^4\left(1-\lambda^2\right)^2\left(2+\lambda^2+3\lambda^2\cos(2\alpha)\right)^2\right)^{\frac{1}{2}}\right] \quad (5.30a)$$

$$\sigma_y = \frac{1}{2\lambda^4}\left[\frac{1}{2}G\lambda^2\left(\lambda^2-1\right)\left(\lambda^2+3\lambda^2\cos(2\alpha)+2\right)-\left(4\lambda^4\left(-G^2+G^2\lambda^2+G^2\lambda^6-G^2\lambda^8+\lambda^4\sigma_0^2\right)+\frac{1}{4}G^2\lambda^4\left(1-\lambda^2\right)^2\left(2+\lambda^2+3\lambda^2\cos(2\alpha)\right)^2\right)^{\frac{1}{2}}\right] \quad (5.30b)$$

The yield stress data at different orientations and at two levels of predeformation, (Figures 5.12 and 5.13), were used to verify Eq. (5.30a). This is depicted in Figure 5.14, which shows the yield stress as a function of orientation at two levels of predeformation and at a given strain rate. The solid line is the prediction of Eq. (5.30a) using the value of the strain-hardening modulus from the uniaxial predeformation experiments $G = 3$ MPa (see Section 5.4.2). Unfortunately, the value of the isotropic yield stress σ_0 was not known, since the exact temperature history of the predeformed samples (large sheets) was unknown. Therefore, one yield point at a given level of predeformation, orientation and strain rate, was needed to determine σ_0, using Eq. (5.30a). From Figure 5.14 it is clear that, like in the case of uniaxial predeformation, simple neo-Hookean behaviour with a constant modulus is able to capture the strain-hardening response accurately.

The good agreement between experiment and predictions observed in Figures 5.11 and 5.14, suggest that simple neo-Hookean behaviour employing a constant shear modulus $G = 3$ MPa, is able to give a quantitative description of the state-of deformation dependence of the strain-hardening response at a temperature of 163 °C up to a draw ratio of $\lambda_p = 1.85$. In particular, no effect of finite extensibility could be observed.

5.4.3 Predeformation Below the Glass-Transition Temperature

Inhomogeneous deformation below the glass-transition temperature is initiated by the nonlinear yield behaviour and promoted by the intrinsic strain-softening response. The nonlinear yield behaviour is a material characteristic and can not be avoided, but the intrinsic strain-softening response can be eliminated by

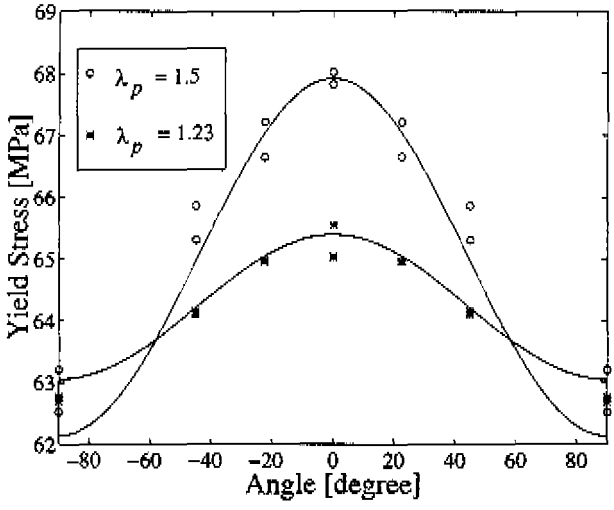

Figure 5.14 *Yield stress versus orientation angle in the planarly predeformed plates, measured at a strain rate of* 10^{-2} s^{-1}.

mechanical conditioning through large-strain plastic deformations. In absence of strain softening, small fluctuations in the stress field can[2] be stabilized by strain-hardening, resulting in homogeneous deformation behaviour (Argon and Hannoosh, 1977). In this study, mechanical conditioning of cylindrical tensile bars was achieved by large-strain to and fro torsion, resulting in isotropic material.

Uniaxial Testing of Samples Predeformed in Torsion

Rejuvenated cylindrical tensile bars were produced by large strain to and fro torsion at room temperature. Heating these samples above the glass-transition temperature did not reveal any residual motion, suggesting that to and fro torsion results in rejuvenated, isotropic samples. A disadvantage of this method is that the predeformation is not distributed homogeneously over the cross-section of the sample. The amount of intrinsic strain softening is maximal on the outside of the sample, and decreases to zero in the central fiber of the tensile bar. A true stress-strain tensile curve of such a mechanically conditioned sample is depicted in Figure 5.15. In this figure, a small load drop can still be observed. This is

[2]Elimination of intrinsic strain softening through mechanical conditioning does not necessarily lead to homogeneous deformation behaviour. For example, due to their low strain-hardening modulus, polyethylene and polypropylene still show necking in a tensile test, despite the fact that they display no intrinsic strain-softening.

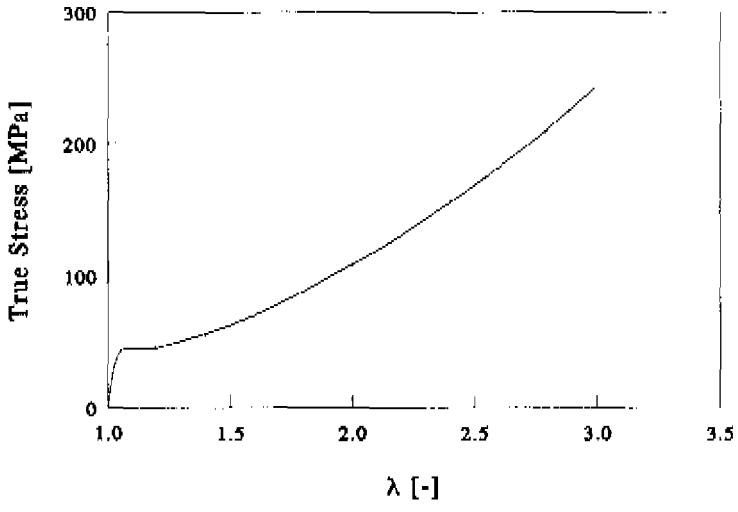

Figure 5.15 *True stress as a function of draw ratio for a cylindrical tensile bar, conditioned in torsion.*

probably due to the central core of the tensile bar which was not deformed and, therefore, has not been rejuvenated. Visually, however, the deformation of the cylindrical tensile bar remained homogeneous. From Figure 5.15 it can also be seen that homogeneous deformations up to $\lambda = 3$ were reached, in contrast to maximum draw ratios of 2.44 and 2.5 reported by respectively Boyce and Arruda (1990) and Donald and Kramer (1982a). To determine the state-of deformation dependence of the strain-hardening response of polycarbonate, also uniaxial compression tests were performed. The results of the uniaxial tensile -and compression tests, plotted as true stress versus $(\lambda^2 - 1/\lambda)$, is depicted in figures 5.16 and 5.17.

In these Figures, the strain-hardening response appears as a straight line of equal slope in both tension and compression, indicative of neo-Hookean behaviour. From the slope the strain-hardening modulus was determined (Eq. (5.20)) to be: $G = 26$ MPa. No effect of finite extensibility was observed, there is no deviation from the straight line in a σ vs. $(\lambda^2 - 1/\lambda)$ plot for both uniaxial tension -and compression experiments. This is again in contrast with uniaxial -and planar compression data of polycarbonate, published by Arruda and Boyce (1993a).

Shear Testing of Samples Predeformed in Torsion

A torsion curve of a mechanically conditioned torsion bar of length L and with a polar moment of inertia I_p is depicted in Figure 5.18. Assuming *linear* behaviour,

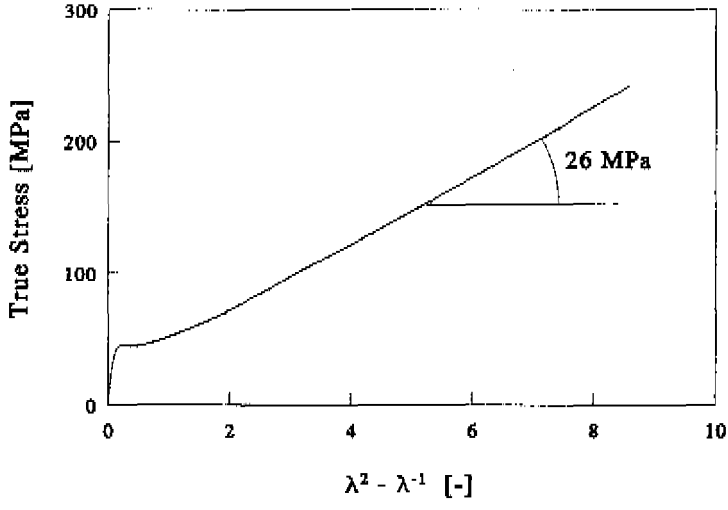

Figure 5.16 *True stress versus* $(\lambda^2 - 1/\lambda)$ *during a tensile test at* $\dot{\epsilon} = 10^{-2}\ s^{-1}$ *of a cylindrical tensile bar, conditioned in torsion.*

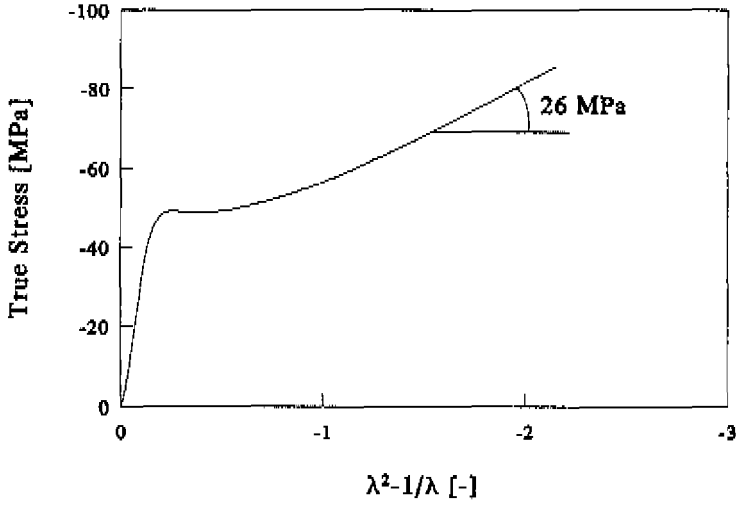

Figure 5.17 *True stress versus* $(\lambda^2 - 1/\lambda)$ *during a compression test at* $\dot{\epsilon} = 10^{-2}\ s^{-1}$ *of a cylindrical tensile bar, conditioned in torsion.*

the relation between torque M_w and torsion angle per unit length ϕ/L, is given by (Roark and Young, 1984):

$$\frac{\phi}{L} = \frac{M_w}{G\, I_p} \tag{5.31}$$

with the shear modulus G.

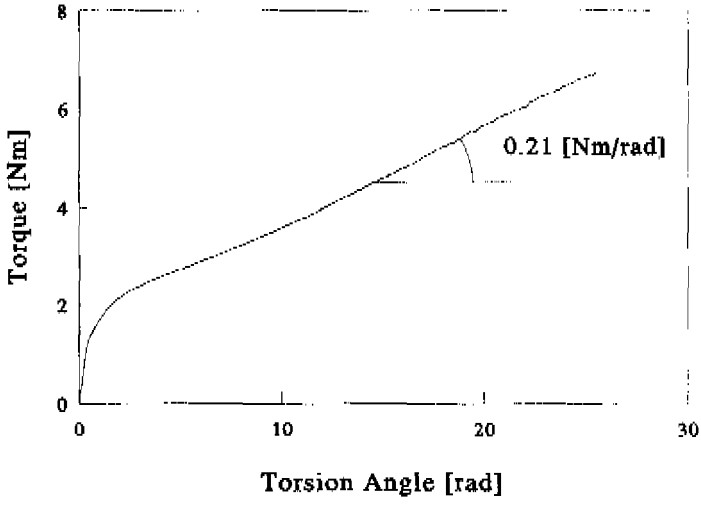

Figure 5.18 *Strain-hardening of polycarbonate measured in torsion, at a rotation speed of 1 rad/s.*

From Figure 5.18 it is clear, that, also in shear deformation, neo-Hookean behaviour is observed. The shear modulus $G = 26$ MPa, obtained from the torsion experiments, is in excellent agreement with the values obtained from the tensile and compression tests. Again, no effect of finite extensibility is observed.

5.4.4 Temperature Dependence of the Strain-Hardening Response

The rejuvenated tensile bars were also used to perform tensile tests over a range of strain rates from 10^{-4} to 10^{-1} s^{-1}, at different temperatures above room temperature. The results are depicted in Figure 5.19. No strain-rate effects could be observed, and at all temperatures the strain-hardening response was essentially elastic until fracture occured. From Figure 5.19, it is clear that neo-Hookean strain-hardening behaviour is observed over the whole temperature range. The strain-hardening modulus as a function of temperature, determined from Figure 5.19, is depicted in Figure 5.20. Although there is no effect of strain rate

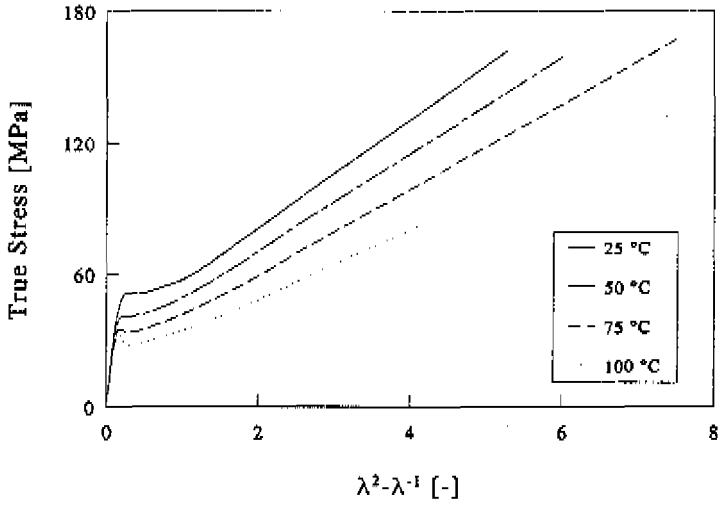

Figure 5.19 *Homogeneous tensile curves of polycarbonate at different temperatures. No strain-rate effects could be observed.*

on the hardening response, the strain-hardening modulus clearly decreases as a function of temperature.

5.5 Discussion and Conclusions

Nowadays, it is generally accepted that the strain hardening response of (glassy) polymers originates from a rubber-elastic response of the entanglement network, characterized by the plateau modulus G_r (which can be measured in the melt, using mechanical spectroscopy). Using the classical theory of rubber elasticity, the plateau modulus can be used to calculate the molecular weight M_e of a single strand in the entanglement network (Kramer, 1983):

$$M_e = \frac{\rho RT}{G_r} \tag{5.32}$$

Assuming that entanglements cannot unravel on the time scale of the experiment, a maximum draw ratio of the network can be estimated as the ratio of the stretched length of a single strand (molecular weight: M_e) and its random walk length:

$$\lambda_{max} = \frac{N_e l_b}{\sqrt{C_\infty N_e l_b^2}} = \sqrt{\frac{N_e}{C_\infty}} \tag{5.33a}$$

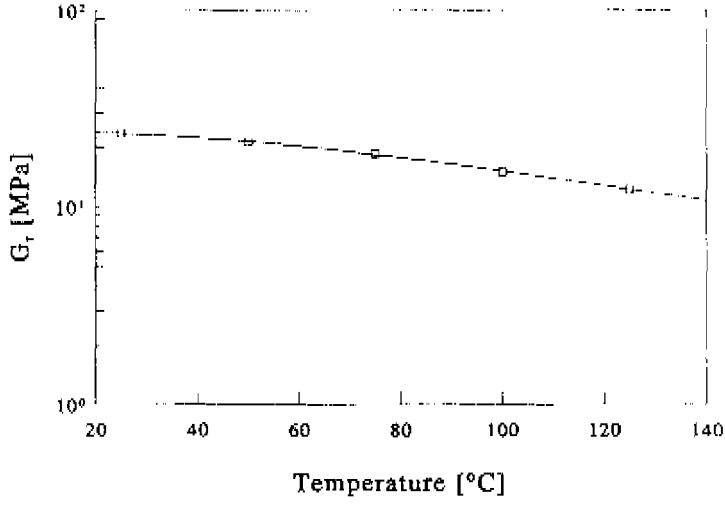

Figure 5.20 *Strain-hardening modulus G_r of polycarbonate as a function of temperature (from Figure 5.19). The solid line is a guide to the eye.*

$$N_e = \frac{M_e}{M_0} \tag{5.33b}$$

Here, N_e is the number of monomer units of an entangled strand, C_∞ is the characteristic ratio (a measure of the chain stiffness), and l_b and M_0 are, respectively, the length and the molecular weight of a monomer unit.

For a number of polymers, Donald and Kramer (1982b, 1982a) determined the draw ratio in craze fibrils and shear deformation zones, using transmission electron microscopy. They found that the experimental values correlated reasonably well with the maximum draw ratio of the entanglement network according to Eq. (5.33a). Their estimate for the maximum draw ratio of polycarbonate was $\lambda_{max} \approx 2.5$. Indications for a finite extensibility of the entanglement network were also found from uniaxial and planar compression tests on polycarbonate and polymethyl methacrylate by Arruda and Boyce (1993a). They estimated, for polycarbonate, from uniaxial compression tests a limiting chain stretch $\sqrt{N} = 1.5$, from which a maximum draw ratio in uniaxial extension can be calculated[3]: $\lambda_{max} \approx 2.5$.

In this study, thermal and mechanical conditioning techniques were used to access the strain-hardening response of glassy polymers, by means of large *homogeneous* deformations. It was shown, that the state-of deformation dependence of

[3]According to the eight-chain model, the maximum draw ratio of the network is obtained when the average chain stretch parameter, Eq. (5.10), equals the limiting chain stretch $\sqrt{N}$.

the strain-hardening response of polycarbonate, is adequately described by neo-Hookean behaviour, with a shear modulus $G = 26$ MPa at room temperature, which decreases at higher temperatures. In particular, no effect of a maximum draw ratio was observed, in contrast to the studies mentioned above. The strain-hardening response remained neo-Hookean until fracture occured at draw ratios $\lambda \approx 3$ (in uniaxial extension).

It should be noticed, that finite extensibility is not a prerequisite to stabilize a local deformation zone. In Chapter 4, it was argued that, *at constant stress*, the evolution of the draw ratio in a deformation zone is determined by the stress dependence, and the intrinsic strain-softening response, of the plastic flow process and by the value of the strain-hardening modulus G_r. Using realistic material parameters, it was estimated that the shear strain γ_{dz} at which the neo-Hookean strain-hardening response stabilizes a plastic deformation zone in polycarbonate, is approximately: $\gamma_{dz} = 1.4$ (see Figure 4.5). This corresponds to an extension ratio of $\lambda_{dz} = 1 + \frac{1}{2}\gamma_{dz} = 1.7$, which is in good agreement with the experimental value as determined by Donald and Kramer (1982a). Thus, in a constant stress situation, stabilisation of a deformation zone can be realized by a neo-Hookean strain-hardening response as well, and does not necessarily result from a finite extensibility of the entanglement network.

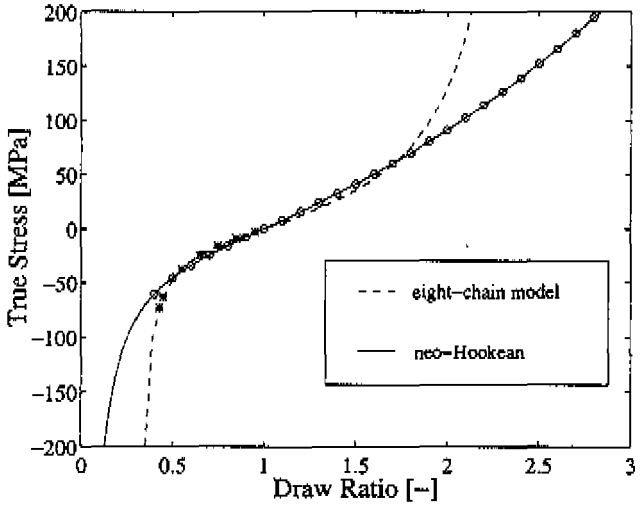

Figure 5.21 *Comparison between the strain-hardening response of polycarbonate as determined by uniaxial tensile and compression experiments on rejuvenated samples (∘), and by uniaxial compression on non-rejuvenated samples (∗).*

A comparison between the uniaxial compression data on non-rejuvenated sam-

ples by Arruda (1992) and our compression and tensile data on rejuvenated samples, is depicted in Figure 5.21. The lines in this figure are the calculated strain-hardening response of polycarbonate according to neo-Hookean behaviour with a modulus of $G = 26$ MPa, and according to the eight-chain model with the network parameters as determined by Arruda (1992). The initial strain-hardening modulus and the maximum draw ratios in uniaxial tensile and compression, calculated from their network parameters (see Table 5.1), equal: $G = 19.5$ MPa, $\lambda_{max}^{compression} = 0.3$ and $\lambda_{max}^{tensile} = 2.44$. From Figure 5.21 it is clear, that the actual compression data do not differ substantially, both rejuvenated and non-rejuvenated samples show an upswing in stress. However, interpreting this stress upswing as resulting from a finite extensibility of the network, using a non-Gaussian spring model, also leads to a maximum draw ratio in *tensile* deformation, which is not observed experimentally.

The temperature dependence of the strain-hardening modulus, as measured in uniaxial tensile deformation on mechanically conditioned samples, was depicted in Figure 5.20. Arruda (1992) assumed that the temperature dependence of the strain-hardening response originated from a change in chain density n (number of elastically active chains), which is equivalent to a change in the number of monomer units between entanglements (N_e), since the total number of monomer units is conserved (Boyce, 1986). Following Raha and Bowden (1972), an empirical relation was proposed, to describe the evolving chain density with temperature.

It is instructive to plot the values of the strain-hardening modulus as a function of temperature, together with a temperature scan of the dynamic modulus at 1 Hz (Figure 5.22). This is allowed, since the strain-hardening response is to a good approximation elastic (even at higher temperatures, strain-rate effects were not observed). In Figure 5.22, it can be seen, that the temperature dependence of the stain-hardening modulus correlates very well with the relaxation behaviour of the entanglement network. This quantitative agreement is a strong indication that strain hardening in polycarbonate indeed originates from a rubber-elastic response of the entanglement network, which becomes operable when segmental motion is allowed. In the polymer rheology field, it is well established that relaxation of the entanglement network results from *reptation* de Gennes (1971). In the reptation theory, the influence of topological interactions on centre-of-mass diffusion of long chain molecules is taken into account by assuming a chain to be confined in a tube in which only snake-like diffusion is allowed. Reptation is a powerful theory, which is able to relate many molecular aspects, such as molecular weight, molecular weight distribution, chain architecture (branching, star polymers), to the relaxation behaviour of polymer melts (Larson, 1988, Chapter 4). If the correspondence between relaxation of the strain-hardening response and relaxation behaviour of the melt, as suggested by Figure 5.22, is correct, the concepts of reptation theory would also apply to the strain-hardening response of glassy polymers.

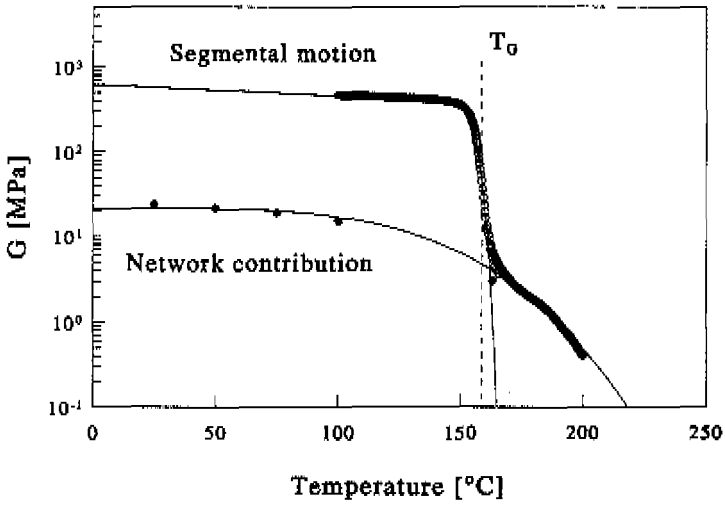

Figure 5.22 *Open symbols: Temperature scan of the dynamic (shear) modulus at 1 Hz. Closed symbols: Strain-hardening modulus as a function of temperature, the lines are guides to the eye.*

Conceptually, it is important that the temperature dependence of the strain-hardening response originates from relaxation behaviour of the network. In principle, this could be described using a second spectrum of Leonov modes, with temperature dependent relaxation times. However, the absence of strain-rate effects in the strain-hardening response at constant temperature, suggests that relaxation of the entanglement network is not very dependent on stress, in contrast to the glass transition (Chapter 3). With respect to modelling, this implies that the use of a single, temperature-dependent neo-Hookean spring, instead of a spectrum of Leonov modes, to describe the temperature dependence of the strain-hardening response is sufficient.

Although we now have a detailed description of the nonlinear viscoelastic behaviour up to the "yield point" (Chapter 3) and of the strain-hardening response, it is still not possible to predict a complete stress-strain curve of polycarbonate, since rejuvenation (intrinsic strain softening) has not been taken into account. Some aspects of physical aging and rejuvenation will be discussed in the next Chapter.

Chapter 6

Aging and Rejuvenation

6.1 Introduction

Important aspects of the deformation behaviour of glassy polymers which have not been discussed so far, are "physical aging", and "rejuvenation". Upon cooling a (polymer) melt, the molecular mobility decreases, and when the relaxation times exceed the experimental time scale, the melt becomes a glass. In the glassy state, thermodynamic variables, like volume and enthalpy, have not been able to attain their equilibrium value, and continue to decrease, a process called *physical aging* (Struik, 1978; McKenna, 1989). Physical aging also has a pronounced effect on mechanical properties. In the sixties it was found that the main influence of physical aging on linear viscoelastic behaviour is to increase all retardation times proportional to aging time (Struik, 1978). With respect to modelling, this implies that the effect of aging on mechanical behaviour can be incorporated similar to the effect of stress and temperature, using a *aging-time shift factor* a_t.

The effect of aging can be erased, either by raising the temperature above the glass-transition temperature, or, alternatively, mechanically, by application of plastic deformation, of which the latter is called *rejuvenation* (McKenna and Kovacs, 1984). Rejuvenation results in a significant decrease of the viscosity during plastic flow after the "yield point", and is, therefore, also referred to as *intrinsic strain softening*. As shown in Chapter 4, intrinsic strain softening plays an important role in the evolution of strain inhomogeneities, such as shear bands and crazes, since it strongly amplifies inhomogeneous behaviour.

Qualitatively, changes in mobility during aging and rejuvenation are often attributed to changes in the so-called *free volume* (Struik, 1978; Hasan *et al.*, 1993), loosely defined as free space, available for segmental diffusion. Unfortunately, attempts to quantify the free-volume concept have met serious difficulties, since there is no known definition of "free volume" that provides a satisfactory relation between "free volume" and mobility, especially below the glass transition temperature (Struik, 1978, Chapter 13). This is related to the fact that a thorough

theoretical understanding of the glass transition is still lacking (Mansfield, 1995), which, in general, frustrates attempts to identify measurable parameters that are able to describe "mobility" (relaxation behaviour) around and below the glass transition temperature (Hodge, 1995). A quantitative description of aging and rejuvenation in the linear and nonlinear range, therefore, deserves a special study, and is considered outside the scope of this thesis. This Chapter has the character of an "epilogue", and is only concerned with some consequences of the modelling strategy, advocated in Chapters 2 and 3, with respect to aging and rejuvenation.

6.2 Rejuvenation and Elastic Dilatation

The free-volume approach is a well-known concept, which states that mobility in an amorphous (liquid) material is determined by the degree of packing, or, equivalently, by the amount of free space, available for diffusion (Hirschfelder *et al.*, 1967; Struik, 1978). One of the most popular relations between free volume and mobility was derived by Doolittle (1951). By measuring the viscosity of n-alkane liquids as a function of temperature and volume, and assuming that variations in viscosity (mobility) are *only* determined by changes in volume (thermal expansion), he observed a quantitative relation between viscosity η and fractional free volume f:

$$\ln \eta = A - \frac{B}{f} \tag{6.1}$$

Here, A and B are material constants ($B \approx 1$), and f is defined as:

$$f = \frac{v - v_0}{v} \tag{6.2}$$

with v the actual specific volume and the v_0 specific occupied volume (extrapolated volume at zero Kelvin). The Doolittle equation, Eq. (6.1), was supported theoretically by Turnbull and Cohen (1961) from the assumption that only free volume sites larger than a critical size contribute to particle diffusion. The Doolittle equation defines a free-volume shift factor a_f:

$$\ln a_f = \ln \left(\frac{\tau}{\tau_{ref}} \right) = \frac{B}{f} - \frac{B}{f_{ref}} \tag{6.3}$$

Here, τ_{ref} is the relaxation time at a reference fractional free volume f_{ref}.

From the Doolittle equation, a temperature shift factor a_T can be derived, presuming that changes in mobility as a function of temperature originate solely from changes in free volume with temperature. Substituting in Eq. (6.3) a linear relation between free volume and temperature:

$$f = f_g + \Delta\alpha (T - T_g) \tag{6.4}$$

leads to the well-known WLF-equation (Williams *et al.*, 1955):

$$\ln a_T = \ln \frac{\tau(T)}{\tau(T_g)} = \frac{-C_1^g(T - T_g)}{C_2^g + (T - T_g)} \tag{6.5}$$

where

$$C_1^g = \frac{B}{f_g} \quad \text{and} \quad C_2^g = \frac{f_g}{\Delta\alpha} \tag{6.6}$$

with f_g the fractional free volume at the glass-transition temperature T_g (reference state), and $\Delta\alpha$ the difference between the thermal expansivity above and below T_g. From the WLF-equation it follows that at high temperatures ($T \gg T_g$), the constant B/f_g is approximately equal to the shift factor $\ln a_T$. Since the relaxation times at the glass-transition temperature ($\tau(T_g)$ typically of the order of 10^2 s), and at high temperatures ($\tau(T) \approx 10^{-13}$ s, bounded by vibrational transitions) differ at most fifteen orders of magnitude, f_g has a "universal" value of approximately $1/\ln(10^{15}) = 0.029$ ($B \approx 1$) (Struik, 1987).

In many types of deformation, dilatation occurs, which finally, if not immediately, should contribute to the amount of free volume. Given the wide applicability of the WLF-equation (Ferry, 1980, Chapter 11), it is not surprising that many authors have considered stress-induced changes of the relaxation times to originate from changes in free volume through dilatation (Ferry, 1980, Chapter 18). If it is assumed that all relaxation times are equally affected by free volume, this leads to a so-called *volume clock*. Some authors even assumed that both, stress and temperature, influence (nonlinear) viscoelastic behaviour *solely* through changes in free volume. Shay, Jr. and Caruthers (1986) combined the free-volume definition ("hole fraction") of the Simha-Somcynsky equation-of state, which is a known function of temperature, pressure and specific volume, with the Doolittle equation, Eq. (6.3), to derive a "volume clock" for the nonlinear viscoelastic constitutive behaviour of polymer glasses. Also O'Dowd and Knauss (1995) used the Doolittle equation to describe yield-like behaviour, using the fractional free volume f as an empirical parameter to describe the thermodynamic state of the material (see also Knauss and Emri (1981, 1987) and Losi and Knauss (1992)). Using only a volume clock, however, these models could not reproduce yield-like behaviour in deformations with a negative dilatation, like uniaxial compression (O'Dowd and Knauss, 1995). Moreover, these models were unable to describe Von Mises-like yield behaviour, since, for example, the dilation in shear deformation is much smaller than in tensile deformation (Shay, Jr. and Caruthers, 1986).

Stress-clock models, like the Leonov model introduced in Chapter 2, do not suffer from the deficiencies mentioned above, but, as they stand, do not describe intrinsic strain softening. Combining a volume clock with a stress clock, could result in a natural way to describe intrinsic strain softening for stress-clock models, retaining their favourable characteristics. A volume clock can be introduced

in the compressible Leonov model, Eq. (2.52), in a straightforward way, if it is assumed that free volume only affects mobility (the viscosity function) and does not contribute to the stress tensor directly. In that case, only a shift function, and an evolution equation for free volume, are needed. The Doolittle equation, Eq. (6.3), is the obvious choice for the free-volume shift function. With respect to the evolution equation, it could be assumed, in principle, that deformation induced dilatation directly contributes to the amount of free volume (O'Dowd and Knauss, 1995). However, an elastic dilatation would enlarge all free volume sites instantaneously, and since only free-volume sites larger than a critical size contribute to particle diffusion (Turnbull and Cohen, 1961), a time-lag is to be expected. A well-known phenomenological evolution equation for the fractional free volume f, at isothermal conditions, in the absence of deformation, is due to Kovacs (1964):

$$\dot{f} = -\frac{f - f_\infty(T)}{\tau(f,T)} \tag{6.7}$$

Here, $f_\infty(T)$ is the equilibrium-free volume at temperature T, and $\tau(f,T)$ is a relaxation time. This equation can be augmented, in a straightforward way, to include the effect of deformation, assuming that the dilatation $(J-1)$ adds to the equilibrium value of the (fractional) free volume (rather than the free volume itself), and that the relaxation time $\tau(f,T)$ is equal to the mechanical relaxation time η/G:

$$\dot{f} = -k\frac{f - (f_\infty(T) + \alpha(J-1))}{\eta(\tau_{eq},T,f)/G} \tag{6.8}$$

where two extra fit parameters, α and k, have been added to generalize Eq. (6.7). This evolution equation for the fractional free volume combined with the Doolittle equation, Eq. (6.3), constitutes a "volume clock", which can be introduced in the compressible Leonov model (Chapter 2, Eq. (2.52)):

$$\mathbf{T} = K(J-1)\mathbf{I} + G\tilde{\mathbf{B}}_e^{\,d} \tag{6.9a}$$

$$\overset{\circ}{\tilde{\mathbf{B}}}_e = (\mathbf{D}^d - \mathbf{D}_p)\cdot\tilde{\mathbf{B}}_e + \tilde{\mathbf{B}}_e\cdot(\mathbf{D}^d - \mathbf{D}_p) \tag{6.9b}$$

$$\dot{J}\mathbf{I} = J\,\mathrm{tr}(\mathbf{D})\mathbf{I} \tag{6.9c}$$

$$\dot{f} = -k\frac{f - (f_\infty + \alpha(J-1))}{\eta(\tau_{eq},f)/G} \tag{6.9d}$$

$$\mathbf{D}_p = \frac{\mathbf{T}^d}{2\eta(\tau_{eq},f)} \tag{6.9e}$$

$$\eta(\tau_{eq},f) = \eta_0\, a_\sigma\, a_f \tag{6.9f}$$

$$a_\sigma = \frac{\left(\frac{\tau_{eq}}{\tau_0}\right)}{\sinh\left(\frac{\tau_{eq}}{\tau_0}\right)} \tag{6.9g}$$

$$a_f = \exp\left(\frac{B}{f} - \frac{B}{f_{ref}}\right) \tag{6.9h}$$

A few remarks with respect to Eq. (6.9) are in place. In Chapter 3, it was shown that the compressible Leonov model, actually, is a single mode approximation of the relaxation time spectrum, describing only the longest relaxation time (see Figure 3.9). Introduction of a volume clock can, therefore, only be expected to account for the effect of aging and rejuvenation on the "yield point". According to Eq. (6.9), the effect of aging (at zero stress) on the "yield point" will be negligible, since the mechanical relaxation time in Eq. (6.9d) is very large (for polycarbonate in the order of 10^{17} s). The effect of rejuvenation will depend on the values of the parameters α, f_∞, f_{ref}, B, k and f_0 (the initial value of f at "zero" time), and can be fitted to experiment[1].

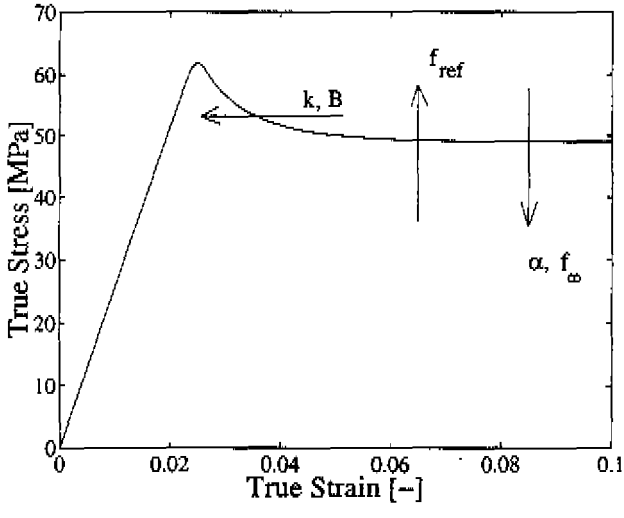

Figure 6.1 *Effect of free-volume parameters, see Eq. (6.8), on strain-softening behaviour in uniaxial tensile deformation of polycarbonate ($\dot{\varepsilon} = 10^{-2}\ s^{-1}$), as described by the compressible Leonov model augmented with a volume clock; schematic.*

A schematic uniaxial tensile response of the compressible Leonov model augmented with a volume clock, Eq. (6.9), is depicted in Figure 6.1. In this figure, some typical free-volume parameters were used: $f_{ref} = f_0 = 0.012$ [-] (in the order of the "universal" value of f at T_g: $f = 0.029$), $k = B = \alpha = 1$ [-] and $f_\infty = 0.01$ [-] (O'Dowd and Knauss, 1995).

[1]Since rejuvenation inevitably results in strain localisation, this requires a numerical evaluation of the inhomogeneous experiments (Timmermans *et al.*, 1995).

From Figure 6.1 it is clear, that combination of a volume clock with a stress clock, can lead to a realistic description of intrinsic strain-softening behaviour in uniaxial tensile deformation. The mechanical relaxation time, which governs the transition to yield-like behaviour, also determines the evolution of free volume (see Eq. (6.9d)). Choosing the initial value of f equal to its reference value ($f_0 = f_{ref}$), the volume clock will only start to work after the stress clock has initiated "yielding". Therefore, an important feature of the stress-clock model, Von Mises-like yield behaviour, is retained.

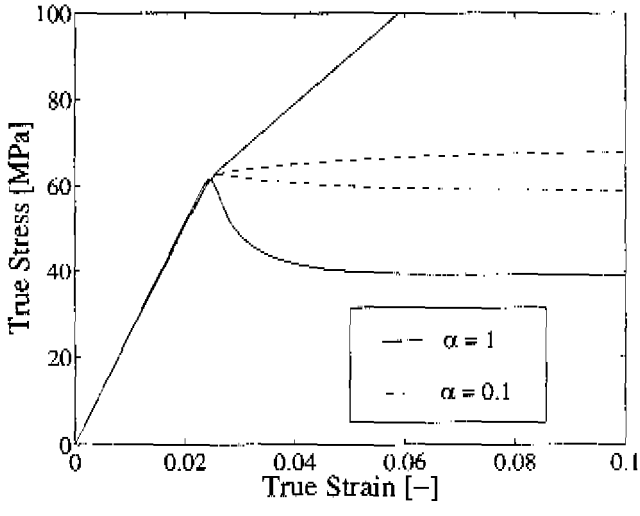

Figure 6.2 *Effect of the free-volume parameter α, see Eq. (6.8), on strain-softening behaviour in uniaxial tension and compression. The two upper lines constitute the response in compression and the two lower lines are the corresponding tensile curves.*

The crucial test of the model, however, is the behaviour in a deformation with negative dilatation (compression). This is depicted in Figure 6.2, showing the influence of the free-volume parameter α on the strain-softening behaviour in uniaxial tensile and compression. In this Figure, the same parameters were used as in Figure 6.1, only f_∞ was equated with f_{ref} and f_0, which is the maximum value from a Physics point of view[2]. As is clear from Figure 6.2, the response of the volume clock in compression, at $\alpha = 1$, is stronger than the stress clock and prohibits yielding. The contribution of the volume clock can be nullified by decreasing the parameter α, which is equivalent to reducing the amount of dilatation to be added to the equilibrium value of the fractional free volume. Unfortunately,

[2]If f_∞ would be larger than f_{ref}, then the (free) volume would *increase* upon aging.

this also reduces the amount of intrinsic strain softening in uniaxial tension. It must be concluded, that the combination of a free-volume clock with the compressible Leonov model, as depicted in Eq. (6.9), is not able to describe intrinsic strain softening in both tensile and compression experiments. The basic idea, advocated in Eq. (6.9), is that deviatoric stress reduces the mechanical relaxation time, while, at the same time, mechanical dilatation lifts the equilibrium free-volume value f_∞ over the actual amount of free volume f, resulting in an increase in mobility (intrinsic strain softening). However, in a deformation with negative dilatation, this will always lead to a *decrease* in mobility, whereas, experimentally, strain softening is also known to occur in, for example, uniaxial compression (Whitney and Andrews, 1967; Brown and Ward, 1968; Boyce and Arruda, 1990). It appears, therefore, that the elastic volume changes which occur during deformation have no (direct) influence on mobility. This was confirmed experimentally by Hasan *et al.* (1993), who observed an *increase* in free volume upon uniaxial *compression*, using positron annihilation lifetime spectroscopy. Also dilatometric experiments by McKenna *et al.* (1991) (see also Santore *et al.* (1991), and Waldron, Jr. *et al.* (1995)) indicate that the thermodynamic (volume) state of a glass is decoupled from the mechanical stress or deformation (McKenna *et al.*, 1994).

6.3 Phenomenological Approach to Rejuvenation

In a uniaxial tensile experiment, after the yield point, necking occurs and a load drop is observed. Part of this drop is due to the geometric instability and part is due to intrinsic strain softening (rejuvenation). The existence of rejuvenation can be demonstrated by comparison of the stress-strain behaviour of two polycarbonate samples, one quenched from the melt, the other annealed close to the glass-transition temperature, as depicted in Figure 6.3. The large difference in thermal history induces a significant difference in yield stress. Yet the stress at which stable neck growth proceeds, as well as the draw ratio in the neck, are approximately equal. This is a strong indication that after large plastic deformations the effect of (thermal) history is erased; the material is rejuvenated. Moreover, the constant value to which the flow stress evolves, appears to be independent of the thermal history (Hasan *et al.*, 1993). The level that is reached is usually regarded as a saturation level of rejuvenation. This was also shown in uniaxial compression experiments on annealed and quenched polycarbonate and poly(methyl methacrylate) by Hasan *et al.* (1993). Using positron annihilation lifetime spectroscopy, they observed an increase in the size of free volume sites following inelastic deformation, and found the initially quenched and annealled specimen to posses the same post-deformation free-volume distribution.

Hasan *et al.* (1993) postulated that shear transformations occur in regions of increased free volume, where the local resistance is low. To model rejuvenation

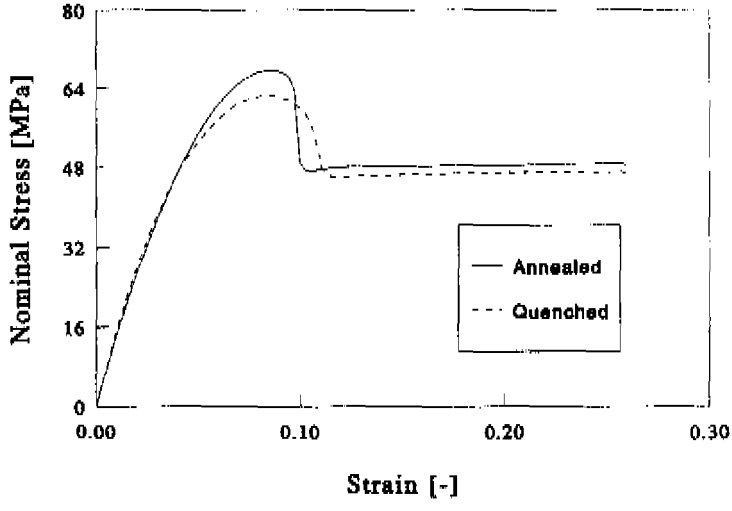

Figure 6.3 *Stress-strain curves at a strain rate* $\dot{\epsilon} = 10^{-2}\ s^{-1}$ *of two polycarbonate samples at room temperature, one annealed close to the glass-transition temperature, the other quenched from the melt. The draw ratio in the neck was equal for both samples.*

they proposed a first order evolution equation for the number density D of such regions as a function of (equivalent) plastic strain:

$$\frac{dD}{d\gamma_p} = -\frac{D - D_\infty}{\tau_p} \tag{6.10}$$

where D_∞ is the equilibrium value of D, and τ_p is a relaxation time. Combination with a "D-shift factor" a_D (actually a plastic-strain shift factor a_γ), defined in Eq. (6.11)[3], these two equations constitute a "D-clock", which can be incorporated in the compressible Leonov model, see Eq. (4.2a) (Timmermans *et al.*, 1995).

$$a_D = \exp(-D) \tag{6.11}$$

Here, D_∞ determines the steady state flow stress and (D_∞/τ_p) the softening slope. This phenomenological description of intrinsic strain softening was used in Chapter 4 to determine the evolution of plastic strain at constant stress (see Eq. (4.2) and Figures 4.5 and 4.6).

[3]Hasan *et al.* (1993) used as shift factor ($a_D = 1/D$), but since D has to change several orders of magnitude, Eq. (6.11) is more convenient (Timmermans *et al.*, 1995).

6.4 Aging, Rejuvenation and Nonlinear Viscoelasticity

It is now widely accepted that in the linear viscoelastic range, time-aging time superposition applies (Struik, 1978). The combined action of aging and nonlinear viscoelastic behaviour, however, is still a controversial area of research (Waldron, Jr. *et al.*, 1995). Large deformations beyond the yield point lead to a saturation level of rejuvenation and result in a complete erasure of the aging history as confirmed by mechanical testing (previous Section), positron annihilation experiments (Hasan *et al.*, 1993) and caloric measurements (Oleinik *et al.*, 1993).

On basis of aging studies, combining large and small stresses, it has been stated (Struik, 1978; Ricco and Smith, 1985; Smith *et al.*, 1988; Yee *et al.*, 1988) that rejuvenation also occurs at moderate stresses below the yield stress. This was disputed by others (Lee and McKenna, 1990; Santore *et al.*, 1991; Waldron, Jr. *et al.*, 1995, and references therein), who argued that the rejuvenation effects observed could be described using a nonlinear viscoelastic constitutive equation with fading memory. McCrum (1984, 1992) proposed a sequential aging hypothesis, in which it is assumed that aging predominantly affects those relaxation times which are comparable to the aging time. According to this hypothesis, time-aging time superposition is a valid approximation in the linear region, where only the "short" relaxation times are probed. At high stress, touching the long relaxation times which have not been able to age, time-aging time superposition does not apply anymore.

In Chapter 3, it was shown that the "yield stress" is determined by the longest relaxation time. Therefore, according to time-aging time superposition, aging far below the glass-transition temperature should equally affect the "yield stress" and linear viscoelastic behaviour (see Figure 6.4). Experimentally, however, the retardation times shift proportionally to aging time in the linear viscoelastic range, whereas the effect of aging on the yield stress is much smaller. This could be due to rejuvenation at moderate stress, below the "yield stress" (Struik, 1978). On the other hand, the increase in "yield stress" upon annealing close to the glass-transition temperature is apparently not affected. Moreover, the good agreement between experiments and predictions for the stress-relaxation experiments at moderate stress (see Figure 3.14), as well as the applicability of time-stress superposition (see Figure 3.5), suggest that for short monotone loading paths up to the "yield stress", rejuvenation effects are not important.

According to the sequential aging hypothesis, the "yield stress" is not affected by aging far below the glass-transition temperature, because the longest relaxation times are much larger than the aging time, and barely change. However, at temperatures close to the glass-transition temperature, the longest relaxation times become comparable to the aging times and are subjected to aging, resulting in an increase of the "yield stress". This was also confirmed by Bauwens (1987), who observed that aging of quenched (young) polycarbonate at room temperature resulted in a significant stiffening of the tensile curve at low stress (determined by

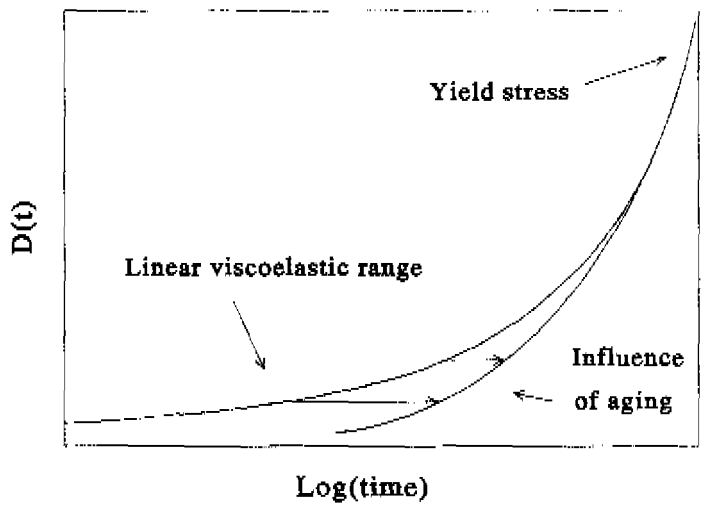

Figure 6.4 *Schematic representation of the influence of aging on the linear compliance curve. From experiment it is well established that at short times, the compliance curve shifts proportional to aging time. However, the yield stress, which is determined by the longest relaxation time, is hardly affected by aging. This indicates that aging not only shifts the compliance curve, but also changes its shape.*

the "shorter" relaxation times), but hardly affected the yield stress, whereas annealing close to the glass transition temperature resulted in a substantial increase of the yield stress, leaving the shape of the tensile curve at low stress unchanged. Since deviatoric stress and temperature have a similar effect on relaxation times, it could very well be that prolonged exposure to elevated stresses results in similar effects as described above. For instance Vincent (1960) already observed that post yielded polyvinyl chloride "quenched" to zero stress exhibits no strain softening upon reloading, whereas the same material after relaxation just below the yield stress (equivalent to annealing just below the glass transition temperature) possesses an increased yield stress and does display strain softening (see Figure 6.5).

There is more experimental evidence that the influence of aging is not to shift the complete compliance curve, but only that part where the relaxation times are of the same order of magnitude as the aging times considered. Venditti and Gillham (1992a, 1992b) used torsional bread analysis to show that by aging at different temperatures it is possible to change specific parts of the relaxation time spectrum.

These complicated effects of aging at elevated stress and temperature, not

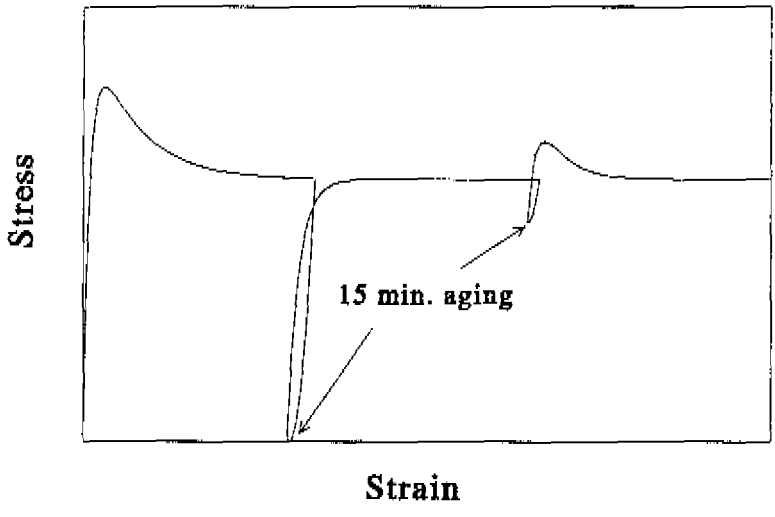

Figure 6.5 *Schematic representation of the post yield behaviour of polyvinyl chloride, as observed by Vincent (1960). After quenching to zero stress the material exhibits no strain softening upon reloading, whereas the same material after relaxation just below the yield stress (equivalent to annealing just below the glass transition temperature) possesses an increased yield stress and does display strain softening.*

only shifting the relaxation time spectrum, but also changing its shape, are not taken into account by the constitutive model proposed in this thesis, which uses only a stress clock (see Figure 7.4). It is therefore to be expected that especially in cyclic loading situations the proposed model will fail.

Chapter 7

Conclusions and Recommendations

The objective of the study described in this thesis was to develop a detailed three-dimensional constitutive equation for the nonlinear viscoelastic behaviour of glassy polymers. Most constitutive models which are known to date, focus on a special aspect of the material behaviour and neglect the rest. For example, to describe the nonlinear viscoelastic behaviour at small deformations, rather detailed models have been proposed, which are only valid in a specific deformation mode. On the other hand, finite three-dimensional constitutive equations developed to describe strain hardening, often totally neglect this non-linear behaviour at small strains.

In this thesis, an attempt is made to combine all these aspects of the deformation behaviour, and to develop a single constitutive equation for the finite, nonlinear viscoelastic behaviour of glassy polymers. To this extent, the "time-stress superposition principle" is invoked, sometimes referred to as a "stress clock". Time-stress superposition states that the main influence of stress is to change equally all relaxation times associated with a specific molecular transition. This nonlinear influence of stress, originating from stress-biased segmental diffusion, is described quantitatively by the Eyring theory, which defines a shift factor a_σ by which all relaxation times are multiplied. In general, the relaxation behaviour of polymer glasses is dominated by two relaxation mechanisms: the glass transition and the reptation process. Therefore, in essence, time-stress superposition states that "yielding" can be envisaged as a stress-induced glass transition, and, tentatively, that ductile fracture is related to stress-induced reptation.

To describe three-dimensional relaxation behaviour, a basic model, a so-called "compressible Leonov mode" is presented in Chapter 2. A single Leonov mode is a Maxwell model (see Figure 7.1), splitting the total rate-of strain tensor $\mathbf{D}$ in an elastic part $\mathbf{D}_e$ and a plastic part $\mathbf{D}_p$. The relaxation time, $\lambda = \eta(\tau_{eq})/G$, depends on an equivalent stress τ_{eq}, proportional to the Von Mises stress. The nonlinearity is determined by the parameter τ_0 (related to the activation volume). At low stress, $\tau_{eq} \ll \tau_0$, the relaxation time is constant $\lambda = \lambda_0$ ($a_\sigma = 1$). At higher stress levels, $\tau_{eq} \geq \tau_0$, the relaxation time decreases rapidly as described by the

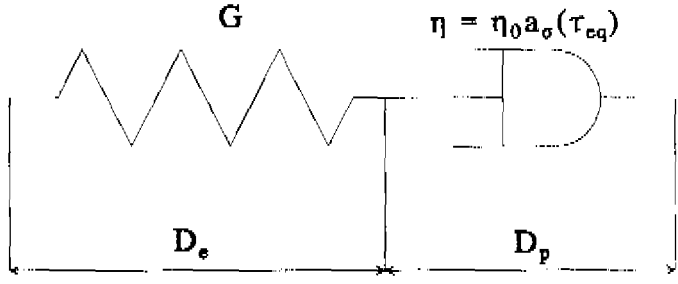

Figure 7.1 *Graphical representation of the deviatoric stress response of a single Leonov mode.*

shift function a_σ[1]. Furthermore, a Leonov mode is capable of describing finite deformations, and correctly separates the (elastic) hydrostatic stress (described by a constant bulk modulus K), and (viscoelastic) deviatoric stress. It is depicted as:

$$\mathbf{T} = K(J-1)\mathbf{I} + G\tilde{\mathbf{B}}_e^{\,d} \tag{7.1a}$$

$$\overset{\circ}{\tilde{\mathbf{B}}}_e = (\mathbf{D}^d - \mathbf{D}_p)\cdot\tilde{\mathbf{B}}_e + \tilde{\mathbf{B}}_e\cdot(\mathbf{D}^d - \mathbf{D}_p) \tag{7.1b}$$

$$\dot{J}\mathbf{I} = J\,\mathrm{tr}(\mathbf{D})\mathbf{I} \tag{7.1c}$$

$$\mathbf{D}_p = \frac{\mathbf{T}^d}{2\eta(\tau_{eq})} \tag{7.1d}$$

$$\eta(\tau_{eq}) = \eta_0\, a_\sigma \tag{7.1e}$$

$$a_\sigma = \frac{\left(\frac{\tau_{eq}}{\tau_0}\right)}{\sinh\left(\frac{\tau_{eq}}{\tau_0}\right)} \tag{7.1f}$$

Here, $\mathbf{T}$ is the Cauchy stress tensor, K is the bulk modulus, G the shear modulus, $\mathbf{I}$ the second order unity tensor, $J-1$ the relative volume deformation, and $\tilde{\mathbf{B}}_e$ an internal variable, describing the isochoric elastic strain stored in the Leonov mode during deformation.

Subsequently, this Leonov model can be extended to a "multi-mode" expression, to describe the bimodal spectrum of relaxation times which rules the complete deformation behaviour of polymer glasses. This is depicted graphically in

[1] up to typically 15 decades changing the stress from zero to the yield stress for polycarbonate at room temperature.

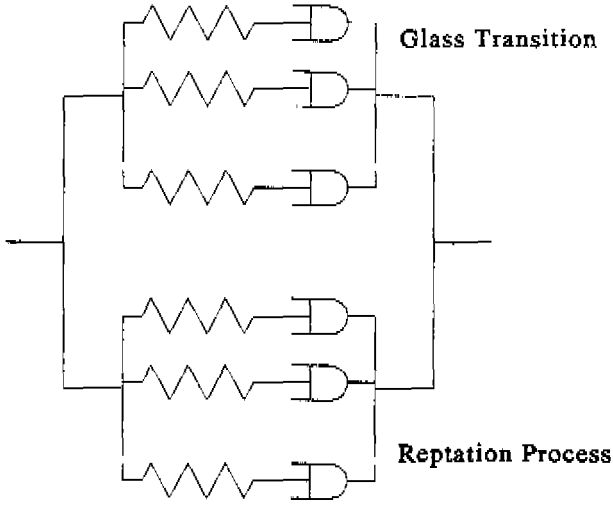

Figure 7.2 *Mechanical analogue of the bimodal spectrum of relaxation times of a polymer glass, composed of the glass transition and the reptation process. In principle, both sets of relaxation times can have their own temperature and stress dependence.*

Figure 7.2, and can be written as:

$$\mathbf{T} = K(J-1)\mathbf{I} + \sum_i G_i \tilde{\mathbf{B}}^d_{e,i} + \sum_j G_j \tilde{\mathbf{B}}^d_{e,j} \tag{7.2a}$$

$$\dot{J}\mathbf{I} = J\,\mathrm{tr}(\mathbf{D})\mathbf{I} \tag{7.2b}$$

$$\overset{\circ}{\tilde{\mathbf{B}}}_{e,i} = (\mathbf{D}^d - \mathbf{D}_{p,i}) \cdot \tilde{\mathbf{B}}_{e,i} + \tilde{\mathbf{B}}_{e,i} \cdot (\mathbf{D}^d - \mathbf{D}_{p,i}) \tag{7.2c}$$

$$\mathbf{D}_{p,i} = \frac{\mathbf{T}^d_i}{2\eta_i(\tau^{(1)}_{eq})} \tag{7.2d}$$

$$\eta_i(\tau^{(1)}_{eq}) = \eta_{0,i}\, a^{(1)}_\sigma \tag{7.2e}$$

$$a^{(1)}_\sigma = \frac{\left(\dfrac{\tau^{(1)}_{eq}}{\tau^{(1)}_0}\right)}{\sinh\left(\dfrac{\tau^{(1)}_{eq}}{\tau^{(1)}_0}\right)} \tag{7.2f}$$

$$\tau^{(1)}_{eq} = \sqrt{\frac{1}{2}\,\mathrm{tr}(\mathbf{T}^d_{(1)} \cdot \mathbf{T}^d_{(1)})} \tag{7.2g}$$

$$\mathbf{T}^d_{(1)} = \sum_i \mathbf{T}^d_i = \sum_i G_i \tilde{\mathbf{B}}^d_{e,i} \tag{7.2h}$$

$$\overset{\circ}{\bar{\mathbf{B}}}_{e,j} = (\mathbf{D}^d - \mathbf{D}_{p,j}) \cdot \bar{\mathbf{B}}_{e,j} + \hat{\mathbf{B}}_{e,j} \cdot (\mathbf{D}^d - \mathbf{D}_{p,j}) \tag{7.2i}$$

$$\mathbf{D}_{p,j} = \frac{\mathbf{T}^d_j}{2\eta_j(\tau^{(2)}_{eq})} \tag{7.2j}$$

$$\eta_j(\tau^{(2)}_{eq}) = \eta_{0,j}\, a^{(2)}_\sigma \tag{7.2k}$$

$$a^{(2)}_\sigma = \frac{\left(\frac{\tau^{(2)}_{eq}}{\tau^{(2)}_0}\right)}{\sinh\left(\frac{\tau^{(2)}_{eq}}{\tau^{(2)}_0}\right)} \tag{7.2l}$$

$$\tau^{(2)}_{eq} = \sqrt{\frac{1}{2}\,\mathrm{tr}(\mathbf{T}^d_{(2)} \cdot \mathbf{T}^d_{(2)})} \tag{7.2m}$$

$$\mathbf{T}^d_{(2)} = \sum_j \mathbf{T}^d_j = \sum_j G_j \bar{\mathbf{B}}^d_{e,j} \tag{7.2n}$$

Here, $a^{(1)}_\sigma$ and $a^{(2)}_\sigma$ are the shift factors for the relaxation times associated with, respectively, the glass transition and the reptation process. The stress dependence of the relaxation times of these two processes, determined by $\tau^{(1)}_0$ and $\tau^{(2)}_0$, is not necessarily the same. If they are different ($\tau^{(1)}_0 \neq \tau^{(2)}_0$), this gives rise to *stress-rheological complex behaviour*.

The model was demonstrated for polycarbonate in Chapter 3. Polycarbonate was chosen as a model system since, with respect to experimental characterisation, it combines a number of attractive properties. It has a single dominant relaxation mechanism at room temperature and, therefore, it behaves like a rheologically simple material. Furthermore, it has a relative strong strain-hardening response, counter-acting fatal strain-localisation phenomena, like crazing.

To determine the multi-mode Leonov parameters for polycarbonate, the virtual[2] linear creep compliance master curve was constructed by horizontal shifting of creep curves at different stress levels (Chapter 3, Figure 3.5). By fitting the shift factors with the Eyring shift function $a^{(1)}_\sigma$, the nonlinearity parameter $\tau^{(1)}_0$ was determined: $\tau^{(1)}_0 = 0.89$ MPa. The linear compliance curve was transformed to the linear shear relaxation modulus, see Figure 7.3, using the correspondence principle (see Appendix A). Eighteen Leonov modes provided an accurate description of the shear relaxation modulus, using an equidistant grid of relaxation times. The resulting eighteen relaxation times and shear moduli, which describe that part of the spectrum which is due to the glass transition, are depicted in Tabel 7.1[3].

In Chapter 5 it was shown experimentally, that the three-dimensional strain-hardening response is accurately described by neo-Hookean behaviour, employing

[2] Aging effects are not included!

[3] In principle, the shear relaxation modulus, depicted in Figure 7.3, also includes the shear relaxation modulus due to the reptation process. However, the network response only contributes three percent to the total ("glassy") shear modulus, and can, therefore, safely be neglected.

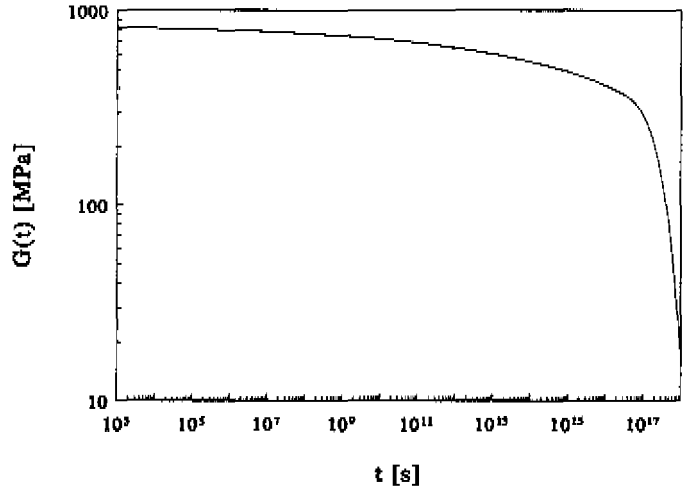

Figure 7.3 *The linear shear relaxation modulus $G(t)$ calculated from the linear tensile compliance curve $D(t)$ as described in Appendix A.*

a shear modulus $G = 26$ MPa at room temperature. It was also shown that the strain-hardening response is essentially elastic, and even at elevated temperatures no strain-rate effects were observed. This indicates that the stress dependence of the reptation process is much smaller compared to the stress dependence of the glass transition. With respect to modelling, this implies that the spectrum due to the reptation process reduces to a single neo-Hookean spring, describing the strain-hardening response.

Summarizing, the multi-mode Leonov model for polycarbonate comprises eighteen modes to describe the glass transition part of the spectrum and a single spring (one Leonov mode with an infinite viscosity) to capture the strain-hardening response. This is depicted graphically in Figure 7.4 and is written as:

$$\mathbf{T} = K(J-1)\mathbf{I} + \sum_i G_i \tilde{\mathbf{B}}^d_{e,i} + G_r \tilde{\mathbf{B}}^d_{e,r} \tag{7.3a}$$

$$\dot{J}\mathbf{I} = J\,\mathrm{tr}(\mathbf{D})\mathbf{I} \tag{7.3b}$$

$$\overset{\circ}{\tilde{\mathbf{B}}}_{e,i} = (\mathbf{D}^d - \mathbf{D}_{p,i}) \cdot \tilde{\mathbf{B}}_{e,i} + \tilde{\mathbf{B}}_{e,i} \cdot (\mathbf{D}^d - \mathbf{D}_{p,i}) \tag{7.3c}$$

$$\mathbf{D}_{p,i} = \frac{\mathbf{T}^d_i}{2\eta_i(\tau^{(1)}_{eq})} \tag{7.3d}$$

i	λ_i [s]	G_i [MPa]	$\eta_{0,i} = \lambda_{0,i} \cdot G_i$ [MPa·s]
1	0.7080e+04	0.2254e+02	0.1596e+06
2	0.3548e+06	0.9810e+01	0.3481e+07
3	0.2512e+07	0.1096e+02	0.2753e+08
4	0.1778e+08	0.1354e+02	0.2407e+09
5	0.1259e+09	0.1633e+02	0.2056e+10
6	0.8913e+09	0.1687e+02	0.1503e+11
7	0.6310e+10	0.2125e+02	0.1341e+12
8	0.4467e+11	0.2331e+02	0.1041e+13
9	0.3162e+12	0.3336e+02	0.1055e+14
10	0.2239e+13	0.3642e+02	0.8153e+14
11	0.1585e+14	0.4226e+02	0.6698e+15
12	0.1122e+15	0.4532e+02	0.5085e+16
13	0.7943e+15	0.5148e+02	0.4089e+17
14	0.5623e+16	0.7140e+02	0.4015e+18
15	0.3981e+17	0.5088e+01	0.2026e+18
16	0.2818e+18	0.3992e+03	0.1125e+21
17	0.1995e+19	0.6563e+01	0.1310e+20
18	0.1413e+20	0.2049e+01	0.2894e+20

Table 7.1 *Linear Leonov parameters obtained by fitting the linear relaxation modulus*

$$\eta_i(\tau_{eq}^{(1)}) = \eta_{0,i}\, a_\sigma^{(1)} \tag{7.3e}$$

$$a_\sigma^{(1)} = \frac{\left(\frac{\tau_{eq}^{(1)}}{\tau_0^{(1)}}\right)}{\sinh\left(\frac{\tau_{eq}^{(1)}}{\tau_0^{(1)}}\right)} \tag{7.3f}$$

$$\tau_{eq}^{(1)} = \sqrt{\frac{1}{2}\,\mathrm{tr}(\mathbf{T}_{(1)}^d \cdot \mathbf{T}_{(1)}^d)} \tag{7.3g}$$

$$\mathbf{T}_{(1)}^d = \sum_i \mathbf{T}_i^d = \sum_i G_i \tilde{\mathbf{B}}_{e,i}^d \tag{7.3h}$$

$$\overset{\circ}{\tilde{\mathbf{B}}}_{e,r} = \mathbf{D}^d \cdot \tilde{\mathbf{B}}_{e,r} + \tilde{\mathbf{B}}_{e,r} \cdot \mathbf{D}^d \tag{7.3i}$$

A numerical prediction of a uniaxial tensile test, using the parameters in Table 7.1 and a strain-hardening modulus $G_r = 26$ MPa, is depicted in Figure 7.5 (see also Figures 3.11-3.15). From these Figures, it is clear that the multi mode Leonov model accurately captures many aspects of the nonlinear viscoelastic behaviour, including rate-dependent "yielding".

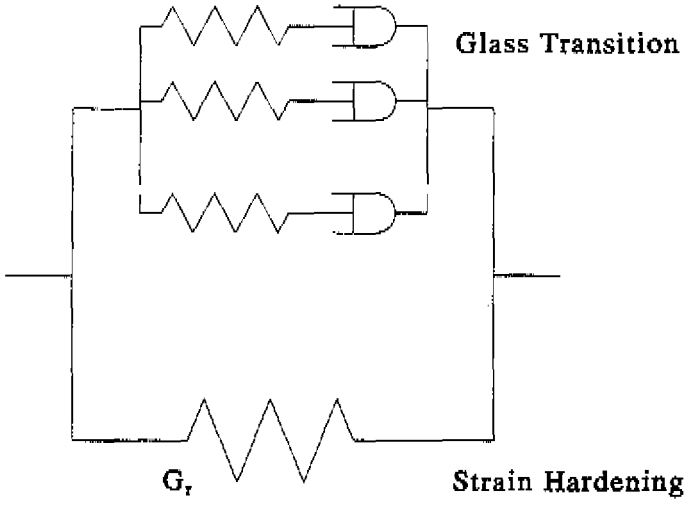

Figure 7.4 *Mechanical analogue of the deviatoric stress response of polycarbonate, consisting of eighteen Leonov modes to describe the glass transition, and a single spring to model the strain-hardening response.*

In Chapter 5, it was also shown that for polycarbonate, even at large strains (up to a draw ratio $\lambda = 3$ in uniaxial tensile deformation), no asymptotic upswing in stress, indicative of a finite extensibility of the entanglement network, was observed. The three-dimensional strain-hardening response was accurately described by neo-Hookean behaviour. However, if compelled to by experiment[4], finite extensibility could easily be incorporated in Eq. (7.3), by replacing the constant shear modulus G_r with, for example, the deformation-dependent shear modulus from the "eight chain model" $G_8(I_{\bar{\mathbf{B}}_r})$ (Arruda and Boyce, 1993b) (see also Eq. (5.15)).

It should also be noted that, especially at elevated temperatures, the relaxation behaviour of the entanglement network ("entanglement slip") finally must become apparent, since polycarbonate is a thermoplast which ultimately can flow. It could be assumed, tentatively, that this will also occur at high stress, leading to ductile fracture. It would be interesting to determine whether ductile fracture at large deformations is rate-dependent, and if so, whether this rate dependence can be captured by a stress-dependent relaxation time (Eq. (7.2) with $j = 1$, equivalent to adding a stress-dependent "dash pot" to the strain-hardening modulus).

If one is only interested in rate-dependent yield behaviour, a useful approx-

[4]e.g., for other polymers, especially thermosets

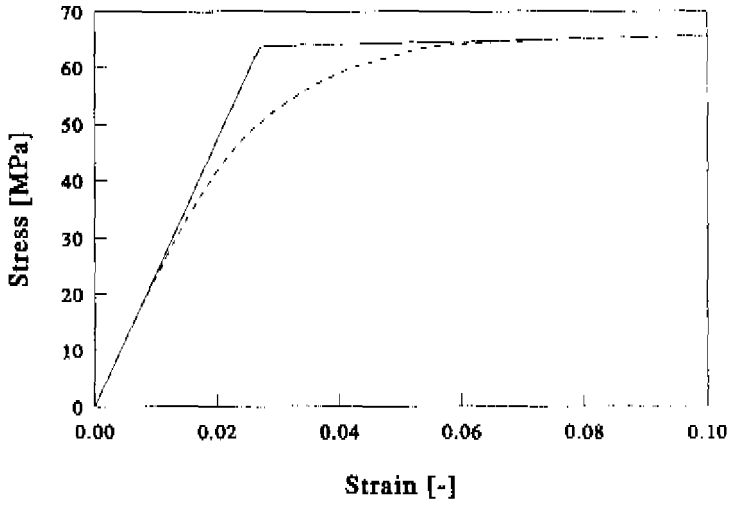

Figure 7.5 *Calculated uniaxial tensile response of the multi-mode Leonov model (dashed line), compared to the single-mode approximation (solid line).*

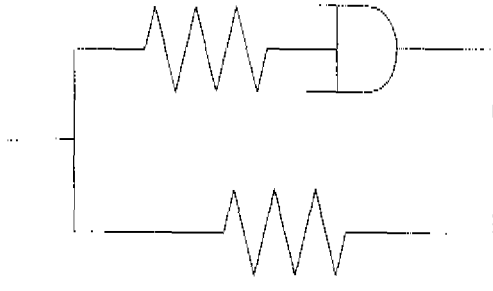

Figure 7.6 *Graphical representation of the "single-mode" approximation of the deformation behaviour of a glassy polymer. The Leonov mode describes rate-dependent yield behaviour, and the spring represents the strain-hardening response.*

imation is to add all moduli G_i and zero-shear viscosities $\eta_{0,i}$ in Table 7.1, and reduce the description of the glass transition part of the spectrum to a single Leonov mode. This is depicted in Figure 7.6 and Eq. (7.3) with $i = 1$. This "single-mode" Leonov model (actually a "double-mode" model) is similar to the well-known Haward-Thackray model (Haward and Thackray, 1968), and its three-dimensional extensions by Boyce *et al.* (1988); Wu and van der Giessen (1993),

and others. A typical uniaxial tensile curve of this single-mode approximation is depicted in Figure 7.5, together with the multi-mode prediction. It is clear that the use of a single stress-dependent relaxation time results in an abrupt transition from elastic to plastic deformation.

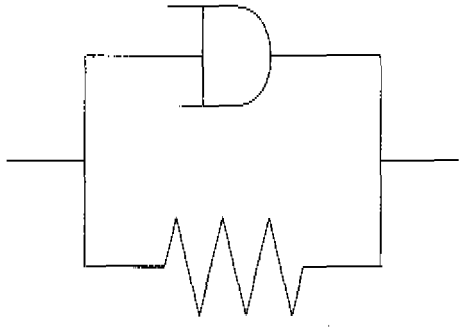

Figure 7.7 *Schematic drawing of the mechanical behaviour of a polymer glass at the yield point. The dashpot depicts the nonlinear flow behaviour, and the (neo-Hookean) spring represents the entropic strain hardening.*

It is of course possible to reduce the model even further, by neglecting the initial elastic response completely, in which case the single mode Leonov model becomes a Kelvin-Voigt model, depicted in Figure 7.7. This approximation was used in Chapter 4, to determine the effect of strain hardening on the evolution of plastic strain, and in Chapter 5, to describe the development of anisotropy as a function of predeformation above the glass transition temperature.

On Localisation Phenomena

In Chapter 4, it is illustrated how the combined action of nonlinear plastic flow behaviour, strain hardening and intrinsic strain softening, can lead to strain localisation. Strain localisation manifests itself in glassy polymers in the form of shear bands and crazes. Using an extremely brittle polystyrene grade as a model polymer, it is shown experimentally, that the strain rate dependence of the plastic flow process and craze initiation are identical. This is a strong indication that the formation of a micro shear band is the rate-determining step in craze initiation. The cavitation of the shear band which leads to a craze, is either a relatively fast, or even time-independent, process. This offers possibilities for defining a local (time-independent) craze criterion, by comparison of detailed finite-element calculations of a given micro-structure with experimental craze studies. Such a local criterion is essential in computer-aided design of new heterogeneous polymer systems, where the morphology is optimized in such a way that shear yielding

prevails crazing (van der Sanden *et al.*, 1993).

On Aging and Rejuvenation

It should be noted that mechanical properties in general, and viscoelastic behaviour especially, are profoundly influenced by physical aging. It is now well established that, under influence of aging, the creep compliance curve shifts toward longer times. However, all samples used in this study had the same age, which by far exceeded the longest time in the experiments. Therefore, to a first approximation, aging was not taken into account (which will cause the model to be less accurate for differently aged samples). As opposed to aging, it has also been observed that plastic deformation beyond the "yield point" can result in a decrease of the viscosity, leading to intrinsic strain softening and a decrease of the yield stress. This phenomenon is called "rejuvenation" and is thought to be the result of mechanically "deaging" the sample by plastic deformation. There are indications in literature, that rejuvenation can occur even at moderate stress levels (Struik, 1978). However, the good agreement between experiments and predictions for the stress-relaxation experiments, as well as the applicability of time-stress superposition, indicate that for polycarbonate, rejuvenation effects are not important for monotone loading paths up to the "yield stress", and for short loading times relative to the age of the material. Although a quantitative description of rejuvenation (and aging) at moderate stresses has yet to be developed, several phenomenological models have been proposed that give an adequate description of strain softening in monotone loading paths after the yield point (Boyce *et al.*, 1988; Hasan *et al.*, 1993). These models can be used as a starting point for the development of rejuvenation models at moderate stress levels.

References

Allison, S. W. and Ward, I. M. (1967). The cold drawing of polyethylene terephtalate. *Brit. J. Appl. Phys.*, **18**, 1151.

Anand, L., Kim, K. H., and Shawki, T. G. (1987). Onset of shear localization in viscoplastic solids. *J. Mech. Phys. Solids*, **35**(4), 407.

Argon, A. S. (1973). A theory for the low-temperature plastic deformation of glassy polymers. *Phil. Mag.*, **28**, 839.

Argon, A. S. and Hannoosh, J. G. (1977). Initiation of crazes in polystyrene. *Phil. Mag.*, **36**(5), 1195.

Arruda, E. M. (1992). *Characterization of the Strain Hardening Response of Amorphous Polymers*. Ph.D. thesis, Massachusetts Institute of Technology.

Arruda, E. M. and Boyce, M. C. (1993a). Evolution of plastic anisotropy in amorphous polymers during finite straining. *Int. J. Plast.*, **9**(6), 697.

Arruda, E. M. and Boyce, M. C. (1993b). A three-dimensional constitutive equation for large stretch behaviour of rubber materials. *J. Mech. Phys. Solids*, **41**, 389.

Astarita, G. and Marrucci, G. (1974). *Principles of Non-Newtonian Fluid Mechanics*. McGraw-Hill, London.

Baaijens, F. T. P. (1991). Calculation of residual stresses in injection molded products. *Rheol. Acta.*, **30**, 284.

Bauwens, J. C. (1987). Differences between the effects of annealing and physical ageing on the mechanical behaviour of polycarbonate. *Plast. Rub. Proc. Appl.*, 7(3), 143.

Beris, A. and Edwards, B. (1990). Poisson bracket formulation of incompressible flow equations in continuum mechanics. *J. Rheol.*, **34**, 55.

Bernstein, B. and Shokooh, A. (1980). The stress clock function in viscoelasticity. *J. Rheol.*, **24**, 189.

Besseling, J. and van der Giessen, E. (1994). *Mathematical Modelling of Inelastic Deformations*. Chapman & Hall, London.

Bird, R., Armstrong, R., and Hassager, O. (1987). *Dynamics of Polymeric Liquids, vol. 1: Fluid Mechanics*. John Wiley & Sons, New York.

Bowden, P. (1970). A criterion for inhomogeneous deformation. *Phil. Mag.*, **22**, 455.

Boyce, M. C. (1986). *Large Inelastic Deformation in Glassy Polymers*. Ph.D. thesis, The Massachusetts Institute of Technology.

Boyce, M. C. and Arruda, E. M. (1990). An experimental and analytical investigation of the large strain compressive and tensile response of glassy polymers. *Pol. Eng. Sci.*, **30**(20), 1289.

Boyce, M. C., Parks, D. M., and Argon, A. S. (1988). Large inelastic deformation of glassy polymers, part 1: rate dependent constitutive model. *Mech. Mater.*, **7**(1), 15.

Brown, N. and Ward, I. M. (1968). Load drop at the yield point of a polymer. *J. Pol. Sci. A2*, **6**, 607.

Cohen, A. (1991). A padé approximant to the inverse langevin function. *Rheol. Acta*, **30**, 270.

Coleman, B. and Noll, W. (1963). The thermodynamics of elastic materials with heat conduction and viscosity. *Arch. Rational Mech. Anal.*, **13**, 167.

de Gennes, P. G. (1971). Reptation of a polymer chain in the presence of fixed obstacles. *J. Chem. Phys.*, **55**(2), 572.

De Koning, G. J. M. and Lemstra, P. J. (1993). Crystallization phenomena in bacterial poly[(*r*)-3-hydroxybutyrate]. 2. embrittlement and rejuvenation. *Polymer*, **34**, 4089.

de Smet, B. J., Bach, P. W., Scholten, H. F., Dortmans, L. J. M. G., and de With, G. (1992). Weakest-link failure predictions for ceramics iii: uniaxial and biaxial bend tests on alumina. *J. Eur. Ceram. Soc.*, **10**, 101.

Dekkers, M. E. J. (1985). *The Deformation Behaviour of Glass Bead-Filled Glassy Polymers*. Ph.D. thesis, Eindhoven University of Technology, Eindhoven, the Netherlands.

Donald, A. M. and Kramer, E. J. (1982a). Deformation zones and entanglements in glassy polymers. *Polymer*, **23**, 1183.

Donald, A. M. and Kramer, E. J. (1982b). The entanglement network and craze micromechanics in glassy polymers. *J. Polym. Sci. Polym. Phys. Ed.*, **20**, 1129.

Doolittle, A. K. (1951). Studies in newtonian flow. ii. the dependence of the viscosity of liquids on free-space. *J. Appl. Phys.*, **22**, 1471.

Ferry, J. D. (1980). *Viscoelastic Properties of Polymers*. John Wiley & Sons, Inc., New York, third edition.

Flory, P. J. (1988). *Statiscal Mechanics of Chain Molecules*. Hanser Publishers, Munich, second edition.

Flory, P. J. and Rehner, Jr., J. (1943). Statistical mechanics of cross-linked polymer networks. *J. Chem. Phys.*, **11**, 512.

Gent, A. N. and Wang, C. (1995). Fracture mechanics and cavitation in rubber-like solids. *J. Mat. Sci.*, **26**, 3392.

Grmela, M. (1985). Stress tensor in generalized hydrodynamics. *Phys. Lett. A*, **111**, 41.

G'Sell, C., Hiver, J. M., Dahouin, A., and Souahi, A. (1992). Video-controlled tensile testing of polymers and metals beyond the necking point. *J. Mater. Sci.*, **27**, 5031.

Hasan, O. A. and Boyce, M. C. (1995). A constitutive model for the nonlinear viscoelastic viscoplastic behaviour of glassy polymers. *Polym. Eng. Sci.*, **35**, 331.

Hasan, O. A., Boyce, M. C., Li, X. S., and Berko, S. (1993). An investigation of the yield and postyield behaviour and corresponding structure of poly(methyl methacrylate). *J. Polym. Sci. Polym. Phys. Ed.*, **31**, 185.

Haward, R. N. (1993). Strain hardening of thermoplastics. *Macromolecules*, **26**, 5860.

Haward, R. N. and Thackray, G. (1968). The use of a mathematical model to describe isothermal stress-strain curves in glassy polymers. *Proc. Roy. Soc. A.*, **302**, 453.

Hirschfelder, O. J., Curtiss, C. F., and Bird, R. B. (1967). *Molecular Theory of Gases and Liquids*. Chapman & Hall, London, fourth edition.

Hodge, I. M. (1995). Physical aging in polymer glasses. *Science*, **267**, 1945.

Huang, Y., Hunston, D. L., Kinloch, A. J., and Riew, C. K. (1993). Mechanism of toughening thermoset resins. In C. K. Riew and A. J. Kinloch, editors, *Toughened Plastics I, Science and Engineering*, Advances in Chemistry Series, page 1. American Chemical Society, Washington, D.C.

Hunter, S. C. (1983). *Mechanics of Continuous Media*. Ellis Norwood, Chichester, second edition.

James, H. M. and Guth, E. (1943). Theory of the elastic properties of rubber. *J. Chem. Phys.*, **11**, 455.

Jongschaap, R. (1990). Microscopic modelling of the flow properties of polymers. *Rep. Prog. Phys.*, **53**, 1.

Jongschaap, R. J. J., de Haas, K. H., and Damen, C. A. J. (1994). A generic matrix representation of configuration tensor rheological models. *J. Rheol.*, **38**, 1.

Kambour, R. P. (1986). Crazing. In J. I. Kroschwitz, editor, *Encyclopedia of Polymer Science and Engineering*, volume 4, page 299. John Wiley & Sons, New York, second edition.

Kinloch, A. J. and Young, R. J. (1985). *Fracture behaviour of polymers*. Elsevier Applied Science Publishers Ltd, London and New York, second edition.

Knauss, W. G. and Emri, I. (1981). Nonlinear viscoelasticity based on free volume considerations. *Comput. Struct.*, **13**, 123.

Knauss, W. G. and Emri, I. (1987). Volume change and the nonlinear thermoviscoelastic constitution of polymers. *Polym. Eng. Sci.*, **27**, 86.

Kovacs, A. J. (1964). Transition vitreuse dans les polymères amorphes. etitude phènomènologique. *Fortschr. Hochpolym.-Forsch.*, **3**, 394.

Kramer, E. (1983). Microscopic and molecular fundamentals of crazing. *Adv. Pol. Sci.*, **52/53**, 1.

Kramer, E. J. and Berger, L. L. (1990). Craze growth and fracture. *Adv. Pol. Sci.*, **91/92**, 1.

Krausz, A. and Eyring, H. (1975). *Deformation Kinetics*. Wiley-Interscience, London.

Kuhn, W. and Grün, F. (1942). Beziehungen zwischen elastischen konstanten und dehnungsdoppelbrechung hochelastischer stoffe. *Kolloidzeitschrifft*, **101**, 248.

Larson, R. G. (1988). *Constitutive Equations for Polymer Melts and Solutions*. Butterworth, Stoneham.

Leaderman, H. (1943). *Elastic and Creep Properties of Filamentous Materials and Other High Polymers*, page 13. The Textile Foundation, Washington D.C.

Lee, A. and McKenna, G. B. (1990). The physical aging response of an epoxy glass subjected to large stresses. *Polymer*, **31**, 423.

Leonov, A. I. (1976). Nonequilibrium thermodynamics and rheology of viscoelastic polymer media. *J. Rheol.*, **15**, 85.

Losi, G. U. and Knauss, W. G. (1992). Free volume theory and nonlinear thermoviscoelasticity. *Polym. Sci. Engng.*, **32**(8), 542.

Macosko, C. W. (1994). *Rheology: Principles, Measurements, and Applications.* VCH Publishers, New York.

Mansfield, M. L. (1995). Model of the glass transition. *J. Chem. Phys.*, **103**(18), 8124.

Matsushige, K., Radcliffe, S., and Bear, E. (1975). The mechanical behaviour of polystyrene under pressure. *J. Mater. Sci.*, **10**, 833.

McCrum, N. G. (1984). Sequential relaxation as the mechanism of physical ageing in amorphous polymers. *Polym. Comm.*, **25**, 2.

McCrum, N. G. (1992). Interpretation of physical ageing in creep and DMTA from sequential ageing theory. *Plas. Rub. Comp. Proc. Appl.*, **18**(3), 181.

McKenna, G. B. (1989). Glass formation and glassy behavior. In C. Booth and C. Price, editors, *Comprehensive Polymer Science, Polymer Properties*, volume 2, page 311. Pergamon, Oxford.

McKenna, G. B. and Kovacs, A. J. (1984). Physical aging of poly(methyl methacrylate) in the nonlinear range: Torque and normal force measurements. *Polym. Eng. Sci.*, **24**, 1138.

McKenna, G. B., Santore, M. M., Lee, A., and Duran, R. S. (1991). Aging in glasses subjected to large stresses and deformations. *J. Non-Crystalline Solids*, **131-133**, 497.

McKenna, G. B., Schultheisz, C. R., and Leterrier, Y. (1994). Volume recovery and physical aging: dilatomeric evidence for different kinetics. In *9th Int. Conf. on Deformation, Yield and Fracture of Polymers*, page 31/1, London. The Institute of Materials.

Mead, D. W. (1994). Numerical interconversion of linear viscoelastic material functions. *J. Rheol.*, **38**(6), 1769.

Neale, K. (1981). Phenomenological constitutive laws in finite plasticity. *Solid Mech. Arch.*, **6**, 79.

Noll, W. (1958). A mathematical theory of the mechanical behaviour of continuous media. *Arch. Rational Mech. Anal.*, **2**, 197.

O'Dowd, N. P. and Knauss, W. G. (1995). Time dependent large principal deformation of polymers. *J. Mech. Phys. Solids*, **43**(5), 771.

Oleinik, E. F., Salamantina, O. B., Rudnev, S. N., and Shenogin, S. V. (1993). A new approach to treating plastic strain in glassy polymers. *Polymer Science*, **35**, 1532. Translated from Vysokomolekulyarnye Soedinenika, vol. 35, 1993, pp. 1819-1849.

Provencher, S. W. (1982a). A constrained regularization method for inverting data represented by linear or integral equations. *Comput. Phys. Commun.*, **27**, 213.

Provencher, S. W. (1982b). Contin: A general purpose constrained regularization program for inverting noisy linear algebraic and integral equations. *Comput. Phys. Commun.*, **27**, 229.

Raha, S. and Bowden, P. (1972). Birefringence of plastically deformed poly (methyl methacrylate). *Polymer*, **13**, 174.

Ricco, T. and Smith, T. L. (1985). Rejuvenation and physical aging of a polycarbonate film subjected to finite tensile strains. *Polymer*, **26**, 1979.

Rice, J. R. (1977). The localization of plastic deformation. In W. T. Koiter, editor, *Theoretical and Applied Mechanics*, New York. North-Holland Publishing Company. Proc. of the 14^{th} IUTAM Congress, Delft (1976).

Roark, R. J. and Young, W. C. (1984). *Formulas for Stress and Strain*. McGraw-Hill, Singapore, fifth edition.

Rubin, M. B. (1987). An elastic-viscoplastic model exhibiting continuity of solid and fluid states. *Int. J. Engng. Sci.*, **25**, 1175.

Rubin, M. B. (1994). Plasticity theory formulated in terms of physically based microstructural variables part 1. theory. *Int. J. Solids Structures*, **31**, 532.

Sansour, C. and Bednarczyk, H. (1993). A study on rate-type constitutive equations and the existence of a free energy function. *Acta Mech.*, **100**, 205.

Santore, M. M., Duran, R. S., and McKenna, G. B. (1991). Volume recovery in epoxy glasses subjected to to torsional deformations: the question of rejuvenation. *Polymer*, **32**, 2377.

Schapery, R. A. (1969). On the characterization of nonlinear viscoelastic materials. *Pol. Eng. Sci.*, **9**, 295.

Shay, Jr., R. M. and Caruthers, J. M. (1986). A new nonlinear viscoelastic constitutive equation for predicting yield in amorphous solid polymers. *J. Rheol.*, **30**, 781.

Simo, J., Taylor, R., and Pister, K. (1985). Variational and projection methods for the volume constraint in finite deformation elasto-plasticity. *Computer Meth. Appl. Mech. Engng.*, **51**(1-3), 177.

Smith, T. L., Levita, G., and Moonan, W. K. (1988). Reversal and activation of physical aging by applied deformation in simple compression and extension. *J. Polym. Sci.: Part B: Polym. Phys.*, **26**, 875.

Struik, L. E. (1978). *Physical Aging in Amorphous Polymers and other Materials.* Elsevier, Amsterdam.

Struik, L. E. (1986/1987). Course on physics of polymers. Technical Report 135020, University Twente, Enschede, the Netherlands.

Struik, L. E. (1990). *Internal Stresses, Dimensional Instabilities and Molecular Orientations in Plastics.* John Wiley & Sons Ltd, Chichester.

Sweeney, J., Duckett, R. A., and Ward, I. M. (1988). The fracture behaviour of oriented polyethylene at high pressures. *Proc. R. Soc. Lond. A*, **420**, 53.

Tervoort, T. A., Brekelmans, W. A. M., and Govaert, L. E. (1994). A 3-d stress-strain relation for glassy polymers. In *9th Int. Conf. on Deformation, Yield and Fracture of Polymers*, page 66/1, London. The Institute of Materials.

Timmermans, P. H. M., Smit, R. J. M., Tervoort, T. A., Brekelmans, W. A. M., and Govaert, L. E. (1995). Simulation of localization of deformation in polymer glasses. In A. Bakker, editor, *7th International Conference on Mechanical Behaviour of Materials*, page 203. European Structural Integrity Society, Delft University Press.

Tobolsky, A. V. and Eyring, H. (1943). Mechanical properties of polymeric materials. *J. Chem. Phys.*, **11**, 125.

Treloar, L. R. G. (1975). *The Physics of Rubber Elasticity.* Clarendon Press, Oxford, third edition.

Tschoegl, N. W. (1989). *The Phenomenological Theory of Linear Viscoelastic Behaviour: an Introduction.* Springer-Verlag, Berlin Heidelberg.

Turnbull, D. and Cohen, M. H. (1961). Free-volume model of the amorphous phase: glass transition. *J. Chem. Phys.*, **34**(1), 120.

Valanis, K. C. (1971). A theory of viscoplasticity without a yield surface. *Arch. Mech.*, **23**, 517.

van der Sanden, M., Tervoort, T., and Meijer, H. (1993). Deformation and toughness of polymeric systems: 2. influence of entanglement density. *Polymer*, **34**, 2961.

van Wijngaarden, H. (1988). *Constitutive Relations for Metals with an Application to the Extrusion of Lead.* Ph.D. thesis, Eindhoven University of Technology, Eindhoven, the Netherlands.

Venditti, R. A. and Gillham, J. K. (1992a). Isothermal physical aging of poly(methyl methacrylate): localization of perturbations in thermomechanical properties. *J. Appl. Polym. Sci.*, **45**(3), 501.

Venditti, R. A. and Gillham, J. K. (1992b). Physical aging deep in the glassy state of a fully cured polyimide. *J. Appl. Polym. Sci.*, **45**(9), 1501.

Vincent, P. I. (1960). The necking and cold-drawing of rigid plastics. *Polymer*, **1**, 7.

Waldron, Jr., W. K., McKenna, G. B., and Santore, M. M. (1995). The nonlinear viscoelastic response and apparent rejuvenation of an epoxy glass. *J. Rheol.*, **39**(2), 471.

Wang, M. C. and Guth, E. J. (1952). Statistical theory of networks of non-gaussian flexible chains. *J. Chem. Phys.*, **20**, 1144.

Ward, I. M. (1990). *Mechanical Properties of Solid Polymers.* John Wiley & Sons, Chichester, second edition.

Westergaard, H. M. (1952). *Theory of Elasticity and Plasticity*, volume 3 of *Harvard Monographs on Applied Science.* John Wiley & Sons, New York.

Whitney, W. and Andrews, R. D. (1967). Yielding of glassy polymers: volume effects. *J. Pol. Sci. C*, **16**, 2981.

Williams, M. L., Landel, R. F., and Ferry, J. D. (1955). The temperature dependence of relaxation mechanisms in amorphous polymers and other glass-forming liquids. *J. Am. Chem. Soc.*, **77**, 3701.

Wu, P. D. and van der Giessen, E. (1992). On improved 3-d non-gaussian network models for rubber elasticity. *Mech. Res. Comm.*, **19**, 427.

Wu, P. D. and van der Giessen, E. (1993). On improved network models for rubber elasticity and their applications to orientation hardening in glassy polymers. *J. Mech. Phys. Solids*, **41**, 427.

Wu, P. D. and van der Giessen, E. (1994). Analysis of shear band propagation in amorphous glassy polymers. *Int. J. Solids Structures*, **31**(11), 1493.

Wu, P. D. and van der Giessen, E. (1995). On neck ropagation in amorphous glassy polymers under plane strain tension. *Int. J. Plasticity*, **11**(3), 211.

Yee, A. F., Bankert, R. J., Ngai, K. L., and Rendell, R. W. (1988). Strain and temperature accelerated relaxation in polycarbonate. *J. Polym. Sci.: Part B: Polym. Phys.*, **26**, 2463.

Appendix A

Interconversion of Linear Viscoelastic Response Functions

Interconversion of linear viscoelastic response functions in various modes of deformation is most readily done by invoking the correspondence principle. According to this principle, the appropriate Laplace transform of an elastic solution to a stress analysis problem corresponds to the viscoelastic solution in the transform plane. The time-dependent solution is then obtained by inverting the transform. The principle can only be applied if the boundaries themselves do not change with time (Tschoegl, 1989).

In case of step response functions, the appropriate Laplace transform is the Carson transform (s-multiplied Laplace transform). As an example, substitution of the Carson transforms $s\bar{E}$ and $s\bar{D}$ in the elastic relation $E = 1/D$ results in:

$$\bar{E}(s)\bar{D}(s) = \frac{1}{s^2}$$

Here, s is the transform variable and the overbar denotes the Laplace transform. Re-transforming then yields the relation between the creep compliance and the relaxation modulus, equation (A.1):

$$\int_0^t D(t - t')E(t')dt' = t \tag{A.1}$$

Conversion of the creep compliance in tensile mode to the shear relaxation modulus can be realized in a similar way. From Hooke's law for isotropic elastic materials, the relation between the shear modulus G, the tensile compliance D, and the bulk modulus K reads:

$$G = \frac{3K}{9KD - 1}$$

The Carson transform relation, therefore, becomes:

$$s\bar{G}(s) = \frac{3s\bar{K}(s)}{9s\bar{K}(s)s\bar{D}(s) - 1}$$

Since it is assumed that the volume response remains elastic, the Laplace transform of the bulk modulus $\bar{K}$ equals K_0/s and the transform equation becomes:

$$s\bar{G}(s) = \frac{3K_0}{9K_0 s\bar{D}(s) - 1} \tag{A.2}$$

This relation can be used to transform the experimental tensile compliance function $D(t)$ (figure 3.9) to the shear relaxation modulus $G(t)$ by collocation. To this extent, the experimental compliance function was first fitted to a generalized Kelvin-Voigt model:

$$D(t) = D_g + \sum_{i=1}^{n} D_i(1 - e^{-\frac{t}{\lambda_i}}) + \frac{t}{\eta_0^e}$$

with the Carson transform:

$$s\bar{D}(s) = D_g + \sum_{i=1}^{n} \frac{D_i}{1 + \lambda_i s} + \frac{1}{s\eta_0^e}$$

The fit was obtained using CONTIN, a constrained regularization program developed to invert ill-posed linear integral equations (Provencher, 1982a, 1982b). The key feature making CONTIN particular suitable for fitting ill-posed problems is the ability to incorporate a priori knowledge of the solution structure, like non-negativity of the Kelvin-Voigt parameters, into the numerical algorithm (Mead, 1994). A satisfactory fit was obtained using a log-equidistant grid of eighteen relaxation times (see figure 3.9). The next step consisted of calculating for a range of s values the Carson transform of the shear relaxation modulus, $s\bar{G}(s)$, by substitution of the Carson transform of the Kelvin-Voigt representation of $D(t)$ into equation A.2. The resulting curve was fitted to a generalized Maxwell model:

$$s\bar{G}(s) = \sum_{i=1}^{n} \frac{G_i\lambda_i s}{1 + \lambda_i s}$$

Again, the fit was obtained using CONTIN, imposing non-negativity of the Maxwell parameters and constraining the zeroth and the first moment of the distribution to the a priori known values of the glassy shear modulus G_g and the zero-shear viscosity η_0:

$$G_g = \sum_{i=1}^{n} G_i = \frac{3K_0}{9K_0 D_g - 1}$$

$$\eta_0 = \sum_{i=1}^{n} \eta_i = \sum_{i=1}^{n} G_i\lambda_i = \frac{\eta_0^e}{3}$$

The first relation follows from Hooke's law, whereas the second relation reflects the Trouton ratio between extensional and shear viscosity. An excellent fit was obtained using a log-equidistant grid of eighteen relaxation times. The resulting shear relaxation modulus is depicted in figure 3.10 and the eighteen shear moduli and relaxation times are tabulated in Table 3.3. A check of the conversion procedure was provided by comparing the original fit of the Carson transform of $D(t)$ with the generalized Maxwell fit of (the Carson transform of) $G(t)$, again using equation A.2. A good agreement was obtained.

Samenvatting

Bij het bestuderen van het deformatiegedrag van polymeren wordt onderscheid gemaakt tussen lineair viscoelastisch gedrag, niet-lineair viscoelastisch gedrag en het vloeigedrag bij hoge spanningen. Het lineair viscoelastisch gedrag wordt, gebruikmakend van de zogenaamde lineaire respons theorie, beschreven met de bekende Boltzmann superpositie-integraal. Het modelleren van niet-lineair viscoelastisch gedrag is een nog altijd actief gebied van onderzoek, waarin verschillende theorieën zijn ontwikkeld. De meeste daarvan beogen een één-dimensionale beschrijving te geven van een specifieke belastingstoestand bij niet al te grote deformaties, zoals bijvoorbeeld kruip. Het vloeigedrag wordt tenslotte in het algemeen beschreven met behulp van vloeicriteria, waarbij meestal wordt gekozen voor het druk- en reksnelheidsafhankelijke Von Mises criterium. Na het vloeipunt vertonen polymeren rekversteviging, soms voorafgegaan door intrinsieke rekverzachting.

In dit proefschrift is getracht al deze aspecten van het mechanisch gedrag van glasachtige polymeren te combineren in één constitutieve vergelijking. Hiertoe is gebruik gemaakt van het "tijd-spanning superpositie-principe", ook wel een "spanningsklok" genoemd. Tijd-spanning superpositie stelt dat de niet-lineaire invloed van spanning voornamelijk bestaat uit het op identieke wijze veranderen van alle relaxatietijden. Met andere woorden, dat de intrinsieke tijdschaal van het materiaal verandert. Dit is analoog aan het bekende "tijd-temperatuur superpositie-principe", waarin alle relaxatietijden op dezelfde manier van de temperatuur afhangen. De mate waarin de relaxatietijden veranderen door de niet-lineaire invloed van spanning, wordt kwantitatief beschreven door de Eyring theorie van spanningsgeïnduceerde diffusie. Voor het experimentele onderzoek naar de geldigheid van spanning-tijd superpositie is gekozen voor polycarbonaat als een modelpolymeer, aangezien in dit polymeer vanaf kamertemperatuur tot aan het glaspunt slechts één relaxatiemechanisme actief is. Het blijkt dat het volledige niet-lineaire viscoelastische gedrag van polycarbonaat, inclusief het reksnelheidsafhankelijke vloeigedrag, wordt bepaald door de combinatie van een lineair relaxatietijden-spectrum met één niet-lineariteitsparameter uit de Eyring theorie, het zogenaamde "activeringsvolume". Tijd-spanning superpositie betekent in essentie, dat het vloeipunt gezien kan worden als een spanningsgeïnduceerde glasovergang.

De rekversteving in polycarbonaat is experimenteel onderzocht door middel van grote homogene deformaties, zowel boven als onder de glasovergangstemperatuur. Voor het realiseren daarvan beneden het glaspunt is gebruik gemaakt van een mechanische conditioneringstechniek, waarbij cilindervormige proefstaven werden getordeerd tot ver in het plastische gebied, waarna de staven weer in hun isotrope uitgangstoestand werden teruggebracht door ze terug te draaien. Het gevolg van deze plastische deformatie is dat, bij het opnieuw belasten van het materiaal, geen rekverzachting meer op optreedt, hetgeen resulteert in homogene deformatie, zelfs bij trekbelasting.

Gebruikmakend van deze mechanisch geconditioneerde proefstaven bleek experimenteel dat het verstevigingsgedrag van polycarbonaat, zowel in trek, druk, als afschuiving, uitstekend kan worden beschreven met neo-Hooke's gedrag, met een afschuifmodulus $G = 26$ MPa. Een asymptotische toename van de spanning, die zou kunnen wijzen op een eindige uitrekbaarheid (maximale strekgraad) van het entanglementnetwerk, werd niet waargenomen. De rekversteviging bleef voldoen aan neo-Hooke's gedrag tot het moment van breuk, dat in trek optrad bij 200 % deformatie. De temperatuursafhankelijkheid van de rekverstevigingsmodulus komt overeen met de temperatuursafhankelijkheid van de plateaumodulus, zoals die wordt waargenomen bij dynamisch mechanische metingen. Dit is een directe aanwijzing dat de rekversteviging in polycarbonaat wordt veroorzaakt door rubberelastisch gedrag van het entanglementnetwerk.

Teneinde al deze aspecten van het mechanisch gedrag van glasachtige polymeren te combineren tot één enkele constitutieve vergelijking, is een basismodel ontwikkeld voor het beschrijven van relaxatiegedrag, een zogenaamd "Leonov element". Een Leonov element is een in feite een Maxwell model, waarvan de relaxatietijd afhankelijk is van een equivalente spanning, evenredig met de Von Mises spanning. Een Leonov element maakt verder, op correcte wijze, onderscheid tussen de (elastische) hydrostatische spanning en (viscoelastische) deviatorische spanning en is geschikt voor het beschrijven van eindige deformaties, rekening houdend met geometrisch complex gedrag als gevolg van het gelijktijdig optreden van elastische en plastische deformaties. Een aantal van deze Leonov elementen is vervolgens parallel geschakeld, resulterend in een benadering van het relaxatietijdenspectrum, hetgeen het volledige deformatiegedrag van glasachtige polymeren afdoende beschrijft. Het resulterende model geeft een kwantitatieve beschrijving van het drie-dimensionale, niet-lineaire, viscoelastische gedrag bij eindige deformaties. Het geeft ook een beschrijving van drie-dimensionale aspecten van rekversteviging, zoals de ontwikkeling van anisotropie tijdens plastische deformatie.

Het in dit proefschrift beschreven onderzoek toont aan dat het lineaire relaxatietijdenspectrum het mechanisch gedrag van glasachtige polymeren bepaalt. De deviatorische spanning (en temperatuur) vervormen slechts de tijdschaal van het materiaal. Opgemerkt dient te worden dat het mechanische gedrag in het algemeen en het lineair viscoelastische gedrag in het bijzonder, in belangrijke

mate wordt beinvloed door fysische veroudering. Het is bekend dat onder invloed van fysische veroudering de kruipcompliantiecurve verschuift naar langere tijden. Echter de proefstaven die werden gebruikt in deze studie, hadden alle eenzelfde leeftijd, die veel hoger was dan de experimenteertijd. Daarom is, als eerste benadering, fysische veroudering niet meegenomen. Het gevolg hiervan is dat het model voor materialen met een andere geschiedenis minder nauwkeurig zal zijn en in kwantitatieve zin dus nog niet universeel toepasbaar is.

Fysische veroudering kan door plastische deformatie teniet worden gedaan. Dit fenomeen, ook wel verjonging genoemd, kenmerkt zich door een verlaging van de viscositeit na het vloeipunt, wat leidt tot intrinsieke rekverzachting. De goede overeenkomst tussen voorspelling en experiment voor de niet-lineaire relaxatie-experimenten en de toepasbaarheid van tijd-spanning superpositie wijzen erop dat, voor polycarbonaat, voor monotone belastingsgeschiedenissen tot aan het vloeipunt, verjongingseffecten relatief onbelangrijk zijn. Daarom zijn in deze studie verjongingseffecten niet meegenomen. Hoewel een nauwkeurige kwantitatieve beschrijving van verjongingseffecten beneden het vloeipunt nog onvoldoende uitgekristalliseerd is, zijn er in de literatuur verscheidene bruikbare fenomenologische modellen beschikbaar voor het beschrijven van rekverzachting na het vloeipunt.

Een belangrijk gevolg van het niet-lineaire vloeigedrag van polymeren in het algemeen en glasachtige polymeren in het bijzonder, is het optreden van rek-lokalisatie. Rek-lokalisatie, hier gedefinieerd als het uitgroeien van inhomogeen gedrag ten gevolge van kleine verstoringen in het rek- of spanningsveld, uit zich in de vorming van shearbands en crazes. Gebruikmakend van een brosse polystyreen-grade als modelmateriaal is experimenteel aangetoond dat de reksnelheidsafhankelijkheid van het breukproces (craze-initiatie) en het vloeiproces identiek zijn. Dit gegeven opent mogelijkheden voor het definiëren van een lokaal craze-initiatie criterium, door eindige-elementen berekeningen voor een gegeven microstructuur te vergelijken met experimentele craze-studies. Een dergelijk lokaal criterium zou een krachtig hulpmiddel kunnen zijn bij het computer-ondersteund ontwerpen van nieuwe heterogene polymere systemen die zodanig zijn geoptimaliseerd dat het breukproces wordt overheerst door het vloeiproces.

Acknowledgments

First of all I want to thank Lena and Sasha for their patience and support.

Furthermore, I thank all my colleagues at the Eindhoven University of Technology, both, at the Department of Polymer Technology, and at the Department of Fundamental Mechanical Engineering, for their contributions to this thesis, and for making my stay at the university such a pleasant one. For their technical support, I am especially indebted to: Johan Boekholt, Sjef Garenveld, Toon van Gils and the Central Technical Service Department ("CTD"), in particular, Erwin Dekkers.

I am also indebted to prof.dr. I.M. Ward, dr. R.A. Duckett and dr. J. Sweeney at the University of Leeds (IRC of Polymer Science & Technology) for stimulating discussions and experimental support.

I gratefully acknowledge the contributions of the graduate students: Edwin Klompen, Robert Smit, Stefan Dusée, Katinka van Aert, Maurice Theuns, Renee Hautvast, and the research students: Hein Schellens, Leo van Kemenade, Dagmar Buzeman, Peter Toonsen, and Paul Roosen.

Finally, last but not least, I want to thank Leon Govaert, without whom this thesis would not have existed.

Curriculum Vitae

The author of this thesis was born in Haarlem, the Netherlands, on May 25th, 1961. From 1979 to 1983 he studied Chemical Technology at the Technical College "Amsterdam", Amsterdam, the Netherlands. In 1983 he came to Eindhoven, the Netherlands, to study Chemical Engineering at the Eindhoven University of Technology, where he received his Master Degree in 1987. That same year he started as Assistant Professor at the Department of Polymer Technology in the research group of prof.dr. P.J. Lemstra at the Eindhoven University of Technology. The study described in this thesis, was initiated in 1991, in collaboration with the Department of Fundamental Mechanical Engineering.

As from March 1996, the author will join the research group of prof.dr. P. Smith at the Swiss Federal Institute of Technology (Eidgenössische Technische Hochschule, ETH) in Zürich, Switzerland.

Stellingen

behorende bij het proefschrift

"CONSTITUTIVE MODELLING OF POLYMER GLASSES"

van T.A. Tervoort

1. Het vloeipunt van polycarbonaat is een spanningsgeïnduceerde glasovergang.

   Dit proefschrift, Hoofdstuk 3

2. Het voorspellen van een maximale rekgraad in trek vanuit (uniaxiale) compressieproeven kan bijzonder onnauwkeurig zijn.

   Dit proefschrift, Hoofdstuk 5

3. De omschrijving: "In the context of the idea of free volume we acknowledge that this physical phenomenon is not necessarily the only one that can play a significant role in large deformation processes. While the presently considered strain states develop exclusively positive dilatation, there are others where a volume decrease would not produce some of the phenomena associated with "yield" in tension." is een erg cryptische manier om te zeggen: "Ons vrij-volume model werkt wel in trek, maar niet in druk.".

   O'Dowd, N.P. and Knauss, W.G. (1995) Time-dependent large principle deformation of glassy polymers. J. Mech. Phys. Solids **43***(3), 771-792. Dit proefschrift, Hoofdstuk 6*

4. De rekgraad zoals gevonden in shearbands ("deformation zones") van glasachtige polymeren is niet noodzakelijkerwijs het gevolg van een maximale uitrekbaarheid van het "entanglementnetwerk".

   Donald, A.M. and Kramer, E.J. (1982). Deformation zones and entanglements in glassy polymers. Polymer, **23***, 1183. Dit proefschrift, Hoofdstuk 4 en 5.*

5. Het is opmerkelijk dat de plasticiteitsleer bijna exclusief gebruik maakt van "spanningsklok" modellen op basis van de tweede invariant van de deviatorische spanningstensor, terwijl deze niet of nauwelijks voorkomen in de rheologie van polymere smelten.

   Besseling, J. and van der Giessen, E. (1994) Mathematical Modelling of Inelastic Deformations. Chapman & Hall, London.
   Larson, R.G. (1988) Constitutive Equations for Polymer Melts and Solutions. Butterworth, Stoneham.

6. Van der Werff en Pennings concluderen uit een lineaire extrapolatie van de vloeispanning als functie van de temperatuur ten onrechte dat vloei in georiënteerd polyetheen het gevolg is van het ontstaan van een hexagonale fase in de kristallijne domeinen.

   *Van der Werff, H. and Pennings, A.J. (1991). Tensile deformation of high strength and high modulus polyethylene fibers. J. Colloid Polym. Sci., **270**, 747.*
   *Govaert, L.E. and Peijs, T. (1995). Tensile strength and work of fracture of oriented polyethylene fibre. Polymer, **36**(23), 4425.*

7. Het is nooit te laat Thermo 1 nog eens te volgen.

   *Figuur 12 in: Honell, K.G. and Hall, C.K. (1991) Theory and simulation of hard-chain mixtures: Equations of state, mixing properties, and density profiles near hard walls. J. Chem. Phys. **95**(6), 4481.*
   Thermodynamica I, collegediktaat Technische Universiteit Eindhoven.

8. Het is opmerkelijk dat Rusland probeert te democratiseren naar Europees model, terwijl Europa steeds meer communiceert volgens oud Russisch model.

9. De Munt valt onder monumentenzorg, de gulden helaas niet.

10. Op de momenten dat je zin hebt *in* het leven, denk je meestal niet na over de zin *van* het leven.

Eindhoven, februari 1996.